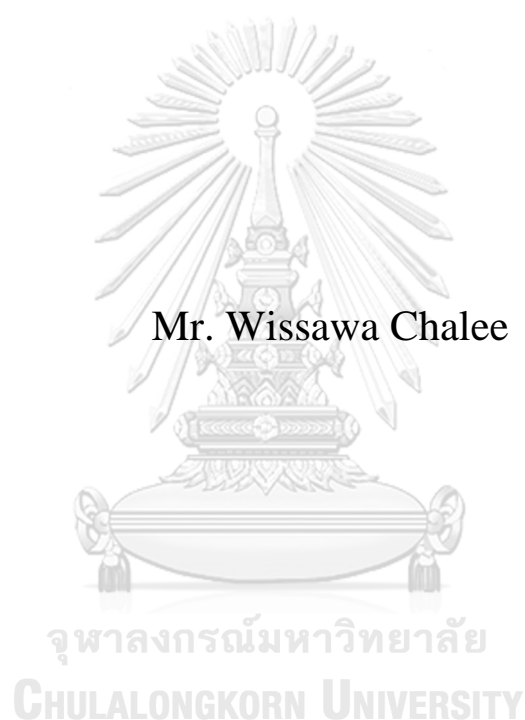


PERFORMANCE ANALYSIS OF THE PROTON-
CONDUCTING SOLID OXIDE ELECTROLYSIS CELL
COUPLING WITH DRY METHANE REFORMING



A Thesis Submitted in Partial Fulfillment of the Requirements
for the Degree of Master of Engineering in Chemical Engineering
Department of Chemical Engineering
Faculty of Engineering
Chulalongkorn University
Academic Year 2019
Copyright of Chulalongkorn University

การวิเคราะห์ประสิทธิภาพของเซลล์อิเล็กโทรไลซิสชนิดออกไซด์ของแข็งแบบนำโปรตอนร่วมกับ
กระบวนการรีฟอร์มมิงของมีเทนแบบแห้ง



วิทยานิพนธ์นี้เป็นส่วนหนึ่งของการศึกษาตามหลักสูตรปริญญาวิศวกรรมศาสตรมหาบัณฑิต
สาขาวิชาวิศวกรรมเคมี ภาควิชาวิศวกรรมเคมี
คณะวิศวกรรมศาสตร์ จุฬาลงกรณ์มหาวิทยาลัย
ปีการศึกษา 2562
ลิขสิทธิ์ของจุฬาลงกรณ์มหาวิทยาลัย

วิชาว ชาติ : การวิเคราะห์ประสิทธิภาพของเซลล์อิเล็กโทรไลซิสชนิดออกไซด์ของแข็งแบบนำโปรตอนร่วมกับกระบวนการรีฟอร์มมิงของมีเทนแบบแห้ง. (PERFORMANCE ANALYSIS OF THE PROTON-CONDUCTING SOLID OXIDE ELECTROLYSIS CELL COUPLING WITH DRY METHANE REFORMING) อ.ที่ปรึกษาหลัก : ผศ. ดร. อมรชัย อภรณ์วิชานพ

เซลล์อิเล็กโทรไลซิสชนิดออกไซด์ของแข็งแบบนำโปรตอน (H-SOEC) เป็นเทคโนโลยีสะอาดสำหรับผลิตแก๊สสังเคราะห์จากน้ำและคาร์บอนไดออกไซด์ผ่านปฏิกิริยาไฟฟ้าเคมีและปฏิกิริยาเคมี อย่างไรก็ตามเทคโนโลยีดังกล่าวมักให้ค่าการเปลี่ยนแปลงคาร์บอนไดออกไซด์ที่ต่ำและมีน้ำปนออกมากับผลิตภัณฑ์แก๊สสังเคราะห์ในปริมาณที่สูง เพราะฉะนั้นเซลล์อิเล็กโทรไลซิสชนิดออกไซด์ของแข็งแบบนำโปรตอนร่วมกับกระบวนการรีฟอร์มมิงของมีเทนแบบแห้ง (H-SOEC/DMR) จึงถูกเสนอขึ้นเพื่อเป็นการปรับปรุงประสิทธิภาพของกระบวนการดังกล่าว แผนผังแบบจำลองของ H-SOEC/DMR ถูกพัฒนาขึ้นโดยใช้โปรแกรม Aspen Plus และใช้แบบจำลองดังกล่าวสำหรับประเมินประสิทธิภาพของ H-SOEC/DMR จากการวิเคราะห์ประสิทธิภาพของ H-SOEC/DMR แสดงให้เห็นว่าภายใต้ช่วงอุณหภูมิตั้งแต่ 1073 K ถึง 1273 K กระบวนการดังกล่าวให้ค่าการเปลี่ยนแปลงของคาร์บอนไดออกไซด์และมีเทนที่สูงมากกว่า 90% และ 80% ตามลำดับและมีปริมาณของน้ำในผลิตภัณฑ์แก๊สสังเคราะห์ที่ต่ำ ทั้งยังพบอีกว่าปริมาณของผลิตภัณฑ์แก๊สสังเคราะห์มีค่าเพิ่มสูงขึ้นตามการเพิ่มขึ้นของความหนาแน่นกระแสและจำนวนเซลล์ จากการวิเคราะห์ทางพลังงานของกระบวนการแสดงให้เห็นว่า H-SOEC/DMR (500 เซลล์) ให้ประสิทธิภาพทางพลังงานสูงสุดอยู่ที่ 72.80% เมื่อดำเนินการภายใต้สภาวะที่มีอุณหภูมิ 1123 K, ความดัน 1 atm, และความหนาแน่นกระแส 2500 A m⁻² การออกแบบเครือข่ายแลกเปลี่ยนความร้อนด้วยการวิเคราะห์จุดพินช์ได้ถูกนำมาประยุกต์ใช้กับ H-SOEC/DMR ซึ่งทำให้ประสิทธิภาพทางพลังงานเพิ่มขึ้นไปที่ 81.46% และจากการวิเคราะห์ทางเอ็กเซอร์จีพบว่าหน่วย H-SOEC/DMR เป็นหน่วยที่มีค่าประสิทธิภาพทางเอ็กเซอร์จีต่ำที่สุดเนื่องจากการปล่อยไอแก๊สอุณหภูมิสูงออกมาจากหน่วยดังกล่าว



สาขาวิชา วิศวกรรมเคมี
ปีการศึกษา 2562

ลายมือชื่อนิสิต
ลายมือชื่อ อ.ที่ปรึกษาหลัก

6070315921 : MAJOR CHEMICAL ENGINEERING

KEYWORD Proton-conducting solid oxide electrolysis cell, Dry methane reforming, Exergy analysis, Syngas production, Simulation

D: Wissawa Chalee : PERFORMANCE ANALYSIS OF THE PROTON-CONDUCTING SOLID OXIDE ELECTROLYSIS CELL COUPLING WITH DRY METHANE REFORMING. Advisor: Asst. Prof. Dr. AMORNCHAI ARPORNWICHANOP, D.Eng.

The proton-conducting solid oxide electrolysis cell (H-SOEC) is a clean technology for syngas production from H₂O and CO₂ through electrochemical and chemical reactions. However, it gives low CO₂ conversion and produces syngas product with high H₂O content. Therefore, the H-SOEC coupling with a dry methane reforming process (H-SOEC/DMR) is proposed to improve its performance. The process flowsheet of the H-SOEC/DMR is developed by using Aspen Plus and used to evaluate the performance of H-SOEC/DMR. The performance analysis of the H-SOEC/DMR shows that under the temperature range of 1073-1273 K, the %CO₂ and %CH₄ conversions of higher than 90% and 80% are observed, and the syngas product with low H₂O content is obtained. The amount of syngas product increases with an increase in operating current density and the number of cells. The energy analysis is also performed, and the result indicates that the H-SOEC/DMR (500 cells) gives the highest energy efficiency of 72.80% when it is operated at temperature of 1123 K, pressure of 1 atm, and current density of 2500 A m⁻². Based on a pinch analysis, the heat exchanger network is applied to the H-SOEC/DMR process, and its energy efficiency is increased to 81.46%. The exergy analysis shows that the H-SOEC/DMR unit gives the lowest exergy efficiency as high-temperature exhaust gas is released.



Field of Study: Chemical Engineering

Student's Signature

Academic 2019

Advisor's Signature

Year:

.....

ACKNOWLEDGEMENTS

First of all, the author would like to express my sincere appreciation to my thesis advisor, Assistant Professor Dr. Amornchai Arpornwichanop, who always introduces me in both research and education. His precious recommendation, as well as motivation throughout the cause of this research, are the important thing to success of this research. Without his support and guidance this thesis would not have been completed.

Moreover, the author most gratefully thanks the chairman, Assistant Professor Dr. Nattaporn Tonanon, and the other member of the thesis committee, Assistant Professor Dr. Palang Bumroongsakulsawat and Assistant Professor Dr. Pornchai Bumroongsri, for their time and useful comment on improving my research.

Finally, the author most gratefully thank my family, especially my father, Mr. Somboon Chalee, and my mother Mrs. Nongnuch Chalee, for their motivation and support, and my friends in the Center of Excellence in Process and Energy System Engineering.

Wissawa Chalee

TABLE OF CONTENTS

	Page
ABSTRACT (THAI)	iii
ABSTRACT (ENGLISH).....	iv
ACKNOWLEDGEMENTS	v
TABLE OF CONTENTS.....	vi
LIST OF FIGURES	ix
LIST OF TABLES.....	xiv
NOMENCLATURES.....	xvi
CHAPTER I INTRODUCTION.....	1
1.1 Background.....	1
1.2 Objective.....	5
1.3 Scopes of work	5
1.4 Research methodology.....	6
CHAPTER II THEORY.....	8
2.1 Proton-conducting solid oxide electrolysis cell (H-SOEC) technology	8
2.1.1 Principle of SOEC.....	9
2.1.2 Configuration of SOEC.....	13
2.1.3 SOEC stack design	13
2.2 Dry methane reforming technology.....	14
2.2.1 Principle of DMR	15
2.2.2 Thermodynamics of DMR.....	16
2.3 Electrochemical model	17
2.3.1 Modelling assumptions.....	17
2.3.2 The voltage of H-SOEC	18
2.4 Gibbs free energy minimization method	32
2.5 Energy analysis.....	37

2.5.1 Energy efficiency	37
2.5.2 Pinch analysis	38
2.6 Exergy analysis	51
CHAPTER III LITERATURE REVIEW	57
3.1 Performance improvement of a solid oxide electrolysis cell for syngas production.....	57
3.2 Proton-conducting solid oxide electrolysis cell.....	60
3.3 Dry methane reforming process.....	65
CHAPTER IV MODELING AND VALIDATION	68
4.1 H-SOEC for syngas production.....	68
4.1.1 MIXER module	68
4.1.2 Electrochemical reaction in ANODE module	69
4.1.3 Proton and oxygen separation in ELECTROL module.....	70
4.1.4 Chemical reaction in CATHODE module.....	70
4.1.5 Cell voltage, power, and overpotentials calculation.....	71
4.1.6 Energy balance	73
4.1.7 H-SOEC validation.....	74
4.2 Dry methane reforming catalyst layer	76
4.3 H-SOEC/DMR for syngas production.....	80
4.4 Other units in H-SOEC/DMR.....	80
4.4.1 Steam generator	80
4.4.2 Syngas compressor	81
4.5 Performance analysis	83
CHAPTER V SENSITIVITY ANALYSIS	86
5.1 Effect of structural parameters.....	86
5.1.1 Effect of thickness of cell and support structure	87
5.1.2 Effect of electrode pore size	91
5.1.3 Effect of electrode porosity	92
5.1.4 Effect of electrode tortuosity	93

5.2 Effect of operational parameters.....	94
5.2.1 Effect of S/C molar ratio	96
5.2.2 Effect of temperature.....	98
5.2.3 Effect of pressure.....	103
5.2.4 Effect of current density	108
5.2.5 Effect of number of cell.....	113
CHAPTER VI ENERGY ANALYSIS AND OPTIMUM CONDITION	118
6.1 Energy analysis.....	118
6.1.1 Effect of temperature on energy efficiency	119
6.1.2 Effect of pressure on energy efficiency.....	122
6.1.3 Effect of current density on energy efficiency	126
6.1.4 Effect of number of cell on energy efficiency.....	130
6.2 Optimum condition.....	134
CHAPTER VII HEAT EXCHANGER NETWORK DESIGN.....	137
7.1 Data extraction.....	137
7.2 Pinch and energy target calculation.....	141
7.3 Heat exchanger network design.....	144
CHAPTER VIII EXERGY ANALYSIS	150
8.1 Exergy analysis of the optimum condition	150
8.2 Effect of operating parameters on exergy efficiency and destruction	157
CHAPTER IX CONCLUSION AND RECOMMENDATIONS	161
9.1 Conclusion	161
9.2 Recommendations.....	164
REFERENCES	165
VITA.....	173

LIST OF FIGURES

	Page
Figure 1.1 The schematics of (a) H-SOEC and (b) H-SOEC combine with a novel layer catalyst of DMR (H-SOEC/DMR) for syngas production.....	3
Figure 1.2 The designed reactor of H-SOEC and dry methane reforming layer.....	4
Figure 2.1 SOEC schematics for CO ₂ /H ₂ O electrolysis based on (a) oxygen ion conducting electrolyte and (b) proton conducting electrolyte (Xiaomin et al., 2017)...	10
Figure 2.2 Relationships between thermodynamic parameters of electrolysis reaction (Wang et al., 2015).....	12
Figure 2.3 SOEC configurations: (a) Tubular and (b) Planar (Ni et al., 2008b).....	13
Figure 2.4 Schematic diagram of the (a) planar (Ebbesen et al., 2011) and (b) tubular (Spacil and Tedmon, 1969) SOECs stacking systems.....	14
Figure 2.5 The effect of overpotentials on the cell voltage due to the increase of current density (Stempien et al., 2013b).....	22
Figure 2.6 Construction of a hot composite curve (Dimian et al., 2014).....	40
Figure 2.7 construction of a cold composite curve (Dimian et al., 2014).....	41
Figure 2.8 Composite curve (Dimian et al., 2014).....	41
Figure 2.9 Streams and temperature interval (Kemp, 2007).....	44
Figure 2.10 Use of heat surplus from an interval (Kemp, 2007).....	46
Figure 2.11 Infeasible and feasible heat cascades (Kemp, 2007).....	46
Figure 2.12 Initial grid diagram for example problem (Kemp, 2007).....	47
Figure 2.13 Above pinch network design for example problem (Kemp, 2007).....	48
Figure 2.14 Below pinch network design for example problem (Kemp, 2007).....	50

Figure 2.15 Heat exchanger network design achieving energy targets (Kemp, 2007)..50	50
Figure 2.16 The energy, entropy, and exergy balances through the system (Çengel et al., 2019).....51	51
Figure 3.1 (a) Schematic diagram of CO ₂ reduction in proton conductor. (b) Cell configuration using single cathode layer, LSCF+GDC and (c) double cathode layers, LSCF+GDC/CMF+LSFM (Shin et al., 2015).....58	58
Figure 3.2 The schematic of CO ₂ /CH ₄ reforming process (Lu et al., 2018).....59	59
Figure 3.3 The geometrical parameters of the designed reactor with SOFC and dry methane reforming layer (Chen et al., 2018).....60	60
Figure 4.1 Process flowsheet of the H-SOEC for syngas production.....69	69
Figure 4.2 A schematic of the hydrogen permeation through the porous ceramic electrode (C. Reid et al., 1959).....71	71
Figure 4.3 Comparison between the experimental data and simulation results.....75	75
Figure 4.4 Dry methane reforming flowsheet simulation.....76	76
Figure 4.5 Schematic drawing of the packed-bed reactor (Herrera Delgado et al., 2015).....77	77
Figure 4.6 Comparison between the simulation results and experiment data of (a) carbon dioxide, (b) methane, and (c) hydrogen, carbon monoxide, and water concentration.....78	78
Figure 4.7 Process flowsheet of the H-SOEC/DMR for syngas production.....80	80
Figure 4.8 Flowsheet simulation of the steam generator unit.....81	81
Figure 4.9 Flowsheet simulation of the 2 stages syngas compressor unit.....83	83
Figure 4.10 Flowsheet simulation of the overall H-SOEC/DMR process.....85	85
Figure 5.1 Effect of thickness of anode, cathode, and electrolyte on the performance of system.....87	87

- Figure 5.2** Evaluation of anode-supported, cathode-supported, and electrolyte-supported for system (a) J-V characteristics, (b) ohmic overpotential of electrolyte-supported and electrode-supported, (c) concentration overpotentials in an anode-supported, and (d) concentration overpotentials in a cathode-supported.....89
- Figure 5.3** Effect of electrode pore size on J-V characteristics of cathode-supported configuration.....91
- Figure 5.4** Effect of electrode porosity on J-V characteristics of cathode-supported configuration.....92
- Figure 5.5** Effect of electrode tortuosity on J-V characteristics of cathode-supported configuration.....93
- Figure 5.6** Effect of the S/C molar ratio (a) on the cell voltage and (b) on the H/C molar ratio.....97
- Figure 5.7** Effect of operating temperature on (a) the cell voltage, equilibrium voltage, activation and ohmic overpotentials, (b) the concentration overpotentials, and (c) the energy demand of system.....99
- Figure 5.8** Effect of operating temperature on (a) product stream molar flow rate and (b) %CO₂ and CH₄ conversions, %Syngas in product, and H/C molar ratio.....101
- Figure 5.9** Effect of operating pressure on (a) the cell voltage, equilibrium voltage, activation and ohmic overpotentials, (b) the concentration overpotentials, and (c) the energy demand of system.....104
- Figure 5.10** Effect of operating pressure on (a) product stream molar flow rate and (b) %CO₂ and CH₄ conversions, %Syngas in product, and H/C molar ratio.....107
- Figure 5.11** Effect of current density on (a) the cell voltage, equilibrium voltage, activation and ohmic overpotentials, (b) the concentration overpotentials, and (c) the energy demand of system.....109

Figure 5.12 Effect of current density on (a) product stream molar flow rate and (b) %CO ₂ and CH ₄ conversions, %Syngas in product, and H/C molar ratio.....	111
Figure 5.13 Effect of number of cell on (a) the cell voltage, equilibrium voltage, activation and ohmic overpotentials, (b) the concentration overpotentials, and (c) the energy demand of system.....	114
Figure 5.14 Effect of number of cell on (a) product stream molar flow rate and (b) %CO ₂ and CH ₄ conversions, %Syngas in product, and H/C molar ratio.....	116
Figure 6.1 Effect of temperature on energy efficiency of process.....	120
Figure 6.2 Effect of temperature on (a) energy demand of H-SOEC/DMR unit and (b) energy demand of SG and SC units.....	121
Figure 6.3 Effect of temperature on syngas production term.....	122
Figure 6.4 Effect of pressure on energy efficiency of process.....	124
Figure 6.5 Effect of pressure on (a) energy demand of H-SOEC/DMR unit and (b) energy demand of SG and SC units.....	125
Figure 6.6 Effect of pressure on syngas production term.....	126
Figure 6.7 Effect of current density on energy efficiency of process.....	128
Figure 6.8 Effect of current density on (a) energy demand of H-SOEC/DMR unit and (b) energy demand of SG and SC units.....	128
Figure 6.9 Effect of current density on syngas production term.....	130
Figure 6.10 Effect of number of cell on energy efficiency of process.....	132
Figure 6.11 Effect of number of cell on (a) energy demand of H-SOEC/DMR unit and (b) energy demand of SG and SC units.....	132
Figure 6.12 Effect of number of cell on syngas production term.....	133

Figure 7.1 Flowsheet simulation of the H-SOEC/DMR process for the heat exchanger network design.....	140
Figure 7.2 Streams and temperature intervals.....	143
Figure 7.3 The cascade diagram of (a) infeasible heat flow and (b) feasible heat flow.....	144
Figure 7.4 Grad diagram of the H-SOEC/DMR process.....	145
Figure 7.5 Stream splitting algorithm for (a) above and (b) below the pinch (Smith, 2016).....	146
Figure 7.6 Above pinch network design.....	147
Figure 7.7 Below pinch network design.....	148
Figure 7.8 Overall network design achieving energy target.....	148
Figure 7.9 Simulation process flowsheet of the H-SOEC/DMR process with heat exchanger network design.....	149
Figure 8.1 %Exergy destruction value of each unit in the H-SOEC/DMR process....	153
Figure 8.2 Exergy efficiency of each unit in the H-SOEC/DMR process.....	154
Figure 8.3 Simulation process flowsheet of the H-SOEC/DMR process after exergy analysis.....	156
Figure 8.4 Effect of temperature on exergy efficiency and destruction value.....	158
Figure 8.5 Effect of pressure on exergy efficiency and destruction value.....	159
Figure 8.6 Effect of current density on exergy efficiency and destruction value.....	159
Figure 8.7 Effect of number of cell on exergy efficiency and destruction value.....	160

LIST OF TABLES

	Page
Table 2.1 Possible gas phase reactions in the dry methane reforming process (Nikoo and Amin, 2011; Wang and Lu, 1996).....	17
Table 2.2 Information of stream data for composite curve construction.....	39
Table 2.3 The information data of process streams example (Kemp, 2007).....	43
Table 2.4 The information data of process streams example with shifted temperature (Kemp, 2007).....	43
Table 2.5 The temperature intervals and heat loads for process streams (Kemp, 2007).....	44
Table 2.6 Standard chemical exergy value for selected substances at the reference environment ($T_0 = 298 \text{ K}$, $P_0 = 1 \text{ atm}$) (Dincer and Rosen, 2013; Evgeny, 2006).....	56
Table 4.1 Cell voltage and overpotentials calculation equations.....	72
Table 4.2 Calculation equation for system operation and evaluation.....	73
Table 4.3 Input parameters and operating conditions.....	75
Table 4.4 Pre-exponential factor and activation energy values.....	76
Table 4.5 Parameters for effective diffusion coefficient calculations (C. Reid et al., 1959).....	76
Table 5.1 Input parameters and operating conditions for operational parameters analysis.....	95
Table 6.1 Summary of effect of parameters on the energy efficiency.....	135
Table 7.1 Input parameters and operating conditions for heat exchanger network design.....	138
Table 7.2 The information data of process streams.....	139

Table 7.3 The information data of process streams with shifted temperature.....141

Table 7.4 The temperature intervals and heat loads for process streams.....143

Table 8.1 Energy and exergy efficiencies of the optimal H-SOEC/DMR process.....155



NOMENCLETURES

A	Cell area (m ²)
a _{ij}	Number of atoms of element j in component i (-)
B _g	Flow permeability (m ²)
C _p	Heat capacity (J mol ⁻¹ K ⁻¹)
C	Sutherland's constant (-)
CP	Heat capacity flow rate (W K ⁻¹)
$\sum CP_H$	Summation of the heat capacity flow rate in hot stream in interval i (W K ⁻¹)
$\sum CP_C$	Summation of the heat capacity flow rate in cold stream in interval i (W K ⁻¹)
C _{pj}	Molar specific heat capacity of stream j (J mol ⁻¹ K ⁻¹)
D _i ^{eff}	Effective diffusion coefficient of species i (m ² s ⁻¹)
d _a	Thickness of anode (m)
d _c	Thickness of cathode (m)
E	Equilibrium voltage (V)
E ⁰	Standard potential (V)
E _{act,i}	Activation energy at the anode (i = a) and cathode (i = c) (J mol ⁻¹)
E _{elec}	Activation energy of ions transport (J mol ⁻¹)
$(\sum Ex)_{in}$	Summation of exergy input (W)
$(\sum Ex)_{out}$	Summation of exergy output (W)
Ex _d	Exergy destruction (W)
$\sum Ex_S$	Total exergy transfer by mass (W)
$\sum Ex_Q$	Total exergy transfer by heat (W)
$\sum Ex_w$	Total exergy transfer by work (W)
Ex _Q	Exergy transfer by heat (W)

Ex_w	Exergy transfer by work (W)
$Ex_{s,j}$	Flow exergy of stream j (W)
$ex_{s,j}$	Specific molar flow exergy of stream j ($J mol^{-1}$)
$ex_{ph,j}$	Physical exergy of stream j ($J mol^{-1}$)
$ex_{ch,j}$	Chemical exergy of stream j ($J mol^{-1}$)
$\overline{ex}_{ch,i}$	Standard specific molar chemical exergy of component i at T_0 and P_0 ($J mol^{-1}$)
F	Faraday constant ($96,485 A s mol^{-1}$)
f_i	Fugacity of species i (atm)
f_i°	Fugacity of species i at standard condition (atm)
F_j	Molar flow rate of stream j ($mol s^{-1}$)
G	Gibbs free energy of system (J)
ΔG	Gibbs free energy change ($J mol^{-1}$)
H	Enthalpy of system ($J mol^{-1}$)
ΔH	Enthalpy change over the temperature interval (W)
h_j	Specific molar enthalpy of stream j at T and P ($J mol^{-1}$)
$h_{0,j}$	Specific molar enthalpy of stream j at T_0 and P_0 ($J mol^{-1} K^{-1}$)
I	Electrical current (A)
J	Current density ($A m^{-2}$)
$J_{0,i}$	Exchange current density at the anode ($i = a$) and the cathode ($i = c$) ($A m^{-2}$)
k_i	Pre-exponential factor at the anode ($i = a$) and cathode ($i = c$) ($A m^{-2}$)
k_B	Boltzmann's constant (-)
l_e	Electrolyte thickness (m)
LHV_{H_2}	Lower heating value of H_2 ($J mol^{-1}$)
LHV_{CO}	Lower heating value of CO ($J mol^{-1}$)
LHV_{CH_4}	Lower heating value of CH_4 ($J mol^{-1}$)
M_{H_2O}	Molar weight of steam ($18 g mol^{-1}$)

M_{O_2}	Molar weight of oxygen (32 g mol ⁻¹)
n	Anode porosity (-)
N_{cell}	Number of cells (cell)
\dot{N}_i	Molar flow rate of species i in the product stream (mol s ⁻¹)
$\dot{N}_{i,in}$	Molar flow rate of species i in the feed stream (mol s ⁻¹)
P	Operating pressure (atm)
P_i	Partial pressure of species i (atm)
P_i^{TPB}	Partial pressures at the triple-phase boundary of species i (Pa)
P_{inter}	Intermediate pressure (atm)
P_{in}	Syngas compressor inlet pressure (atm)
P_{out}	Syngas compressor outlet pressure (atm)
Q	Thermal energy input rate of process (W)
Q_r	Energy for all of the reactions in system (W)
Q_E	External heat (W)
Q_{ovp}	Heat of overpotential (W)
Q_{loss}	Energy losses of system (W)
R	Gas constant (8.314 J mol ⁻¹ K ⁻¹)
R_e	Resistance of the electrolyte (m ² S ⁻¹)
r	Mean pore radius (m)
S	Entropy (J mol ⁻¹ K ⁻¹)
ΔS	Entropy change (J mol ⁻¹ K ⁻¹)
S_i	Shift temperature of interval i (K)
S_{i+1}	Shift temperature of interval $i+1$ (K)
s_j	Specific molar entropy of stream j at T and P (J mol ⁻¹ K ⁻¹)
$s_{0,j}$	Specific molar entropy of stream j at T_0 and P_0 (J mol ⁻¹ K ⁻¹)
T	Operating temperature (K)
T^*	Dimensionless temperature (-)
T_0	Reference environment temperature (K)
U_s	Steam utilization factor (-)

V	Cell voltage (V)
W	Electrical power (W)
$x_{i,j}$	Mole fraction of component i in liquid phase, in stream j (-)
y_i	Molar fraction of species i (-)
$y_{i,j}$	Mole fraction of component i in gas phase, in stream j (-)
$z_{i,j}$	Mole fraction of component i in solid phase, in stream j (-)

Greek symbols

v_B	Stoichiometric number of reactants ($v_B > 0$) or products ($v_B < 0$) in the reaction
v_i	Stoichiometric coefficients of component i
$\eta_{act,i}$	Activation overpotentials at the anode (i = a) and cathode (i = c) (V)
η_{ohm}	Ohmic overpotential (V)
$\eta_{conc,i}$	Concentration overpotentials at the anode (i = a) and cathode (i = c) (V)
η_{en}	Energy efficiency of process (%)
η_{ex}	Exergy efficiency of the overall process (%)
$\eta_{ex,k}$	Exergy efficiency of a single unit in the process (%)
α	Charge transfer coefficient (-)
ρ_e	Conductivity of electrolyte ($S\ m^{-1}$)
ρ_0	Pre-exponential factor ($S\ m^{-1}$)
ξ	Anode tortuosity (-)
$\frac{\xi}{n(D_{H_2O-O_2})}$	Reciprocal of the effective molecular diffusion coefficient for an $H_2O - O_2$ binary system
$\frac{\xi}{n(D_{H_2O,k})}$	Reciprocal of the effective Knudsen diffusion coefficient for steam
$\frac{\varepsilon_{H_2O}}{k_B}$	Lennard-Jones Potentials of steam (K)

$\frac{\varepsilon_{O_2}}{k_B}$	Lennard-Jones Potentials of oxygen (K)
$\sigma_{H_2O-O_2}$	Mean characteristic length of species H ₂ O and O ₂ (Å)
σ_{H_2O}	Collision diameter of steam (Å)
σ_{O_2}	Collision diameter of oxygen (Å)
Ω_D	Dimensionless diffusion collision integral (-)
ϕ_i	Fugacity coefficient of species i
μ	Dynamic viscosity of hydrogen (kg m ⁻¹ s ⁻¹)



CHAPTER I

INTRODUCTION

1.1 Background

Nowadays, the world consumption rate of fossil fuels (e.g., oil, coal, and natural gas) extremely increases, especially in developing countries (Gurney, 2018; Gurney, 2019), resulting in high greenhouse gas emissions. To relieve such an environmental problem, the utilize of greenhouse gas (e.g., carbon dioxide and methane) to produce high value-added products is considered an effective way, apart from reducing emitted gases (Arvidsson et al., 2015; Dominguez et al., 2015; Zhang et al., 2015). Among the various products that can be produced from greenhouse gases, a synthesis gas (syngas), a mixture of hydrogen and carbon monoxide is interest because it is an important intermediate that can be used to synthesize various hydrocarbons such as long-chain hydrocarbons, methanol, ethanol, and synthetic diesel.

In general, conventional syngas production processes involve hydrogenation, steam reforming process as well as the gasification process. In addition, a dry methane reforming (DMR) process using CO_2 and CH_4 as reactants can be applied to the syngas production that given a high CO_2 and CH_4 conversion values (Muradov and Smith, 2008). A proton-conducting solid oxide electrolysis cell (H-SOEC) is another promising technology for syngas production using electricity. When water and CO_2 are introduced to the H-SOEC, syngas can be produced via an electrochemical process.

In the proton-conducting solid oxide electrolysis cell, electrochemical reactions proceed by electrical and thermal energies to generate hydrogen and syngas. The electrochemical conversion is of interest in terms of energy efficiency, compared with other CO_2 conversion processes. The higher energy efficiency of the SOEC can be achieved when electrical energy is supplied from renewable sources. Currently, the growth of green electricity generated via renewable energy technologies has motivated research towards chemical industry electrification. From the power-to-chemical concepts of the SOEC process, cheap resources could be converted into base chemicals and fuels. The operation temperature of H-SOEC is in a range of 800-1000 °C (high

temperature) However, H-SOEC still has some limitations regarding low CO₂ conversion, around 65% (Xie et al., 2010) due to without of catalyst used for the reversible water gas shift reaction (RWGS) that is a reaction to consumed CO₂ and produce CO for syngas production. In addition, the occurrence of H₂O from RWGS is usually produced by H₂O cooperate with CO influence low of syngas selectivity obtained from H-SOEC.

One of another promising technology is the dry methane reforming (DMR) that is an oxidation process of CH₄ for syngas production by using CO₂ as an oxidizing agent. It is carried out in a fixed-bed reactor with a heterogeneous catalyst consisting of active metal site, supporter, and the promoter such as NiO/SiO₂, NiO/TiO₂, and NiO/Al₂O₃ (Aramouni et al., 2018). The DMR is of interest in terms of syngas production, which high CO₂ and CH₄ conversions and syngas selectivity can be obtained from this process. The CH₄ conversion of 94% can be obtained when using Ni-based/mixed oxide supported heterogeneous catalysts at 700 °C and CO₂/CH₄ molar ratio of 1 as reported by Tungkamani et al. (2013). Moreover, Hamzehlouia et al. (2018) reported that the CO₂ and CH₄ conversions of 95% and 85% were achieved with the H₂ and CO selectivity of 90% and 85% at the operating temperature of 800 °C and equivalent ratio of reactant (CO₂/CH₄ = 1) using nickel-based alumina supported catalyst. Although DMR is the high conversion and selectivity process, it is an extremely endothermic reaction ($\Delta H_{298K} = 247 \text{ kJ mol}^{-1}$), which needs high heat energy demand to carry out the reaction. Moreover, the syngas product of DMR is obtained at the equivalent ratio (H₂/CO = 1), but sometimes this molar ratio is lower than 1 due to the presence of a reversible water gas shift reaction which consumes H₂ (Lavoie, 2014).

For improvement term, Chen et al. (2018) investigated the DMR in the proton-conducting solid oxide fuel cell reactor (H-SOFC) in which a catalyst layer of DMR is added to the anode of H-SOFC then CO₂ and CH₄ were introduced to the anode side of the SOFC. The DMR occurred at the anode side of the H-SOFC to produce syngas production and hydrogen product was used to generate electricity through H-SOFC. The results showed that the conversion of CO₂ raised higher than 90%. Moreover, the selectivity of syngas was increased due to the use of H₂O that was generated by the side reaction (RWGS), through steam methane reforming (SMR) reaction with CH₄. From

the above concept, it could be adapted to the H-SOEC process in order to improve the low syngas production of this process.

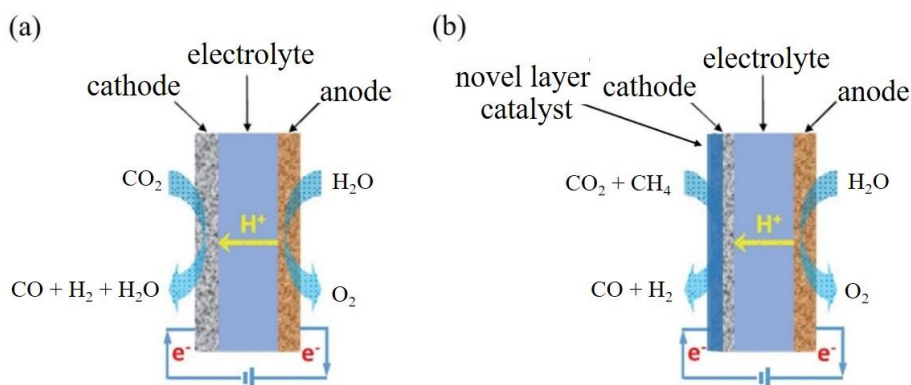


Figure 1.1 The schematics of (a) H-SOEC and (b) H-SOEC combine with a novel layer catalyst of DMR (H-SOEC/DMR) for syngas production.

The H-SOEC coupling with a dry methane reforming process (H-SOEC/DMR) is performed by adding a catalyst layer of DMR to the cathode of H-SOEC and changing the feed from CO_2 to CH_4 and CO_2 mixture on the cathode side (Figure 1.1). The advantage of this process are: (i) high CO_2 and CH_4 conversion, (ii) high syngas selectivity, (iii) energy storage route to store renewable energy (wind or solar) as a power-to-gas process by using CO_2 and CH_4 with heat, (iv) highly energy efficiency process due to using electrical energy (supplied from renewable sources) with heat energy (exhaust heat from exothermic or nuclear plants processes), and (v) environmental friendly because using CO_2 and CH_4 as feeds and without exhaust gas emission (vi) highly H/C ratio in syngas product (H/C ratio ≥ 2), which suitable for methanol and long-chain hydrocarbon synthesis. However, this process is an extremely endothermic process that needs higher energy to sufficient, thus the energy analysis and improvement of the process are necessary to aim to achieve the process that has high in both syngas production and energy efficiency terms.

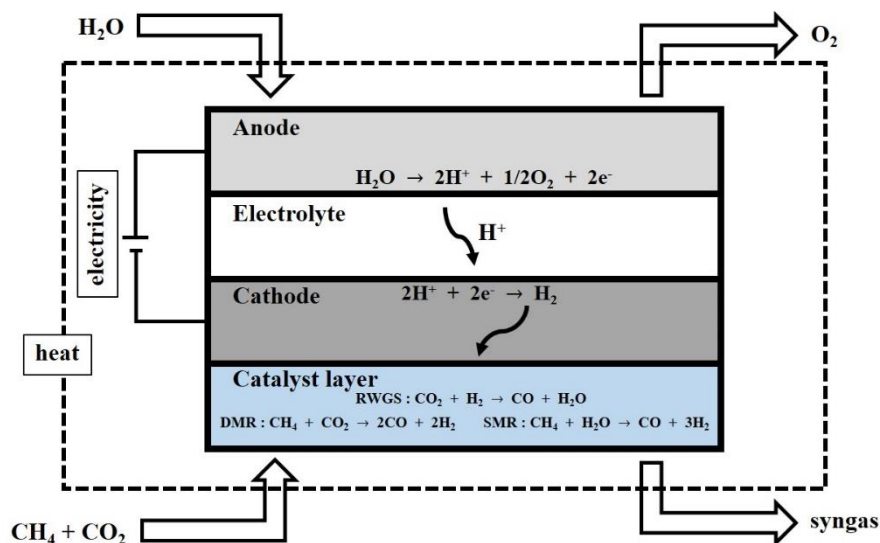


Figure 1.2 The designed reactor of H-SOEC and dry methane reforming layer.

This work aims to design and evaluate the performance of the H-SOEC coupling with a dry methane reforming process (H-SOEC/DMR) in order to receive the process that has high in both syngas production and efficiency terms. The reactor design of this process is illustrated in Figure 1.2. The electrochemical model and flowsheet simulation model are used to evaluate the performance of the process. Energy analysis is also performed to determine the effect of the operating condition on the energy efficiency of the process and the operating condition that given the highest energy efficiency is selected as the optimum condition of the process. Then, to improve the energy efficiency, the heat exchanger network design (HEN) is performed to achieve the maximum heat recovery of the process. Additionally, the exergy analysis of the process is performed to determine the exergy efficiency and exergy destruction that can indicate which part of the process is inefficient, leading to the decision for the modification of the process for improving the efficiency of the process.

1.2 Objective

This study aims to design and evaluate the performance of the H-SOEC coupling with a dry methane reforming process (H-SOEC/DMR) process for syngas production.

1.3 Scopes of work

1.3.1 To develop the electrochemical model of the H-SOEC/DMR process.

1.3.2 To propose the H-SOEC/DMR flowsheet simulation model by using the existing function and unit operation of the Aspen Plus software.

1.3.3 To evaluate the effect of structural parameters of H-SOEC/DMR on performance in cell voltage term that the study conditions consist of (i) thickness of anode, cathode, and electrolyte in the range of 50 to 500 (μm) and support structures; (ii) pore size of 0.3, 0.4, and 0.5 (μm); (iii) porosity of 0.3, 0.4, and 0.5 (-); and (iv) tortuosity of 1.12, 1.14, and 1.16 (-)

1.3.4 To evaluate the effect of operational parameters of H-SOEC/DMR on performance in both cell voltage and syngas production terms. The studied conditions consisted of (i) S/C ratio in the range of 0.5 to 2 (-); (ii) temperature in the range of 1073 to 1273 (K); (iii) pressure in the range of 1 to 5 (atm); (iv) current density in the range of 500 to 2500 (A m^{-2}); and (v) number of cells in the range of 100 to 500 (cell).

1.3.5 To analyze the energy efficiency of H-SOEC/DMR process and to evaluate the effect of key operational parameters on the energy efficiency. The studied conditions consist of (i) temperature; (ii) pressure; (iii) current density; and (iv) number of cells.

1.3.6 To determine the optimal condition of the H-SOEC/DMR process that the highest energy efficiency was obtained.

1.3.7 To perform the heat exchanger network design of the H-SOEC/DMR process.

1.3.8 To analyze the exergy efficiency of the H-SOEC/DMR process and to evaluate the effect of key operational parameters on the exergy efficiency. The studied conditions consist of (i) temperature; (ii) pressure; (iii) current density; and (iv) number of cells.

1.4 Research methodology

For this work, the research methodology consists of several steps as described below:

1.4.1 Study the problems of H-SOEC for syngas production, which given low CO₂ conversion and syngas selectivity.

1.4.2 The H-SOEC process is improved by adding the catalyst layer of DMR into the electrode of H-SOEC (H-SOEC/DMR) and changing feedstock to water, CO₂, and CH₄, as shown in Figure 1.2, to improve the conversion and selectivity of syngas production.

1.4.3 The electrochemical model is developed by using the Fick's model and permeation model, to evaluate process performance in cell voltage term.

1.4.4 The flowsheet model simulation of the H-SOEC/DMR process is performed by using the Aspen Plus software. The reactor modules, which consist of RStoic, RGibbs, and separator, are used to simulate the H-SOEC/DMR process and used to evaluate process performance in terms of syngas production.

1.4.5 The developed electrochemical model is used to analyze the effect of the structural parameters (i.e., pore size, porosity, tortuosity, and thickness of cell) on process performance, then choose the promised value of structural parameters that minimize the cell voltage to use as constant variables for the next step.

1.4.6 The developed model of the H-SOEC/DMR process is used to analyze the effect of operating parameters (i.e., S/C molar ratio, current density, temperature, pressure, and a number of cells) on process performance.

1.4.7 Perform the energy efficiency analysis of the H-SOEC/DMR process. The influence of changes in operational parameters on energy efficiency is investigated.

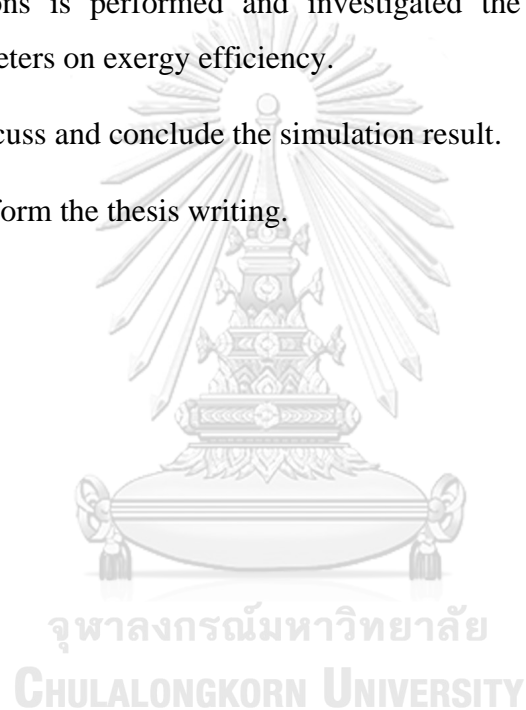
1.4.8 The optimum operating condition is selected based on the highest value of the energy efficiency

1.4.9 Under the optimum conditions of the H-SOEC/DMR process, the heat exchanger network is performed based on the pinch design method.

1.4.10 The exergy efficiency analysis of the H-SOEC/DMR process under the optimum conditions is performed and investigated the influence of changes in operational parameters on exergy efficiency.

1.4.11 Discuss and conclude the simulation result.

1.4.12 Perform the thesis writing.



CHAPTER II

THEORY

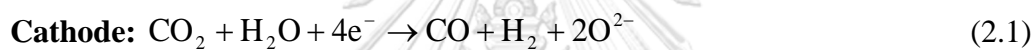
2.1 Proton-conducting solid oxide electrolysis cell (H-SOEC) technology

High-temperature solid oxide electrolysis cell (SOEC) is a technology to produce synthesis gas ($H_2 + CO$) by converting water and carbon dioxide. This technology is carried on by using both electrical energy and thermal energy for electrochemical reactions. When compared with the different type of CO_2 conversion, electrochemical conversions are interesting technology in both energy efficiency and cost terms as described below:

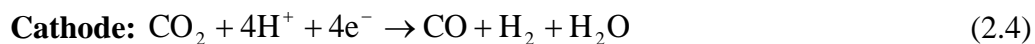
- It can be achieved transportation fuel by CO_2 , water, and renewable energy for hydrocarbon fuel production.
- The process is more accurate and is easier to control by controlling the temperature process and electrode potentials.
- These systems are highly efficient, clean, compact, modular, on-demand, and scalable.
- The process can utilize clean electrical energy sources such as wind, solar, tidal, geothermal, etc., as well as surplus electricity from hydroelectric and nuclear sources (Whipple and Kenis, 2010).
- The integration of the system with exothermic reforming processes can utilize waste heat from reforming reactions to improve energy efficiency.
- This technology is compatibility (environmentally compatible with reduced CO_2 emissions), flexibility (fuel flexible and suitable for integration with various energy sources, especially sustainable energies), capability (can be used for different functions), adaptability (suitable for a variety of applications or different local energy needs), and affordability (competitiveness in cost).

2.1.1 Principle of SOEC

At present, SOEC can be divided into two types, depending on solid electrolyte property that allows oxygen ions (O^{2-}) and proton (H^+) transfer as shown in Figure 2.1. Comparing with the oxygen ion-conducting SOEC (O-SOEC), the proton-conducting SOEC (H-SOEC) has a higher ionic conductivity, especially at intermediate operating temperature (300-700°C). In addition, syngas obtained from O-SOEC has more concentration than H-SOEC, which is often diluted by steam produced from reversible water gas shift reaction (RWGS) ($CO_2 + H_2 = CO + H_2O$). For O-SOEC, both H_2O and CO_2 together flow into SOEC cathode and receive the electrons supplied by the external electricity to associate into H_2 , O^{2-} , and CO on the cathode side, afterward O^{2-} ions permeate through the electrolyte and evolve as O_2 on the anode side as shown below.



For H-SOEC, water that is fed into the SOEC becomes steam due to the high-temperature operation and flows through the anode side. The products that occur at the anode side is O_2 , H^+ , and electrons, and then H^+ permeates through the electrolyte and accepts the electrons into H_2 at the triple-phase boundary on the cathode side, afterward H_2 reacts with CO_2 that is fed into the cathode by RWGS reaction converts into CO and H_2O as shown below.



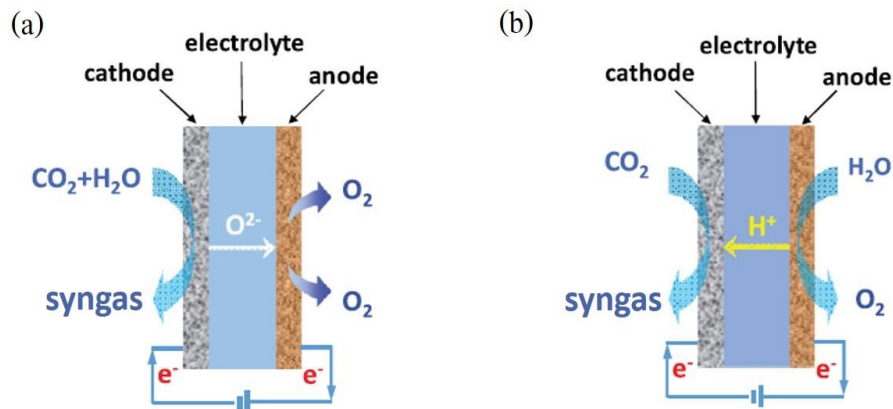


Figure 2.1 SOEC schematics for $\text{CO}_2/\text{H}_2\text{O}$ electrolysis based on (a) oxygen ion conducting electrolyte and (b) proton conducting electrolyte (Xiaomin et al., 2017).

The material and microstructure of SOEC play an important role to achieve high electronic efficiency. The porosity, microstructure, and active area of cell materials should be considered. It is generally recognized that electronic conduction (EC), ionic conduction (IC), and catalytic activation are the three essential functionalities for SOEC electrodes. The EC and IC can also be provided by mixing electronic and ionic conductor as materials such as metal, fluoride, perovskites, double perovskites, and Ruddlesden-Popper (RP). Porous fuel electrode is used as active sites to provide reactions for the decomposition of H_2O and CO_2 . The nickel-Yttria-stabilized zirconia (Ni-YSZ) as known as cermet is widely used as a fuel electrode due to its reasonable electrode catalytic activity, excellent chemical stability, suitable thermal expansion coefficient, and low cost. The properties of material of SOEC consist of: (i) the electrolyte must be chemically stable and can bring ions well, but must not conduct electricity well because both this value will have a reversal of each other, (ii) the electrolyte must be wide enough to prevent the recombination of hydrogen and oxygen, but must not be too wide in order to minimize an ohmic overpotential, (iii) both electrodes must have the appropriate porosity and pore size, (iv) the materials used to make both the electrodes and the electrolyte should have similar thermal expansion coefficient, in order to prevent the occurrence of material failure of the electrolyte due to the high mechanical stress due to the difference in the thermal expansion coefficient and (v) low cost.

The high-temperature electrolysis reductions of CO₂ and H₂O are both endothermic with their proportional electrochemical reactions. As the thermodynamic parameters (i.e., the enthalpy change (ΔH), the Gibbs free energy change (ΔG), and the entropy change (ΔS)) are a function of temperature. The parameter's value of reactions at 298.15 K can be calculated as Eqs. (2.7) - (2.9) (Wang et al., 2015).

$$\Delta H(298.15\text{K}) = \sum_B v_B \Delta_f H_B(298.15\text{K}) \quad (2.7)$$

$$\Delta S(298.15\text{K}) = \sum_B v_B S_B(298.15\text{K}) \quad (2.8)$$

$$\Delta G = \Delta H - T\Delta S \quad (2.9)$$

The thermodynamic parameters of reactions at various temperatures can be calculated according to Eqs. (2.9) - (2.12) (Wang et al., 2015).

$$\Delta H(T) = \Delta H(298.15\text{K}) + \int_{298.15\text{K}}^T \Delta C_p dT \quad (2.10)$$

$$\Delta S(T) = \Delta S(298.15\text{K}) + \int_{298.15\text{K}}^T \Delta C_p dT \quad (2.11)$$

$$\Delta C_p = \sum_B v_B C_p(B) \quad (2.12)$$

Both ΔH and ΔG are related to cell voltage as shown in the relationship below (Eqs. (2.13) and (2.14)) (Wang et al., 2015).

$$E^* = -\frac{\Delta G}{nF} \quad (2.13)$$

$$E^n = -\frac{\Delta H}{nF} \quad (2.14)$$

where ΔH is the enthalpy change (kJ mol⁻¹), B is one of the reactants or products in the reaction, v_B is the stoichiometric number of reactants ($v_B > 0$) or products ($v_B < 0$) in the reaction, $\Delta_f H_B$ is the enthalpy of formation of B, S is the entropy (kJ mol⁻¹ K⁻¹), ΔS is the entropy change (kJ mol⁻¹ K⁻¹), T is the electrolysis temperature (K), ΔG is

the Gibbs free energy change (kJ mol^{-1}), C_p is the heat capacity ($\text{J mol}^{-1} \text{K}^{-1}$), ΔC_p is the heat capacity change ($\text{J mol}^{-1} \text{K}^{-1}$), E^* is the Nernst potential (equilibrium potential) (V), E^n is the thermo-neutral potential (V), n is the number of electrons involved per reaction for the electrolysis reaction (n is equal to 2 for $\text{CO}_2/\text{H}_2\text{O}$ electrolysis), and F is the Faraday constant ($96,485 \text{ A s mol}^{-1}$).

Figure 2.2 illustrates the energy demands of the electrochemical reactions. It is well known that enthalpy is made up of entropy and a Gibbs free energy terms as shown in Eq. (2.9). As indicates in this figure, ΔH , ΔG , and $T\Delta S$ represent the total energy demand, electrical energy demand, and heat energy demand, respectively. With increasing temperature, the total energy demand is almost invariant, but the decreasing electrical energy demand and the increasing heat energy demand are shown for reactions due to positive entropy change ($\Delta S > 0$). The decrease of electrical energy demand is almost equal to the increase in heat energy demand with increasing temperature. The energy efficiency of the process can be improved by using industrial waste heat or electricity from renewable energy.

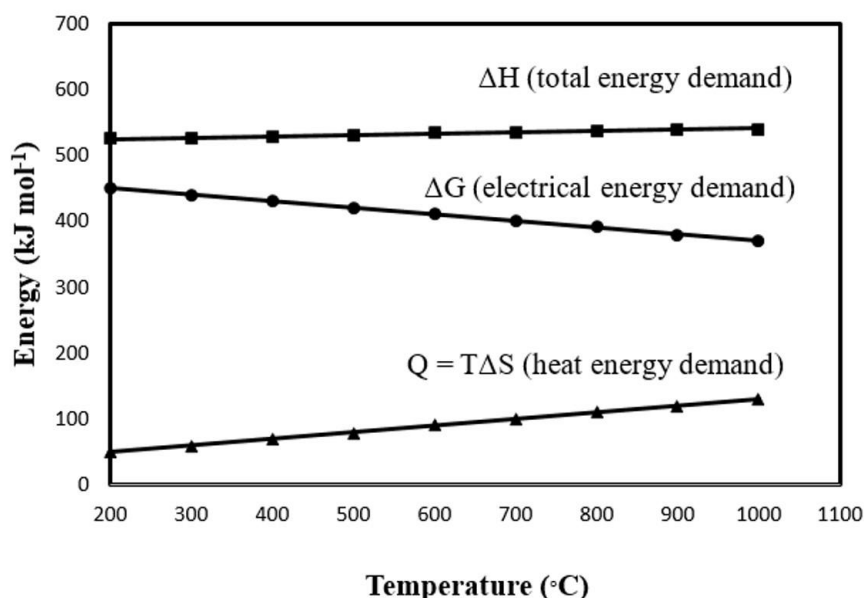


Figure 2.2 Relationships between thermodynamic parameters of electrolysis reaction (Wang et al., 2015).

2.1.2 Configuration of SOEC

In general, SOEC consists of stacking multiple layers in order to achieve syngas production efficiency. When focus at a single unit, the smallest unit of SOEC can be divided into 2 configurations such as (1) tubular and (2) planar as demonstrates in Figure 2.3. The tubular type provides better mechanical strength and facilitates sealing values than planar configuration, while the planar provides better syngas production efficiency due to the better dispersion ability of the gas in planar form and their much shorter current collection paths and significantly higher volumetric density.

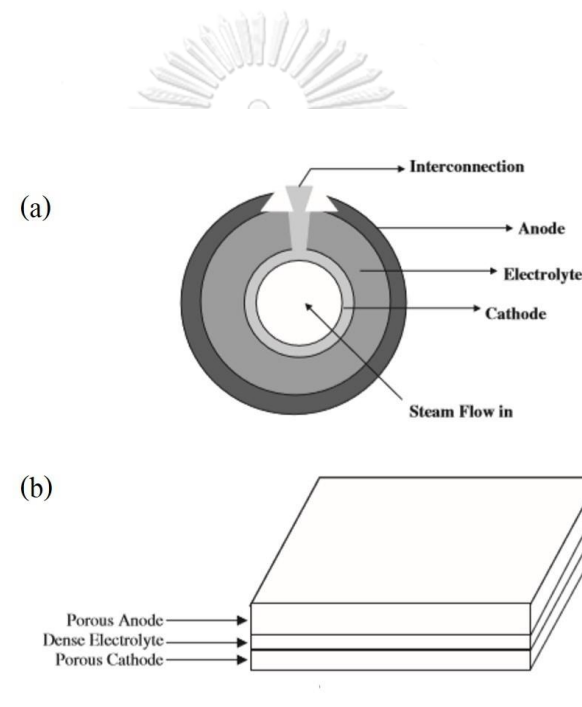


Figure 2.3 SOEC configurations: (a) Tubular and (b) Planar (Ni et al., 2008b).

2.1.3 SOEC stack design

In order to improve the product output of a single cell SOEC system, the cell active area much be enlarged. An increasing of the active area of single cell is restriction. Firstly, it is hard to control the temperature across a large cell area. Secondary, it is challenging to manufacture large and low-cost ceramic films. In order

to treat these issues, a stack consisting of multiple cells is necessary, the structure of the SOECs stack system both tubular and planar configurations are shown in Figure 2.4. In addition, interconnects must be added in a stack, in order to provide adequate electrical connections between the oxygen electrode of one single cell to the fuel electrode of the adjacent one without gas permeation.

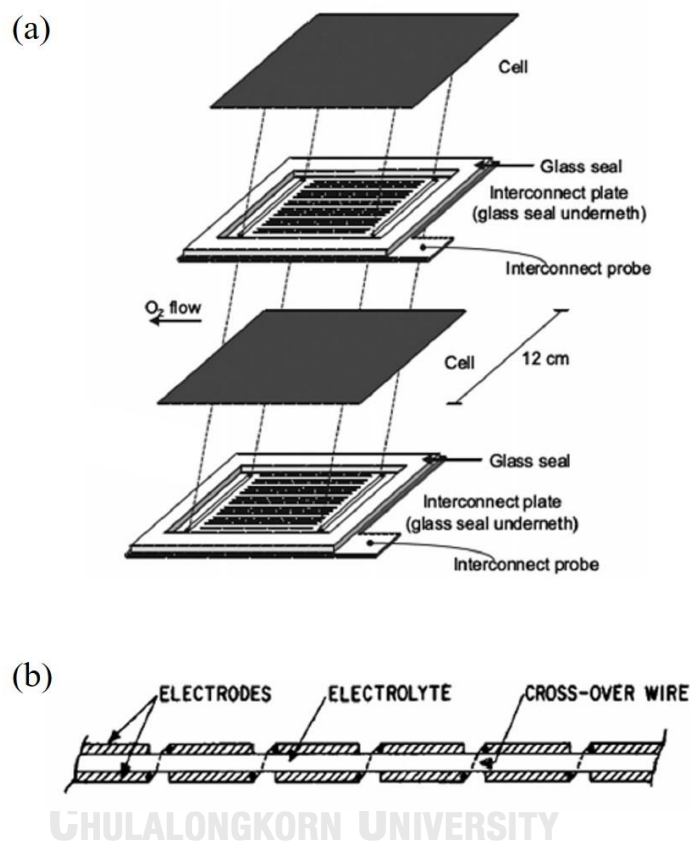
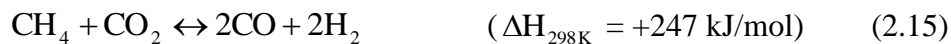


Figure 2.4 Schematic diagram of the (a) planar (Ebbesen et al., 2011) and (b) tubular (Spacil and Tedmon, 1969) SOECs stacking systems.

2.2 Dry methane reforming technology

In current, the production of syngas by the methane oxidation process used many oxidizing agents such as oxygen (partial oxidation of methane (POX) and auto-thermal reforming (ATR)) or water (steam methane reforming (SMR)). Carbon dioxide is considered as an oxidizing agent via a reaction called dry methane reforming (DMR)

(Eq. 2.15). This equation involves the most oxidized form of carbon (CO₂) that interacts with the most reduced form (CH₄) (Wang and Lu, 1996).



Thermodynamics for the DMR reaction is not as popular as the ATR, POX, and SMR reactions. However, according to DMR (Eq. 2.15), consumption of one mole of CO₂ per mole of CH₄ could reduce the carbon impact, which could lead to the consumption of natural gas that is environmentally friendly. The thermodynamic limitation is a big challenge that would rely simply on heat to convert the two molecules with high conversion values. Moreover, DMR also requires a steady and pure carbon dioxide source which may not available in all industrial processes. The used of catalytic systems could lead to the energy consumption reduction of the process which would promote the dry methane reforming to get closer to a conventional process.

2.2.1 Principle of DMR

The dry methane reforming is a chemical process that involves the conversion of CO₂ and CH₄, which identified as the most abundant greenhouse gases in the world to syngas product with an H₂/CO molar ratio of 1. As a result, this process has the performance to relieve the environmental challenge. Moreover, the low H₂/CO molar ratio of syngas products can be adjusted by integrating with another process to achieve a higher molar ratio (H₂/CO > 1) that favorable for the long-chain hydrocarbon production through Fischer-Tropsch synthesis process and methanol through the methanol synthesis process.

The DMR is an extremely endothermic process, which needs a high-temperature range to operation. The operating temperature of DMR usually in the range of 900-1273 K, in order to obtain the high conversion value. In addition, this reaction is favored at low pressures (atmospheric pressure). Moreover, kindly be noted that a CO₂/CH₄ molar ratio higher than the stoichiometric of 1 can also lead to high syngas produced but it reduces an H₂/CO molar ratio of syngas product. The advantage effects of high operating temperatures, low operating pressures and high CO₂/CH₄ molar ratios

of feed on the CO₂ and CH₄ conversion values were investigated and reported in many researches. Although the DMR is considered as an environmental performance process, it is not considered as an industrial favor process. The extremely high endothermic reaction coupling with high carbon composition can also lead to the catalyst deactivation. Moreover, the high reaction time and the pure and steady CO₂ source requirement, result in the DMR is an unappropriated process that needs further development. The heat integration of exothermic with DMR processes is one of an effective way that can improve the DMR energy efficiency.

2.2.2 Thermodynamics of DMR

The dry methane reforming is the high extremely endothermic reaction, compared to ATR and SMR. This can be reminded of the fact that CO₂, the oxidizing agent used in DMR, is the most stable compared to steam and O₂, which oxidizing agents used in SMR and ATR, respectively. Although DMR is consisted by the reaction between CO₂ and CH₄ (Eq. 2.15), several side reactions can also occur during the operation. Table 2.1 summarizes these reactions occur from DMR, equilibrium constants as a function of temperature and enthalpy of reactions. The equilibrium composition of the reaction system was analyzed based on the minimize Gibbs free energy method.

According to Table 2.1, the reversible water gas shift, RWGS (Eq. 2.16), which is the reaction that leads H₂/CO ratio less than unity, is dependent on the equilibrium at an operating temperature range and is usually present during DMR. On the other hand, the RWGS reactions will not occur at temperatures higher than 1093 K. Finally, due to their exothermic nature and negative ln(K) values, Eqs. 2.17 and 2.18 have the possibility of occurring at temperatures lower than 800 K For the syngas production process, it should be operated at high temperature to prevent the presence of Eqs. 2.17 and 2.18.

Table 2.1 Possible gas-phase reactions in the dry methane reforming process (Nikoo and Amin, 2011; Wang and Lu, 1996).

Eqs NO.	Reactions	ΔH_{298K} (kJ mol ⁻¹)	L_n (K _{eq}) at 573 K	L_n (K _{eq}) at 1373 K
2.15	$\text{CH}_4 + \text{CO}_2 \leftrightarrow 2\text{CO} + 2\text{H}_2$	247	-20	13
2.16	$\text{CO}_2 + \text{H}_2 \leftrightarrow \text{CO} + \text{H}_2\text{O}$	41	-5	2
2.17	$\text{CO}_2 + 4\text{H}_2 \leftrightarrow \text{CH}_4 + 2\text{H}_2\text{O}$	-165	14	-10
2.18	$\text{CO} + 3\text{H}_2 \leftrightarrow \text{CH}_4 + \text{H}_2\text{O}$	-206.2	14	-11

2.3 Electrochemical model

The electrochemical model explains the relationship between the current density and cell voltage that depend on the operation parameters (e.g., current density, temperature, and pressure) and structural parameters (e.g., pore size, porosity, and thickness of cell). The aim of this study is to analyze the effect of parameters on process performance by using an electrochemical model that calculates under isothermal conditions. Although the model seems quite simplistic, it can accurately predict the effect of parameters on the cell performance and advantage to use for design and evaluate the process.

จุฬาลงกรณ์มหาวิทยาลัย
CHULALONGKORN UNIVERSITY

2.3.1 Modelling assumptions

The electrochemical model is calculated under the main assumptions that are described as below:

1. Steady state calculation
2. One dimension calculation
3. All of the gases follow ideal gas behavior
4. No heat loss and pressure drop
5. The exchange current density does not depend on electrolyte materials

2.3.2 The voltage of H-SOEC

The cell voltage or cell potential of H-SOEC is depended on both operational and structural parameters due to the electrochemical model that uses to calculate cell voltage is included both equilibrium voltage and overpotential terms, which are functions of condition parameters. The overpotential can be called as voltage losses, cell polarizations or irreversible losses, it mainly consists of activation, ohmic, and concentration overpotentials at anode and cathode sides. Therefore, the cell voltage of H-SOEC can be calculated by Eq. 2.19 (Stempien et al., 2013b).

$$V = E + \eta_{act,a} + \eta_{act,c} + \eta_{ohm} + \eta_{conc,a} + \eta_{conc,c} \quad (2.19)$$

where V is the cell voltage (V), E is the equilibrium voltage (V), $\eta_{act,i}$ is the activation overpotentials at the anode ($i = a$) and cathode ($i = c$) (V), η_{ohm} is the ohmic overpotential (V), and $\eta_{conc,i}$ is the concentration overpotentials at the anode ($i = a$) and cathode ($i = c$) (V).

Equilibrium voltage

For the equilibrium voltage or open circuit voltage or electrochemical potential, the electrochemical potential is the minimum potential required to split steam, or in SOFC mode as the maximum electromotive force obtained from converting fuel gases. For the control volume operating at steady state, it can be calculated by considering the minimum work (W_{min}) concept of thermodynamic, which represent minimum work required for the electrochemical reaction, the energy balance can be written as below (Stempien et al., 2013b).

$$0 = H_i - H_0 + T(S_0 - S_i) - W_{min} \quad (2.20)$$

The concept of minimum work the assumption of reversible operation is necessary that for the reversible system requires minimum work input to operate. The minimum work can be definition by using the Gibbs free energy change (ΔG) as shown in Eq. 2.21. In addition, from the basic electrochemistry relation, the Gibbs free energy change also relates to equilibrium voltage that can be written as Eq. 2.22 (Stempien et al., 2013b).

$$W_{\min} = -\Delta G \quad (2.21)$$

$$-\Delta G = zFE \quad (2.22)$$

where z is the number of the electron for electrochemical reaction (For electrolysis, z is 2 electrons) and F is the Faraday constant ($96,487 \text{ C mol}^{-1}$).

The Gibbs free energy change for ideal gas mixtures assumption can be calculated using Eq. 2.23, which it can be express in partial pressure terms for the gaseous case (Stempien et al., 2013b).

$$\Delta G = \Delta G^0 + RT \ln \left(\frac{\prod P_{\text{products}}^{v_i}}{\prod P_{\text{reacts}}^{v_i}} \right) \quad (2.23)$$

where ΔG^0 is the standard Gibbs free energy, R is the gas constant ($8.314 \text{ J mol}^{-1} \text{ K}^{-1}$), T is the reaction temperature (K), P_i is the partial pressure of component i , and v_i is the stoichiometric coefficient of component i .

From the relationship between the Gibbs free energy change and equilibrium voltage, to calculate equilibrium voltage can be using Eqs. 2.24 and 2.25 that equilibrium voltage depends on temperature and partial pressure of components.

$$E = -\frac{\Delta G^0}{zF} - \frac{RT}{zF} \ln \left(\frac{\prod P_{\text{products}}^{v_i}}{\prod P_{\text{reacts}}^{v_i}} \right) \quad (2.24)$$

$$E = E^0 + \frac{RT}{zF} \ln \left(\frac{\prod P_{\text{products}}^{v_i}}{\prod P_{\text{reacts}}^{v_i}} \right) \quad (2.25)$$

where E^0 is the standard potential (V)

From the steam electrolysis reaction (Eq. 2.26), the Eq. 2.25 can be rearranged to Eq. 2.27 that called Nernst equation. The partial pressure of reactant is steam and the partial pressure of products is hydrogen and oxygen. In addition, the number of electrons transfer of electrolysis reaction (z) is two. This equation is used to calculate the electrical energy demand of steam electrolysis reaction. The standard potential, which calculated by thermochemical ($\Delta G/(2F)$) can be calculated by using Eq. 2.28. At 600 K and 1200 K, the values of standard potential are 1.109017 V and 0.940172 V, respectively (reported by NIST-JANAF thermochemical tables). Assuming linear variation of standard potential between 600 K and 1200 K, the linear equation was received, as reported by (Ni, 2012; Ni et al., 2007a). In addition, the CO_2 was not involved in the electrochemical reaction. It is assumed that the CO_2 was converted through the RWGS reaction (Namwong et al., 2016).



$$E = E^0 + \frac{RT}{2F} \ln \left(\frac{P_{\text{H}_2} P_{\text{O}_2}^{1/2}}{P_{\text{H}_2\text{O}}} \right) \quad (2.27)$$

$$E^0 = 1.253 - 0.00024516(T) \quad (2.28)$$

where $P_{\text{H}_2\text{O}}$, P_{H_2} , and P_{O_2} are the partial pressure of steam, hydrogen, and oxygen (atm), respectively.

Activation overpotential

The activation overpotential is the energy loss due to the chemical kinetics of the electrochemical reaction, which depend on two phenomena on both electrodes. The first is chemical (i.e., the chemical equilibrium state of ions at the triple-phase boundary). The second is electrical (i.e., transfer of charged particles through the interface by ions influent overcoming of the electric field). So, the free energy of activation has two complements consist of the chemical energy of activation and the electrical contribution. The activation overpotentials on both electrodes occur when operating at low current density follow the relationship as shown in Figure 2.5. This overpotential can calculate by using the Butler-Volmer equation (Eq. 2.29) (Guan et al., 2006; Stempien et al., 2013b).

$$J = J_{0,i} \left[\exp\left(\frac{\alpha z F \eta_{\text{act},i}}{RT}\right) - \exp\left(-\frac{(1-\alpha) z F \eta_{\text{act},i}}{RT}\right) \right] \quad (2.29)$$

where J is the current density (A m^{-2}), $J_{0,i}$ is the exchange current density at the anode ($i = a$) and the cathode ($i = c$) (A m^{-2}), and α is the charge transfer coefficient (-).

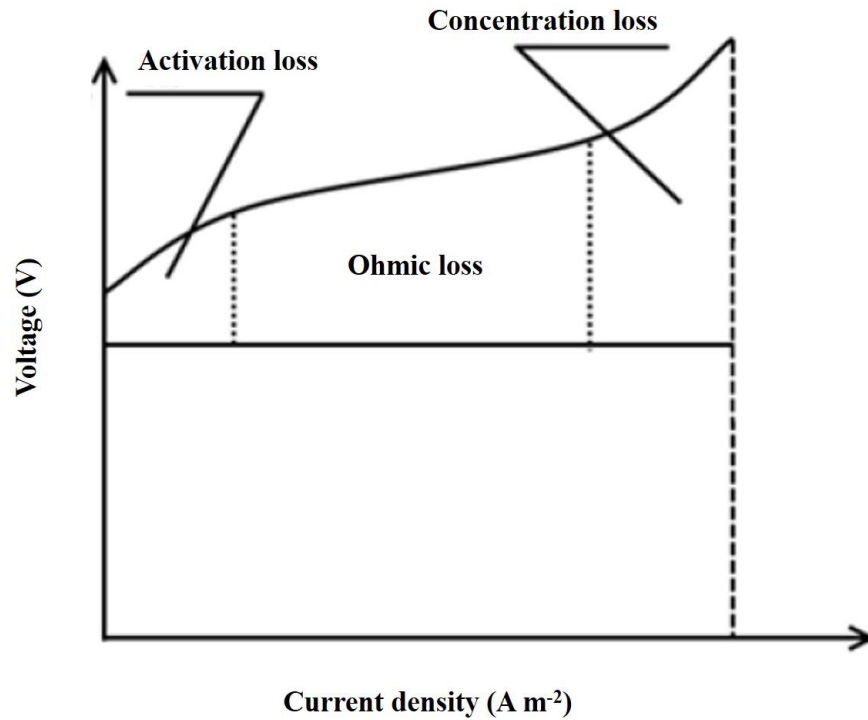


Figure 2.5 The effect of overpotentials on the cell voltage due to the increase of current density (Stempien et al., 2013b).

The charge transfer coefficient is usually assumed to be 0.5. In order to simplify, the equation can be derived into natural logarithm form and called as Tafel equation, which good approximation of Butler-Volmer, then the equation is derived into sin hyperbolic form as Eq. 2.30. and Eq. 2.31. In addition, the exchange current density can be calculated using Eq. 2.32, which is linked to the kinetics of the reaction of the electrode. It has been similar to the Arrhenius exponential equation that depends on temperature.

$$\eta_{\text{act},i} = \frac{RT}{F} \sinh^{-1} \left(\frac{J}{2J_{0,i}} \right) \quad (2.30)$$

$$\eta_{\text{act},i} = \frac{RT}{F} \ln \left[\frac{J}{2J_{0,i}} + \sqrt{\left(\frac{J}{2J_{0,i}} \right)^2 + 1} \right] \quad (2.31)$$

$$J_{0,i} = k_i \exp\left(-\frac{E_{\text{act},i}}{RT}\right) \quad (2.32)$$

where k_i is the pre-exponential factor at the anode ($i = a$) and cathode ($i = c$) (A m^{-2}) and $E_{\text{act},i}$ is the activation energy at the anode ($i = a$) and cathode ($i = c$) (J mol^{-1}).

Ohmic overpotential

The ohmic overpotential is the loss due to the ionic, electronic, and contact resistance of the cell, which can be described by Ohm's law as Eq. 2.33. Commonly, only ionic resistance of electrolyte layer is considered, other resistances are assumed to be negligible due to lower of magnitude; therefore, the equation can be derived into Eq. 2.34 (Menon et al., 2014).

$$\eta_{\text{ohm}} = J \cdot (R_e + R_i + R_a + R_c) \quad (2.33)$$

$$\eta_{\text{ohm}} = J \cdot R_e = J \cdot \frac{l_e}{\rho_e} \quad (2.34)$$

where R_e , R_i , R_a , and R_c are the resistances of the electrolyte, interface, anode, and cathode, respectively ($\text{m}^2 \text{ S}^{-1}$), l_e is the electrolyte thickness (m), and ρ_e is the conductivity of electrolyte (S m^{-1}).

The conductivity of electrolyte can be calculated by Eq. 2.35.

$$\rho_e = \rho_0 \cdot T^{-1} \cdot \exp\left(-\frac{E_{\text{elec}}}{RT}\right) \quad (2.35)$$

where ρ_0 is the pre-exponential factor (S m^{-1}) and E_{elec} is the activation energy of ions transport (J mol^{-1}).

Concentration overpotential

The concentration overpotential is caused due to the mass transfer between the electrode and electrolyte, which especially at a high current density (see Figure 2.5). For this overpotential, it follows the principle of the mass transfer limitations of the porous electrodes. In case that no current is passing through the cell, the concentration of gas species in the electrodes is the same as the free steam concentration. However, when the current starts to pass through the electrodes, the concentration of gas species at the interface decrease influent voltage drop is present. In order to calculate concentration overpotential, the Nernst equation is applying with the concentration of gas species at the interface and can write as Eqs. 2.36 and 2.37 (Namwong et al., 2016; Stempien et al., 2013b).

$$\eta_{\text{conc,a}} = \frac{RT}{2F} \ln \left[\left(\frac{P_{\text{H}_2\text{O}}}{P_{\text{H}_2\text{O}}^{\text{TPB}}} \right) \left(\frac{P_{\text{O}_2}^{\text{TPB}}}{P_{\text{O}_2}} \right)^{1/2} \right] \quad (2.36)$$

$$\eta_{\text{conc,c}} = \frac{RT}{2F} \ln \left[\left(\frac{P_{\text{H}_2}^{\text{TPB}}}{P_{\text{H}_2}} \right) \right] \quad (2.37)$$

where $P_{\text{H}_2\text{O}}^{\text{TPB}}$, $P_{\text{O}_2}^{\text{TPB}}$, and $P_{\text{H}_2}^{\text{TPB}}$ are the partial pressures (Pa) of steam, oxygen, and hydrogen, respectively, at the triple-phase boundary.

At the anode side, only steam and oxygen are gas species that present at this side. The partial pressures at the triple-phase boundary can be calculated by using the diffusion models such as Fick's model (FM), Stefan-Maxwell's model (SMM), and Dusty Gas Model (DGM). FM is selected to be used because it can describe gas transport effectively and non-complicate model. For the Fick's model, the diffusion process, which is driven by concentration gradient or partial pressure gradient, can be determined by Eq. 2.38. At the anode-electrolyte interface, the diffusion rate of steam towards the interface is equal to steam consumption rate under steady state condition, under the assumption that steam consumption is governed by the current density; therefore, the mass transfer rate can be written as Eq. 2.39 (Ni et al., 2006).

$$N_i = -\frac{D_i^{\text{eff}}}{RT} \frac{\partial(y_i P)}{\partial x} = -\frac{D_i^{\text{eff}}}{RT} \frac{\partial(P_i)}{\partial x}, \quad i = 1, 2, \dots \quad (2.38)$$

$$N_{\text{H}_2\text{O}} = \frac{J}{2F} \quad (2.39)$$

จุฬาลงกรณ์มหาวิทยาลัย
CHULALONGKORN UNIVERSITY

where N_i and $N_{\text{H}_2\text{O}}$ are the rates of mass transfer of species i and steam, P is the operating pressure (Pa), x is the depth measured from the electrode surface (m), P_i , y_i , and D_i^{eff} are the partial pressure, molar fraction, and effective diffusion coefficient of species i , respectively.

To obtain the partial pressure of steam at the anode-electrolyte interface, the boundary condition method is performed, thus the equation that derived as Eq. 2.40.

$$P_{\text{H}_2\text{O}}^{\text{TPB}} = P_{\text{H}_2\text{O}} - \frac{RT}{D_{\text{H}_2\text{O}}^{\text{eff}}} \frac{J}{2F} d_a \quad (2.40)$$

where $D_{\text{H}_2\text{O}}^{\text{eff}}$ is the effective diffusion coefficient of steam ($\text{m}^2 \text{s}^{-1}$) and d_a is the thickness of anode (m).

The partial pressure of oxygen at the anode-electrolyte interface can be calculated using the Dalton's law of anode total pressure (Eq. 2.41), which can be derived into Eq. 2.42 (Dale et al., 2008).

$$P_{\text{O}_2} = P - P_{\text{H}_2\text{O}} \quad (2.41)$$

$$\begin{aligned} P_{\text{O}_2}^{\text{TPB}} &= P - P_{\text{H}_2\text{O}}^{\text{TPB}} \\ &= P_{\text{O}_2} + \frac{RT}{D_{\text{H}_2\text{O}}^{\text{eff}}} \frac{J}{2F} d_a \end{aligned} \quad (2.42)$$

จุฬาลงกรณ์มหาวิทยาลัย
CHULALONGKORN UNIVERSITY

The effective diffusion coefficient of steam ($D_{\text{H}_2\text{O}}^{\text{eff}}$) can be expressed by combining the Molecular diffusion and the Knudsen diffusion mechanisms using the Bosanquet formula as Eq. 2.43 (Hernández et al., 2004; Veldsink et al., 1995).

$$\frac{1}{D_{\text{H}_2\text{O}}^{\text{eff}}} = \frac{\xi}{n} \left(\frac{1}{D_{\text{H}_2\text{O}-\text{O}_2}} + \frac{1}{D_{\text{H}_2\text{O},k}} \right) \quad (2.43)$$

where ξ is the anode tortuosity (-), n is the anode porosity (-), $\frac{\xi}{n(D_{\text{H}_2\text{O}-\text{O}_2})}$ is the reciprocal of the effective molecular diffusion coefficient for an $\text{H}_2\text{O} - \text{O}_2$ binary system, and $\frac{\xi}{n(D_{\text{H}_2\text{O},k})}$ is the reciprocal of the effective Knudsen diffusion coefficient for steam.

For the Knudsen diffusion, it is diffusion occurs when the scale length of system (pore size) is comparable to or smaller than mean free path of molecules that make gas molecules frequently collide with the walls of the pores. The transport of molecules can be modeled using the kinetic theory express by Knudsen's equation (Eq. 2.44).

$$D_{\text{H}_2\text{O},k} = \frac{2}{3} r \sqrt{\frac{8RT}{\pi M_{\text{H}_2\text{O}}}} \quad (2.44)$$

where r is the mean pore radius (m) and $M_{\text{H}_2\text{O}}$ is the steam molar weight (18 g mol^{-1}).

The molecular binary diffusion coefficient can be obtained from the Chapman-Enskog theory of ideal gas (Eq. 2.45).

$$D_{\text{H}_2\text{O}-\text{O}_2} = \frac{(2.66 \times 10^{-7}) T^{3/2}}{P \left[2 \left(\frac{1}{M_{\text{H}_2\text{O}}} + \frac{1}{M_{\text{O}_2}} \right)^{-1} \right]^{1/2} \sigma_{\text{H}_2\text{O}-\text{O}_2}^2 \Omega_D} \quad (2.45)$$

where M_{O_2} is the molar weight of oxygen (32 g mol^{-1}), $\sigma_{\text{H}_2\text{O}-\text{O}_2}$ is the mean characteristic length of species H_2O and O_2 (\AA), and Ω_D is the dimensionless diffusion collision integral.

The analytical values of dimensionless diffusion collision integral and mean characteristic length of species H₂O and O₂ can be calculated by Eqs. 2.46 – 2.49.

$$\sigma_{\text{H}_2\text{O}-\text{O}_2} = \frac{\sigma_{\text{H}_2\text{O}} + \sigma_{\text{O}_2}}{2} \quad (2.46)$$

$$\Omega_D = \frac{1.06036}{(T^*)^{0.15610}} + \frac{0.19300}{\exp(0.47635T^*)} + \frac{1.03587}{\exp(1.52996T^*)} + \frac{1.76474}{\exp(3.8941T^*)} \quad (2.47)$$

$$T^* = \frac{k_B T}{\varepsilon_{\text{H}_2\text{O}-\text{O}_2}} \quad (2.48)$$

$$\frac{\varepsilon_{\text{H}_2\text{O}-\text{O}_2}}{k_B} = \sqrt{\frac{\varepsilon_{\text{H}_2\text{O}}}{k_B} \cdot \frac{\varepsilon_{\text{O}_2}}{k_B}} \quad (2.49)$$

where $\sigma_{\text{H}_2\text{O}}$ and σ_{O_2} are the collision diameter of steam and oxygen (Å), T^* is the dimensionless temperature (-), k_B is the Boltzmann's constant, and $\frac{\varepsilon_{\text{H}_2\text{O}}}{k_B}$ and $\frac{\varepsilon_{\text{O}_2}}{k_B}$ are the Lennard-Jones Potentials of steam and oxygen (K) (C. Reid et al., 1959).

For the cathode side, H₂ is just one type of gas that is located at this electrode. $P_{\text{H}_2}^{\text{TPB}}$ can be calculated by using Darcy's model (Eq. 2.50), which also governed by the current density (Eq. 2.51), then the boundary method is performed so the equation is derived as Eq. 2.52.

$$N_{H_2} = -\frac{P_{H_2} B_g}{RT\mu} \nabla P_{H_2} \quad (2.50)$$

$$N_{H_2} = -\frac{J}{2F} \quad (2.51)$$

$$P_{H_2}^{TPB} = \sqrt{(P_{H_2})^2 + \frac{JRT\mu}{FB_g} d_c} \quad (2.52)$$

where N_{H_2} is the mass transfer of hydrogen, μ is the dynamic viscosity of hydrogen ($\text{kg m}^{-1} \text{s}^{-1}$), d_c is the thickness of cathode (m), and B_g is the flow permeability (m^2).

The flow permeability can be determined by the Kozeny-Carman relationship as Eq. 2.53 (Zhu et al., 2005).

$$B_g = \frac{n^3}{72\xi(1-n)^2} (2r)^2 \quad (2.53)$$

จุฬาลงกรณ์มหาวิทยาลัย
CHULALONGKORN UNIVERSITY

For the dynamic viscosity, Sutherland's model is appropriate due to the accuracy at the intermediate temperature that is the operating temperature of H-SOEC; therefore, the dynamic viscosity can be calculated by Eqs. 2.54 – 2.56 (Crane, 1988).

$$\mu = \mu_0 \left(\frac{a}{b} \right) \left(\frac{T/0.555}{T_0} \right)^{3/2} \quad (2.54)$$

$$a = 0.6T_0 + C \quad (2.55)$$

$$b = T + C \quad (2.56)$$

where μ_0 is the reference dynamic viscosity at T_0 (cP), T_0 is the reference temperature ($^{\circ}\text{R}$), and C is the Sutherland's constant (-).

The electrical current, a theoretical current based on a steam utilization factor (U_s), can be calculated by Eq. 2.57. It is noted that the steam utilization factor is defined as a ratio of the molar flow rate of steam used to produce hydrogen to that of the steam feed or conversion of steam to produce hydrogen. The current density can be calculated by electrical current and cell area from Eq. 2.58. Moreover, the electrical power required for the operation can be calculated according to Eq. 2.59.

$$\dot{N}_{\text{H}_2\text{O},\text{in}} = \frac{JAN_{\text{cell}}}{2FU_s} \quad (2.57)$$

$$I = JA \quad (2.58)$$

$$W = IVN_{\text{cell}} \quad (2.59)$$

where I is the electrical current (A), U_s is the steam utilization factor (-), $\dot{N}_{\text{H}_2\text{O},\text{in}}$ is the molar flow rate of the steam feed (mol s^{-1}), N_{cell} is the number of cells (cell), A is the cell area (m^2), and W is the electrical power (W).

The energy efficiency of process can be calculated by Eq. 2.60, which considers the heating value of syngas, power, thermal energy input, and heating value of reactant.

$$\eta_{\text{en}} = \frac{\text{heating value of syngas}}{Q + W + \text{heating value of feed}} \quad (2.60)$$

where η_{en} is the energy efficiency of process (-), Q is the total thermal energy input rate of process (W), and W is the total electrical power (W).

For the thermal energy demand, the overpotentials (irreversibilities) involved in process operation will result in heat production due to entropy generation, which called as Joule heat or heat of overpotential that can be supported to be thermal energy for process. The heat of overpotential can be determined by Eq. 2.61. The thermal energy supported from heat of overpotential can be separated into three cases based on relationship of thermal energy demand ($T\Delta S$), heat of overpotential (Q_{ovp}), and external heat demand (Q_{E}), as shown in Eq. 2.62. In the first case, the thermal energy demand for occurrence of the reactions is larger than heat of overpotential produced ($Q_{\text{ovp}} < T\Delta S$); as a result, the system can be operated as the endothermic mode. In this mode, the heat coming from the external heat source is needed to support heat of system sufficiency for occurrence of the reaction. The external heat demand can be calculated by Eq. 2.62. In the second case, the thermal energy demand is less than the heat of overpotential produced ($Q_{\text{ovp}} > T\Delta S$), hence the system can be operated as the exothermic mode. In this case, the external heat for the system is not required and the excess heat can be utilization, so that the efficiency of the system is enhanced. In the final case, the thermal energy demand is equal to heat generation due to overpotentials irreversibilities ($Q_{\text{ovp}} = T\Delta S$). Moreover, this case is such ideal case (Ni et al., 2007a; Udagawa et al., 2007; Zhang et al., 2010).

$$Q_{\text{ovp}} = (\eta_{\text{act,a}} + \eta_{\text{act,c}} + \eta_{\text{ohm}} + \eta_{\text{conc,a}} + \eta_{\text{conc,c}}) J A N_{\text{cell}} \quad (2.61)$$

$$Q_{\text{E}} = (T\Delta S - Q_{\text{ovp}}) \quad (2.62)$$

where Q_{ovp} is the heat of overpotential (W) and Q_{E} is the external heat demand (W).

2.4 Gibbs free energy minimization method

The Gibbs free energy, which is one of the thermodynamic properties, is usually used to identify the equilibrium state of the system. The Gibbs free energy can be calculated by Eq. 2.63

$$G = H - TS \quad (2.63)$$

where G is the Gibbs free energy of the system (J), H is the enthalpy of the system (J mol^{-1}), and T is the temperature of the system (K).

At the equilibrium condition, the thermodynamic analysis of the process can be performed by using the Gibbs free energy minimization method. Under defined temperature (T) and pressure (P) of the system, the total Gibbs free energy (G^t) of N species in the system can be calculated by Eq. 2.64.

$$G^t = \sum_{i=1}^N n_i G_i = \sum_{i=1}^N n_i \mu_i = \sum_{i=1}^N \left(n_i G_i^\circ + n_i RT \ln \frac{f_i}{f_i^\circ} \right) \quad \text{at } T, P \quad (2.64)$$

where G_i is the Gibbs free energy of species i (J mol^{-1}), G_i° is the Gibbs free energy of species i at standard condition (273 K, 1 atm) (J mol^{-1}), N is the number of species, n_i is the mole of species i , μ_i is the chemical potential of species i , R is the universal gas constant ($\text{J mol}^{-1} \text{K}^{-1}$), f_i is the fugacity of species i (atm), and f_i° is the fugacity of species i at standard condition (atm).

At the standard state, the G_i° of each element is equal to zero, while at any conditions the G_i° is set equal to the Gibbs free energy change of formation for species

i at standard condition (ΔG_{fi}°) and can be calculated by Eq. 2.65. Under the gas phase condition, f_i is determined by Eq. 2.66 and f_i° is equal to 1 bar, which is standard state pressure.

$$\frac{\Delta G_{fi}^{\circ}}{RT} = \frac{\Delta G_{f0i}^{\circ} - \Delta H_{f0i}^{\circ}}{RT_0} + \frac{\Delta H_{f0i}^{\circ}}{RT} + \frac{1}{T} \int_{T_0}^T \frac{\Delta C_{Pi}^{\circ}}{R} dT - \int_{T_0}^T \frac{\Delta C_{Pi}^{\circ}}{R} \frac{dT}{T} \quad (2.65)$$

$$f_i = y_i \phi_i P \quad (2.66)$$

where ΔH_{f0i}° and ΔG_{f0i}° are the enthalpy and Gibbs free energy change of formation for species i at reference condition, respectively (J mol^{-1}), ΔC_{Pi}° is the heat capacity change of reaction to form species i ($\text{J mol}^{-1} \text{K}^{-1}$), T_0 is the reference temperature (K), y_i is the mole fraction of species i , and ϕ_i is the fugacity coefficient of species i .

As the process operation, the total Gibbs free energy of the process is decreased until the process reaches the equilibrium and the total Gibbs free energy is minimum. Thus, the equilibrium components and the thermodynamic value of the system can be determined by the minimization of the Gibbs free energy as shown in Eq. 2.67.

$$\min_{n_i} (G^t)_{T,P} \quad (2.67)$$

In order to follow the conservation of atomic species, the constraints of n_i should be performed as Eq. 2.68

$$\sum_{i=1}^N a_{ji} n_i = b_j \quad \text{for } 1 \leq j \leq M \quad (2.68)$$

where a_{ij} is the number of atoms of element j in component i , b_j is the total number of atoms of element j , and M is the total number of elements.

To perform the optimization, Eqs. 2.65 and 2.66 are substitution into Eq. 2.64, then the objective function equation has become as shown below.

$$\min_{n_i} (G^t)_{T,P} = \sum_{i=1}^N (n_i \Delta G_{fi}^{\circ} + n_i RT \ln \frac{y_i \phi_i P}{P^{\circ}})$$

$$\text{subject to } \sum_{i=1}^N a_{ji} n_i - b_j = 0$$

The aim of this objective function problem is to find n_i that minimization the G^t value in order to defined T and P of the system following the given constraints. The Lagrange multiplier method is basically used to solve the optimization problem. For example, the problem of the single-phase reaction under the ideal gas condition at high temperature and 1 bar, the ϕ_i and P_0/P are unity. Therefore, the optimization problem can be reduced as shown below

$$\min_{n_i} (G^t)_{T,P} = \sum_{i=1}^N (n_i \Delta G_{fi}^{\circ} + n_i RT \ln y_i) = \sum_{i=1}^N (n_i \Delta G_{fi}^{\circ} + n_i RT \ln \frac{n_i}{\sum_i n_i})$$

$$\text{subject to } \sum_{i=1}^N a_{ji} n_i - b_j = 0$$

This objective function problem was solved using the Lagrange multiplier method by defining the value of the quantity Lagrange multiplier (λ_j) and applied it into the constraint to obtain the Lagrange function (L) according to Eq. 2.69.

$$L(n_1, n_2, \dots, n_N, \lambda_1, \lambda_2, \dots, \lambda_M) = \sum_{i=1}^N (n_i \Delta G_{fi}^o + n_i RT \ln \frac{n_i}{\sum_i n_i}) + \sum_{j=1}^M (\lambda_j (\sum_{i=1}^N a_{ji} n_i - b_j)) \quad (2.69)$$

This optimization problem is performed in order to find the value of n_i and λ_j , which are obtained from the minimization of the problem. To solve this problem, the necessary conditions of each equation are shown below

$$\frac{\partial L}{\partial n_1} = 0, \frac{\partial L}{\partial n_2} = 0, \dots, \frac{\partial L}{\partial n_N} = 0$$

$$\frac{\partial L}{\partial \lambda_1} = 0, \frac{\partial L}{\partial \lambda_2} = 0, \dots, \frac{\partial L}{\partial \lambda_M} = 0$$

In the optimization problem, the results n_i and λ_j can be solve following the above procedure. But, the Lagrange multiplier method that is used to solve the problem is very complicated when applied to real gas complicated process because of the complex step for the Gibbs free energy minimization to calculated ΔG_{foi}^o and ϕ_i (Bonilla et al., 2011). Therefore, the use of simulation software such as Aspen Plus to

solve this minimization problem in order to perform the thermodynamic analysis of the complicated process is useful. The reactor module in Aspen Plus can calculate equilibrium composition and thermodynamic value following the Gibbs free energy minimization method by using RGibbs reactor module.



2.5 Energy analysis

2.5.1 Energy efficiency

The energy analysis is the quantitative analysis of energy methods, based on the first law of thermodynamics that can be used to evaluate the thermal efficiency of the process. The energy efficiency can be determined by calculating the energy demand and energy release through the energy balance. All form of energy is treated as an equivalence for energy analysis. The H-SOEC/DMR process is involved in the electrochemical and chemical reactions that electrical energy, heat energy, and reactant feed need to carry out a process for syngas production. Thus, the energy efficiency of the process can be calculated by Eq. 2.70 (Dinh et al., 2018; Zhang et al., 2010).

$$\begin{aligned} \eta_{\text{en}} (\%) &= \frac{\text{Energy}_{\text{syngas product stream}}}{\text{Total energy to system}} \times 100 \\ &= \frac{\left(\dot{N}_{\text{H}_2} \times \text{LHV}_{\text{H}_2} \right) + \left(\dot{N}_{\text{CO}} \times \text{LHV}_{\text{CO}} \right)}{Q_{\text{total}} + W_{\text{total}} + \left(\dot{N}_{\text{H}_2, \text{in}} \times \text{LHV}_{\text{H}_2} \right) + \left(\dot{N}_{\text{CH}_4, \text{in}} \times \text{LHV}_{\text{CH}_4} \right)} \times 100 \end{aligned} \quad (2.70)$$

where \dot{N}_{H_2} , \dot{N}_{CO} are the molar flow rates of H₂ and CO in the product stream (mol s⁻¹), respectively, $\dot{N}_{\text{H}_2, \text{in}}$ and $\dot{N}_{\text{CH}_4, \text{in}}$ are the molar flow rates of H₂ and CH₄ in the feed stream (mol s⁻¹), respectively, LHV_{H_2} , LHV_{CO} , and LHV_{CH_4} are the lower heating values of H₂, CO, and CH₄ (J mol⁻¹), respectively, Q_{total} is the total thermal energy input to the process (W), and W_{total} is the total electrical energy input to the process (W).

2.5.2 Pinch analysis

In order to achieve maximum energy recovery of process, the pinch point analysis or pinch technology is a one of widely used method to energy management of process. The pinch analysis is the method to determine the optimal structure of the heat exchanger and aims to receive the maximum energy recovery and minimum utility requirement based on the thermodynamic. The advantage of this method is that it no need of advanced or complex unit operating in order to process efficiency improvement but it just generates the heat integration system based on concept of finding the minimum energy requirement and the maximum energy recovery of the operating process by matching hot and cold streams in process. The pinch technology can be achieved by two methods that consist of a graphical method and problem table algorithm.

2.5.2.1 Graphical method

A graphical method is the fundamental and basic method for analysis of pinch. The concept of this method is composite curves that illustrate the flow of heat from heat integration between the hot and cold streams of a process. A composite curve can be achieved by plotting the enthalpy change accumulated of the hot or cold stream with temperature. The minimum temperature difference (ΔT_{\min}) which set in the appropriate value is involve to the position of the hot and cold composite curves. This is the setting of the pinch area to the place that the transfer of heat between hot and cold streams are the most restrictive. The hot and cold composite curves are used to determine the minimum energy requirements from the data stream with no need of heat exchanger design. In order to performed the heat exchanger network design, the minimum energy requirements are consist of the minimum hot (Q_h) and cold (Q_c) utilities requirement with ΔT_{\min} , which represent as driving force at pinch point. From the principle of pinch point, the heat must not transfer across the pinch due to a higher of energy demand was received. Therefore, the pinch point analysis to perform the HEN can be divided the system into 2 parts included above pinch and below pinch.

The construction of the composite curve is explained according to the below example. The stream data that are presented in Table 2.2 are chosen to display the structure of the composite curve. The necessary pinch analysis data consists of stream or segment temperature, the heat capacity of each stream or segment, and the enthalpy change of the stream or segment. Those data can be received by the mass and energy balance from the simulation of the process or the measurement from the real process. The enthalpy change can be calculated according to Eq. 2.71.

$$\Delta H = \dot{m} C_p (T_t - T_s) = CP(T_t - T_s) \quad (2.71)$$

where ΔH is the enthalpy change over the temperature interval (kW), \dot{m} is the mass flow rate (kg s^{-1}), C_p is the mass heat capacity ($\text{kW s kg}^{-1} \text{ }^\circ\text{C}^{-1}$), T_t and T_s are the target and supply temperatures ($^\circ\text{C}$), and CP is the heat capacity flow rate ($\text{kW } ^\circ\text{C}^{-1}$)

Table 2.2 Information of stream data for composite curve construction

Stream	Name	T_s ($^\circ\text{C}$)	T_t ($^\circ\text{C}$)	CP ($\text{kW } ^\circ\text{C}^{-1}$)	ΔH (kW)
1	hot 1	220	60	100	-16,000
2	hot 2	180	90	200	-18,000
3	cold 1	50	150	150	15,000
4	cold 2	130	180	400	20,000

In this study, the value of CP of each stream is assumed to be the constant value, thus the value of enthalpy change is the amount of heat for changing the supply into target temperature (sensible heat) and phase (latent heat) of streams. The illustration of hot composite curve construction is shown in Figure 2.6. The hot 1 and hot 2 streams (hot stream) are illustrated by the ad and cd segments with the value of CP_1 and CP_2 are equal to 100 and 200 $\text{kW}/^\circ\text{C}$, respectively. In addition, the total enthalpy change is

equal to 34,000 kW ($\Delta H_h = \Delta H_1 + \Delta H_2 = 16,000 + 18,000 = 34,000$ kW). The interval between the supply and target temperature can be divided into 3 subintervals (e.g., 60 – 90, 90 – 180, and 180 – 220°C). In each interval, the calculation of overall CP performed by adding the CP of the streams in each interval. For the first and third intervals, there is only hot 1 is the activity stream so that CP is equal to 100 kW/°C. For the second interval, active stream are hot 1 and 2 streams, therefore total CP is equal to the summation of CP1 and CP2, which equal to 300 kW/°C. Thus, the slope in the second interval is changed depending on the new CP value. In the case of phase transitions, if the slope close to zero (horizontal position) that means CP is very high.

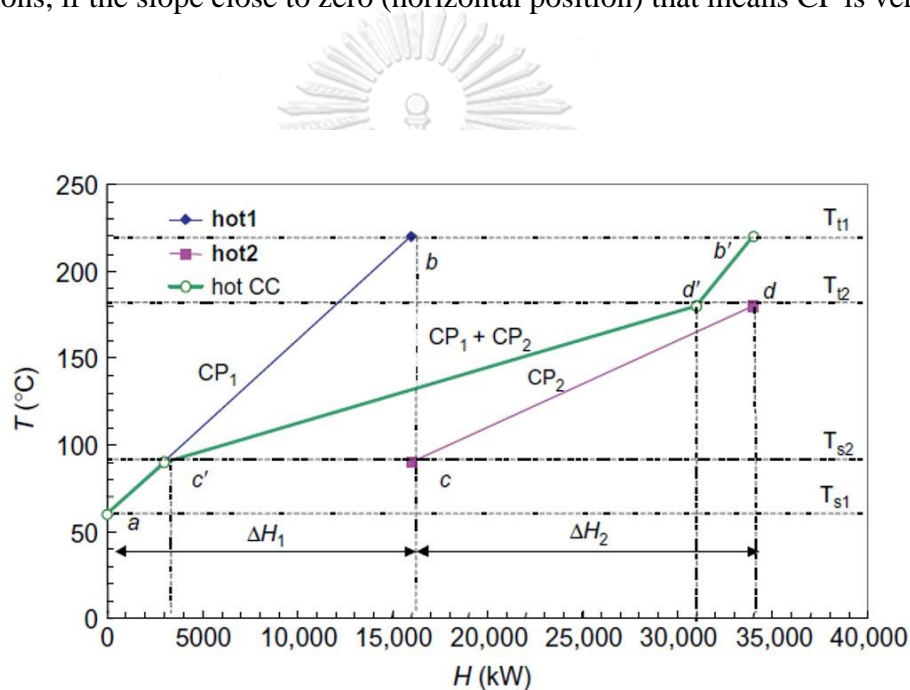


Figure 2.6 Construction of a hot composite curve (Dimian et al., 2014).

The construction of the cold composite curve can be performed using the graphical method as shown in Figure 2.7. The 3 temperature intervals are illustrate: 50 – 130, 130 – 150, and 150 – 180°C, where $CP_3 = 150$, $CP_4 = 400$, and $CP_3 + CP_4 = 550$ kW/°C and the total enthalpy variation is 35,000 kW ($\Delta H_c = \Delta H_3 + \Delta H_4 = 15,000 + 20,000 = 35,000$ kW).

The hot and cold composite curves are showed on the same graph as illustrated in Figure 2.8. The hot composite curve is fixed at the old position, while the cold composite curve is shifted until achieving the ΔT_{min} by given a hot utility. The result shows that for ΔT_{min} is equal to 10°C , Q_h is equal to 7,000 kW and Q_c is equal to 6,000 kW with the pinch point is located between 130 and 140°C .

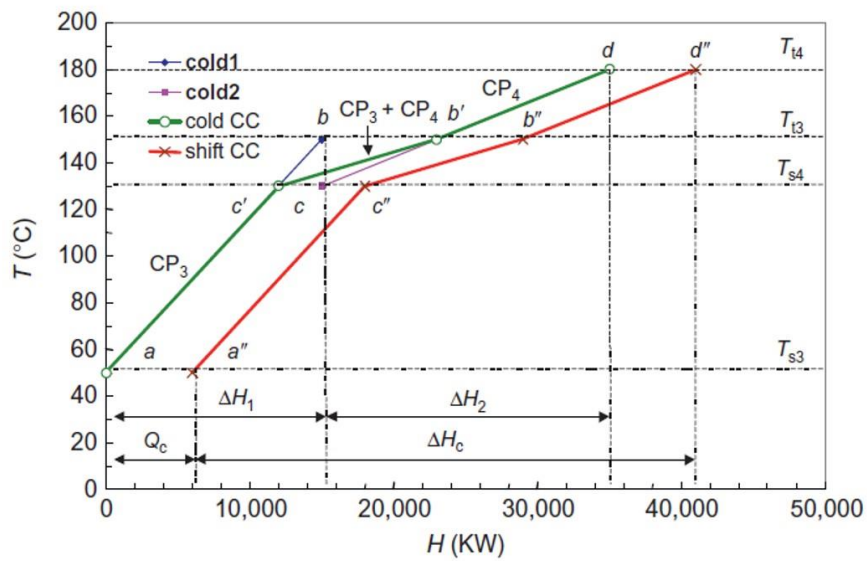


Figure 2.7 construction of a cold composite curve (Dimian et al., 2014).

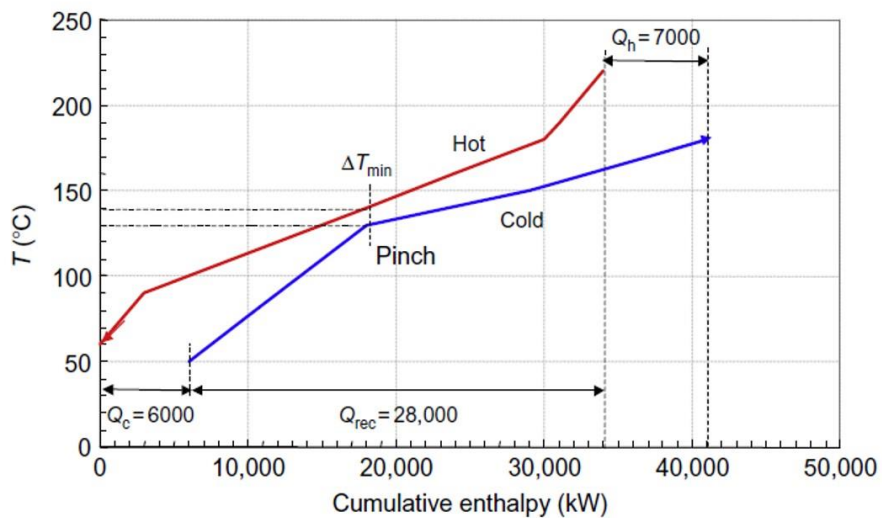


Figure 2.8 Composite curve (Dimian et al., 2014).

2.5.2.2 Problem table algorithm

The problem table algorithm is the other method and is used to find the minimum energy target. This method is simple and accurate more than the graphical method because without drawn of the composition curve. The steps of this method are given below:

In the first step, the ΔT_{\min} value of the process is set and the hot and cold streams of the process are identified. For example, the four process streams are chosen for hot or cold streams according to the data that are shown in Table 2.3 and the ΔT_{\min} is set of 10°C . For the next step, the target and supply temperature of both hot and cold streams are shifted by half of the ΔT_{\min} . For the hot streams, the temperature is shifted below the normal temperature (or 5°C). For the cold streams, the temperature is shifted above the normal temperature as shown in Table 2.4. And then, the value of normal and shift temperature change of each hot and cold streams are put to the schematic form in vertical scale as shown in Figure 2.9. The temperature shift is performed in this way to ensure that each temperature interval is possible to exchange heat between hot and cold streams. According to Figure 3.3, the temperature interval 2 shows the range of shift temperature between 145°C and 140°C . In this interval, the hot streams are consist of 2 and 4 stream with the range of temperature between 150°C and 145°C with the cold stream is 3 stream with the range of temperature between 135°C and 140°C . Therefore, the hot stream temperature is higher than the cold stream temperature through this interval. In addition, the net enthalpy change in each interval temperature can be calculated by Eq. 2.72. The results of each interval calculation are shown in Table 2.5.

$$\Delta H_i = (S_i - S_{i+1})(\sum CP_H - \sum CP_C)_i \quad (2.72)$$

where S_i and S_{i+1} are the shift temperatures of intervals i and $i+1$ ($^\circ\text{C}$), $\sum CP_H$ is the summation of the heat capacity flow rate of hot stream in interval i ($\text{kW } ^\circ\text{C}^{-1}$), and $\sum CP_C$ is the summation of the heat capacity flow rate of cold stream in interval i ($\text{kW } ^\circ\text{C}^{-1}$).

Table 2.3 The information data of process streams example (Kemp, 2007).

Stream number	Type of stream	Heat capacity flow rate (kW °C ⁻¹)	Supply temperature (°C)	Target temperature (°C)	Stream heat load (kW) (positive for heat release)
1	cold	2.0	20	135	2.0(20-135) = -230
2	hot	3.0	170	60	3.0(170-60) = 330
3	cold	4.0	80	140	4.0(80-140) = -240
4	hot	1.5	150	30	1.5(150-30) = 180

Table 2.4 The information data of process streams example with shifted temperature (Kemp, 2007).

Stream number and type	CP (kW °C ⁻¹)	Actual temperature		Shift temperature	
		T _s (°C)	T _t (°C)	S _s (°C)	S _t (°C)
1. cold	2	20	135	25	140
2. hot	3	170	60	165	55
3. cold	4	80	140	85	145
4. hot	1.5	150	30	145	25

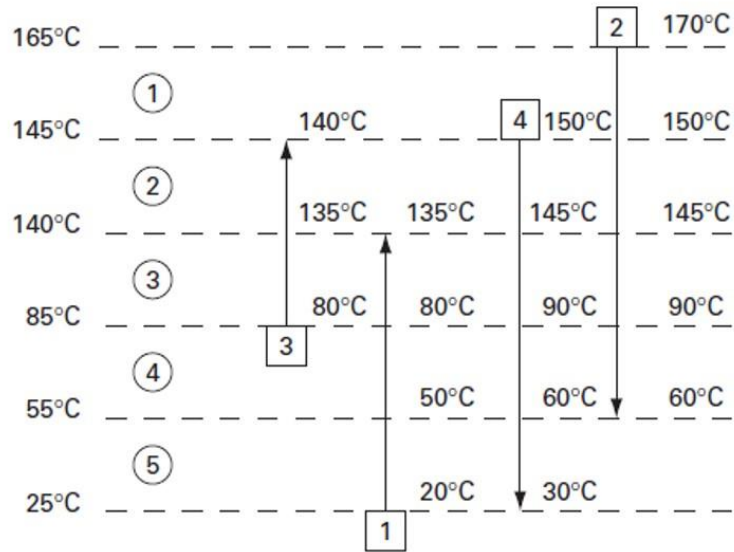


Figure 2.9 Streams and temperature interval (Kemp, 2007).

Table 2.5 The temperature intervals and heat loads for process streams (Kemp, 2007).

Shift temperature (°C)	Interval number	$S_i - S_{i+1}$ (°C)	$\sum CP_H - \sum CP_C$ (kW °C ⁻¹)	ΔH_i (kW)	Surplus or deficit
$S_1 = 165$	1	20	+3.0	+60	Surplus
$S_2 = 145$	2	5	+0.5	+2.5	Surplus
$S_3 = 140$	3	55	-1.5	-82.5	Deficit
$S_4 = 85$	4	30	+2.5	+75	Surplus
$S_5 = 55$	5	30	-0.5	-15	Deficit
$S_6 = 25$					

For the next step, the cascade calculation is performed under the assumption that is the temperature of temperature interval $i + 1$ with enthalpy change is lower than temperature interval i . Therefore, the heat can be transferred from interval i to $i+1$. Figure 2.10 shows a calculation of transfer between intervals 1 and 2. According to cascade, a 60 kW surplus heat of interval 1 is transfer to interval 2 that has 2.5 kW surplus heat and accumulated to 62.5 kW. Then, an accumulated heat is transfer to interval 3 that has 82.5 kW deficit heat and accumulated to 20 kW deficit heat. Additionally, a 20 kW deficit heat is transfer to temperature interval 4 and 5, respectively. The net heat transfer at the end of interval 5 is 40 kW surplus that need the cold utility to transfer out of system. According to the cascade calculation is illustrated in Figure 2.11(a), between the temperature interval of 3 and 4 are given a negative value that is call as thermodynamically infeasible, which represent as heat from cold stream is transfer to hot stream that is impossible for thermodynamics. Therefore, to solve this problem, the hot utility of 20 kW is adding to this system as shown in Figure 2.11(b). In this method, the pinch point temperature is located at the point that given zero net heat transfer. The minimum of hot and cold utilities is 20 kW and 60 kW. In this example, the pinch point has been located at the interval boundary with a shifted temperature of 85 °C (i.e. hot streams at 90 °C and cold streams at 80 °C). The calculation results from both graphical and problem table algorithm methods must be the same. However, the problem table algorithm is suitable for large scale and complicate process because it no need of composite curve drawing and can be used through computational calculation.

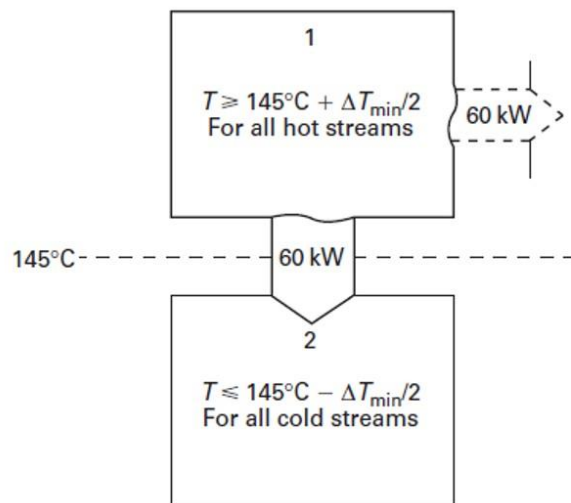


Figure 2.10 Use of heat surplus from an interval (Kemp, 2007).

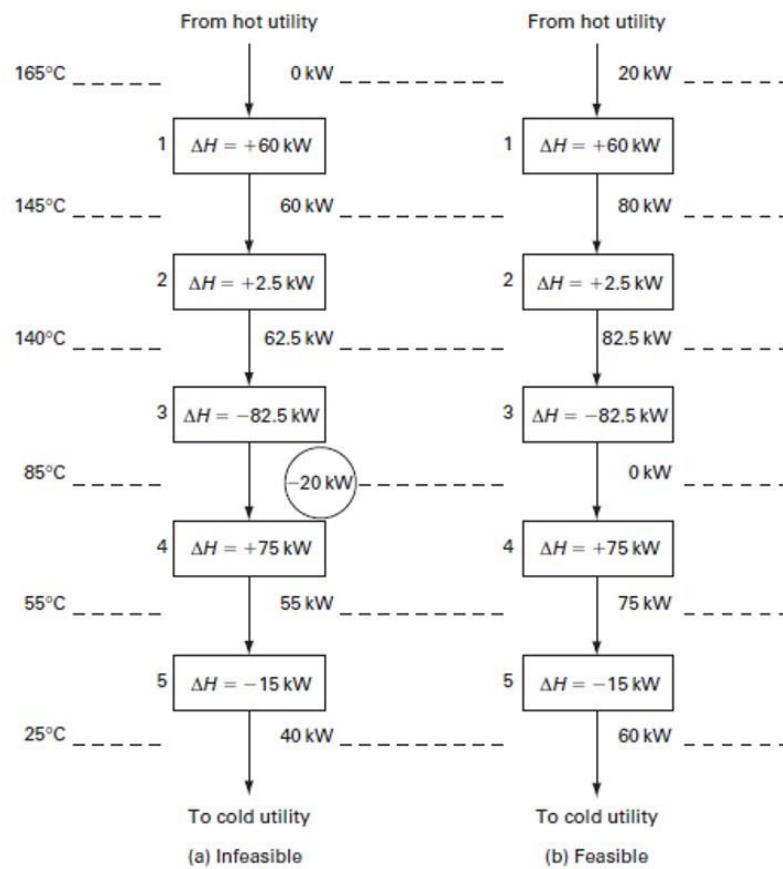


Figure 2.11 Infeasible and feasible heat cascades (Kemp, 2007).

2.5.2.3 Heat exchanger network design

The graphical and problem table algorithm methods are used to find the minimum energy target of the process. Then, the heat exchanger network is performed to obtain that energy target. In the first step, the grid diagram of the process stream is drawn. For this example, the grid diagram of the process stream according to Table 2.3 is performed as shown in Figure 2.12. Basically, the grid diagram is divided into 2 parts include the above pinch and the below pinch. For the above pinch consideration, only the hot utility is needed. In the below pinch, only the cold utility can be used. Thus, it is possible to cool the hot streams by using cold streams with a heat exchanger to obtain temperature at the pinch temperature. Then, the hot utility is used to reach a remaining cold stream to the target temperature. Therefore, the matches of hot and cold streams must find aim to receive heat recovery.

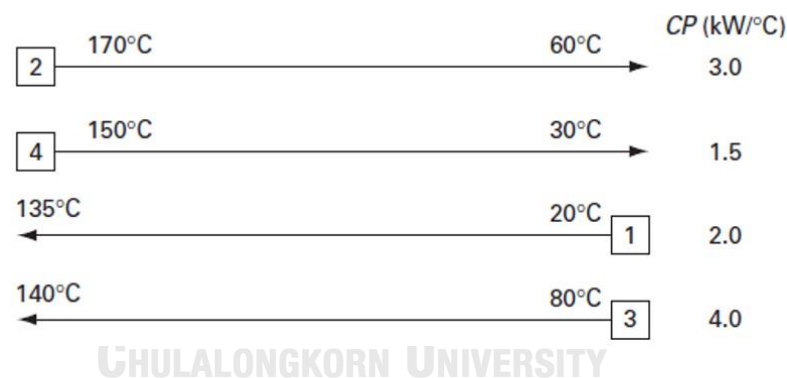


Figure 2.12 Initial grid diagram for example problem (Kemp, 2007).

According to the example problem in Table 2.3, the pinch temperatures of hot and cold streams are 90 °C and 80 °C with the energy target of 80 kW (i.e., the hot utility of 20 kW and cold utility of 60 kW) and setting ΔT_{\min} of 10 °C. In the case of the above pinch temperature, the criteria to matching stream is the hot stream heat capacity flow rate must lower than or equal to cold stream (Eq. 2.73). This criterion is performed to prevent the different hot and cold streams temperatures in the exchanger

more than ΔT_{\min} . The hot stream 2 and cold stream 3 are considered by the following of criterion ($CP_2 < CP_3$), thus the hot and cold streams are matched. In order to reach the pinch temperature, the heat of 240 kW $((90 - 170)3 = 240 \text{ kW})$ must be transfer from hot stream 2. In order to increase the temperature from pinch to target temperature, the heat of 240 kW $((140-80)4 = 240 \text{ kW})$ must be transfer to cold stream 3. Thus, the matching between both streams results in an offer the full fills heat for both streams. In addition, the hot stream 4 and the cold stream 1 are considered by the following criterion ($CP_4 < CP_1$). For heat exchange, the hot stream 4 needs to discharge of 90 kW $((90 - 150)1.5 = 90 \text{ kW})$ to cooling. While 90 kW of heat can be driven the cold stream 1 temperature just 125°C from the target of 135°C that means this match can't fulfill heat demand. Therefore, the external heat utility of 20 kW is needed to heat cold stream 1 to the target temperature of 135°C. The construction of matching hot and cold streams is illustrated in Figure 2.13. It should be noted that the heat utility of 20 kW from the above pinch analysis is equal to the result of the target energy calculation.

$$CP_{\text{HOT}} \leq CP_{\text{COLD}} \quad (2.73)$$

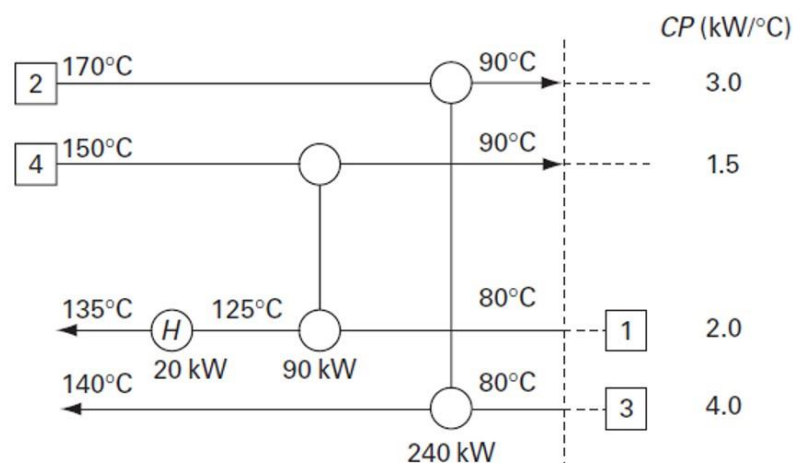


Figure 2.13 Above pinch network design for example problem (Kemp, 2007).

In the case of the below pinch point temperature, the heat exchanger network design can be calculated follow the criteria that difference from above pinch. For the below pinch temperature, the criterion that used in this part is the hot stream heat capacity flow rate must be more than or equal to the cold streams (Eq. 2.74). The below pinch design is performed and aims to guarantee that the cold streams are sufficiently heated to the pinch temperature by using a heat exchanger and heat streams and only the cold utility is used. For example, as shown in Figure 2.12, only the cold stream 1 is considered due to below the pinch temperature and matching with hot stream 2 ($CP_1 < CP_2$). The hot stream 2 is discharged only 90 kW to reach the target temperature of 60 °C ($(60 - 90)3 = 90 \text{ kW}$), which does not satisfy for the cold stream 1 that reaches just 65 °C from the target temperature of 80 °C. The 30 kW of remaining cold stream 1 is supplied from the hot stream, while the hot stream 4 is the opposite. According to the CP criterion, the CP value of cold stream 1 and hot stream 4 are not following the CP criterion that means heat cannot be exchanged between these streams, but in this case, can be possible due to it is away from pinch that the cold stream 1 only heated by 90 kW to the point, which far from the pinch temperature. The promising of this match can be checked using the balance of energy transfer by heat exchange according to Figure 2.14. When the match is a success, the cold stream 1 reaches the target temperature of 80 °C while the hot stream 4 does not satisfy and it needs an external cold utility of 60 kW to reach the target temperature of 30 °C. The value of cold utility that needs in below pinch is equal to the calculation of target energy.

$$CP_{\text{HOT}} \geq CP_{\text{COLD}} \quad (2.74)$$

The final step of the heat exchanger network design is shown the grid of above and below pinch design on the same grid diagram as illustrates in Figure 2.15. The grid diagram shows the promising design of heat recovery when setting ΔT_{min} of 10 °C and this process consists of 6 heat exchangers (4 heat exchangers, 1 heater, and 1 cooler).

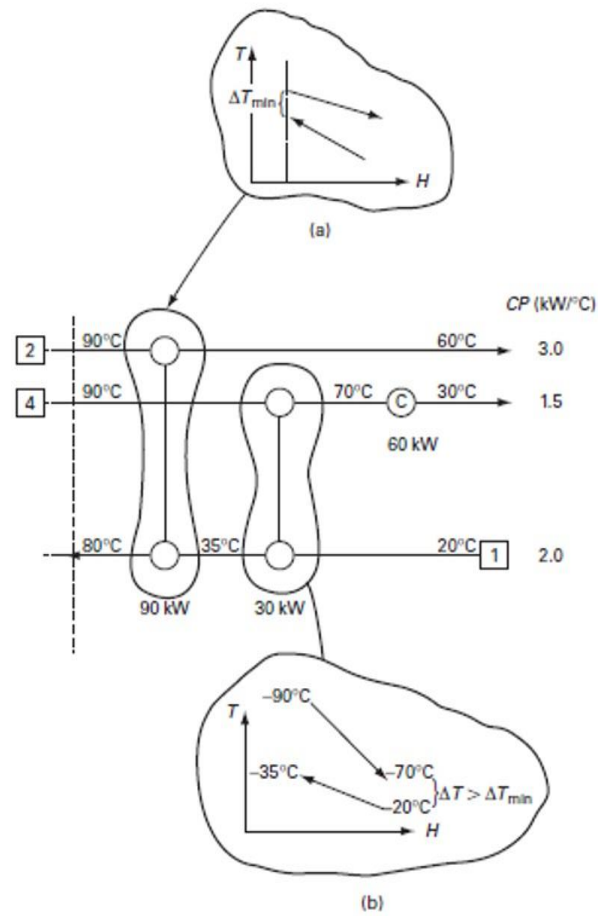


Figure 2.14 Below pinch network design for example problem (Kemp, 2007).

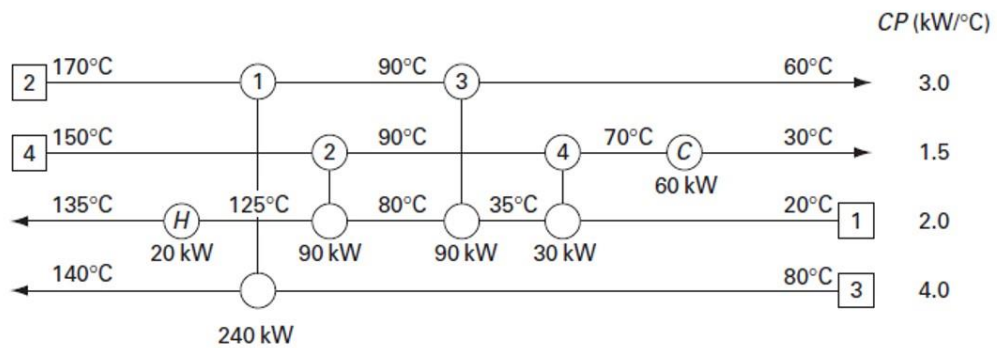


Figure 2.15 Heat exchanger network design achieving energy targets (Kemp, 2007).

2.6 Exergy analysis

Energy analysis is the quantity analyzer tool based on the first law of thermodynamics (FLT). The first law of thermodynamics is the law of the conservation of energy, which describes that although energy can change into another form, it cannot be created or destroyed. Energy analysis is only analyzing the input and output energy from the process, but it does not offer that how much useful work of energy is destroyed when transforms. Exergy is the difference from energy, it is based on both the first and second laws of thermodynamics. Exergy is the maximum theoretical useful work that can be received when the control volume system is operated under initial state (T, P) is brought to equilibrium at reference environment state (T_0, P_0) . In this thesis, the reference environment state is $T_0 = 298 \text{ K}$ and $P_0 = 1 \text{ atm}$ (Dincer and Rosen, 2013; Zhu et al., 2018).

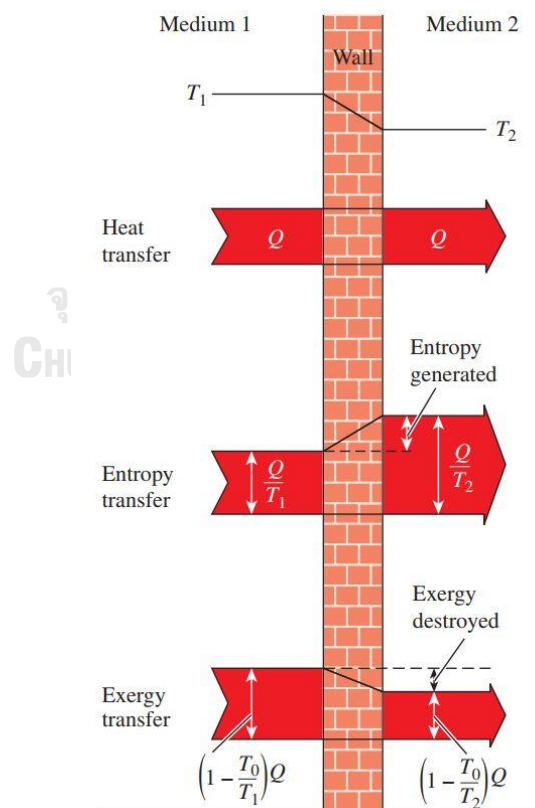


Figure 2.16 The energy, entropy, and exergy balances through the system (Çengel et al., 2019).

Figure 2.16 gives information about the energy, entropy, and exergy balances, in which the wall is represented as the system. According to the energy balance, it can be transformed but cannot be generated or lost. The entropy and exergy balances are different from the energy, the entropy must always be generated through the system, while the exergy is always destroyed by the system. The cause of exergy destroy can be divided into two different ways. The first is the external losses, exhaust or the exergy content in the matter streams, which are not utilized (e.g., cooling water, and purge stream or smoke). The second is the internal destruction or losses due to the irreversibility of the system (e.g., reactions and heat transfer). Therefore, the analysis of exergy of the process can indicate which parts of the process that are using energy inefficient and help to decide what design of process should be and retrofit plant modification.

The important parameter to evaluate the exergy efficiency is the exergy destruction, which can be calculated by the exergy balance at steady-state under the constant volume system operated with input and output stream as performed in Eq. 2.75 (Dincer and Rosen, 2013; Kasemanand et al., 2017).

$$\left(\sum \text{Ex}\right)_{\text{in}} = \left(\sum \text{Ex}\right)_{\text{out}} + \text{Ex}_d \quad (2.75)$$

where $\left(\sum \text{Ex}\right)_{\text{in}}$ and $\left(\sum \text{Ex}\right)_{\text{out}}$ are the summation of exergy inlet and exergy outlet, respectively (W) and Ex_d is the exergy destruction (W).

The exergy transfer is the summation of three types of exergy included the exergy transfer by mass (flow exergy), exergy transfer by heat, and exergy transfer by work. In this study, the exergy transfer by potential and kinetic energies are negligible due to those are few when compared with the other exergy transfer in the thermal chemical process. Additionally, the calculation of the total exergy transfer is following Eq. 2.76 (Dincer and Rosen, 2013).

$$\sum Ex = \sum Ex_s + \sum Ex_Q + \sum Ex_w \quad (2.76)$$

where $\sum Ex_s$, $\sum Ex_Q$, and $\sum Ex_w$ are the total exergy transfers by mass, heat, and work, respectively (W).

The exergy transfer by heat is a quality of the thermal energy that is depended on heat and operating temperature of system and can be calculated by Eq. 2.77 (Dincer and Rosen, 2013).

$$Ex_Q = \left(1 - \frac{T_0}{T_s}\right) Q_s \quad (2.77)$$

where Ex_Q is the exergy transfer by heat (W), T_0 is the reference environment temperature (K), T_s is the temperature of the system (K), and Q_s is the heat transfer through the process (W).

The exergy transfer by work is involve with shaft work done by the process. The shaft work consist of all terms of work (e.g., mechanical and electrical works), but it not involve with work done from the system that without control volume. The calculation of exergy transfer by work is following Eq. 2.78, which is equal to work that transfers through each system (Dincer and Rosen, 2013).

$$Ex_w = W \quad (2.78)$$

where Ex_w is the exergy transfer by work (W) and W is the work transfer through the process (W).

When heat and work transfer to the process, the exergy transfer by heat and work are considered as the exergy transfer to the process term. Inversely, when the heat and work out from the process, those are considered as the exergy transfer out the process term. This thesis, the source of heat supply to the process is not regarded. Therefore, the heat of Q_s of process operation at T_s , the source of heat is also assumed to supply the heat at T_s .

The exergy transfer by mass can be calculated by Eq. 2.79.

$$Ex_{s,j} = F_j \times ex_{s,j} \quad (2.79)$$

where $Ex_{s,j}$ is the flow exergy of stream j (W), F_j is the molar flow rate of stream j (mol s^{-1}), and $ex_{s,j}$ is the specific molar flow exergy of stream j (J mol^{-1}).

The specific molar flow exergy is a summation of specific physical exergy and specific chemical, as shown in Eq. 2.80 (Ghannadzadeh et al., 2012).

$$ex_{s,j} = ex_{ph,j} + ex_{ch,j} \quad (2.80)$$

where $ex_{ph,j}$ is the physical exergy of stream j (J mol^{-1}) and $ex_{ch,j}$ is the chemical exergy of stream j (J mol^{-1}).

The physical exergy is the maximum useful work received by passing a matter stream at the general state (T, P) to the reference environment state (T_0, P_0) through physical process and can be calculated by Eq. 2.81; moreover, it can be transformed to the molar specific heat capacity (C_p) form (C_p constant) as shown in Eq. 2.82.

$$ex_{ph,j} = (h_j - h_{0,j}) - T_0 (s_j - s_{0,j}) \quad (2.81)$$

$$ex_{ph,j} = Cp_j(T_j - T_0) - T_0 \left[Cp_j \ln \left(\frac{T_j}{T_0} \right) - R \ln \left(\frac{P_j}{P_0} \right) \right] \quad (2.82)$$

where h_j and s_j are the specific molar enthalpy ($J \text{ mol}^{-1}$) and specific molar entropy ($J \text{ mol}^{-1} \text{ K}^{-1}$) of stream j at T and P , respectively, $h_{0,j}$ and $s_{0,j}$ are the specific molar enthalpy ($J \text{ mol}^{-1}$) and specific molar entropy ($J \text{ mol}^{-1} \text{ K}^{-1}$) of stream j at T_0 and P_0 , respectively, Cp_j is the molar specific heat capacity of stream j ($J \text{ mol}^{-1} \text{ K}^{-1}$), T_j is the temperature of stream j (K), and P_j is the pressure of stream j (atm).

The chemical exergy is the maximum of useful exergy that could be received via passing the substance to the equilibrium under the reference environment condition (dead state) from the reference environment condition (T_0, P_0). The calculation of the chemical exergy is according to Eq. 2.83 (Dincer and Rosen, 2013; Xiang et al., 2004).

$$ex_{ch,j} = f_j^V \left(\sum y_{i,j} \overline{ex}_{ch,i} + RT_0 \sum y_{i,j} \ln y_{i,j} \right) + f_j^L \left(\sum x_{i,j} \overline{ex}_{ch,i} \right) + f_j^S \left(\sum z_{i,j} \overline{ex}_{ch,i} \right) \quad (2.83)$$

where f_j^V , f_j^L , and f_j^S are the mole fractions of gas, liquid, and solid contained in stream j (-), respectively. $y_{i,j}$, $x_{i,j}$, and $z_{i,j}$ are the mole fractions of component i in gas, liquid, and solid phase contained in stream j (-), respectively. $\overline{ex}_{ch,i}$ is the standard specific molar chemical exergy of component i at T_0 and P_0 ($J \text{ mol}^{-1}$). $\overline{ex}_{ch,i}$ of the all components at the reference environment in the H-SOEC/DMR process are shown in Table 2.6.

Finally, the overall process (η_{ex}) and the exergy efficiency of a single unit in the process ($\eta_{ex,k}$) and is determined the exergy destruction of each unit in the process

are calculated to performed the exergy analysis. The exergy efficiency and exergy destruction are the helpful tool that can be indicate which part of process is inefficiency. The exergy destruction is represent the evaluation of energy potential that is used in every single unit that this value is a positive value. The explanation of the exergy efficiency of the H-SOEC/DMR process for syngas production is the syngas product exergy output process divided by the overall input exergy of the process and can be calculated by Eq. 2.84 that involve to the energy efficiency of the process. In addition, the calculation of exergy efficiency of a single unit is according to Eq. 2.85 (Dincer and Rosen, 2013; Ni et al., 2007a; Yan et al., 2019).

$$\eta_{\text{ex}} (\%) = \frac{\text{Ex}_{\text{syngas product stream}}}{(\sum \text{Ex})_{\text{in}}} \times 100 \quad (2.84)$$

$$\eta_{\text{ex,k}} (\%) = \frac{(\sum \text{Ex})_{\text{out}}}{(\sum \text{Ex})_{\text{in}}} \times 100 = \left(1 - \frac{\text{Ex}_d}{(\sum \text{Ex})_{\text{in}}} \right) \times 100 \quad (2.85)$$

Table 2.6 Standard chemical exergy value for selected substances at the reference environment ($T_0 = 298 \text{ K}$, $P_0 = 1 \text{ atm}$) (Dincer and Rosen, 2013; Evgeny, 2006).

Substance	Phase	Standard chemical exergy (J mol^{-1})
CO_2	g	19870
CH_4	g	831600
H_2O	g	9500
H_2	g	236100
CO	g	275100
O_2	g	3970
H_2O	l	900

CHAPTER III

LITERATURE REVIEW

In this chapter, the kinds of literature that related to the H-SOEC/DMR process are summarized. The topics of this chapter are categorized the interesting literature into three major parts included the performance improvement of a solid oxide electrolysis cell for syngas production, the proton-conducting solid oxide electrolysis cell process, and the dry methane reforming process.

3.1 Performance improvement of a solid oxide electrolysis cell for syngas production

For syngas production via the H-SOEC process, it is facing the problems of low CO₂ conversion and high content of H₂O in syngas product due to production of water as a by-product, which should be receiving an improvement. Xie et al. (2010) studied syngas production through proton-conducting solid oxide electrolysis cell. The experimental carry out by steam is feed into the anode and carbon dioxide is feed into cathode under conditions that applied a current of 1.5 A cm⁻² at 614 °C. The results show the maximum 65% CO₂ conversion is received and water is present as a by-product in this process.

In order to achieve a higher performance of solid oxide electrolysis cell (SOEC), improvement of material and structure of cell compositions become an interesting way. Shin et al. (2015) was design the novel layer catalyst of H-SOEC for syngas production aims to avoid the coking formation at the cathode side of H-SOEC. The experimental is carried out by adding a Ce(Mn, Fe)O₂–(La,Sr)(Fe,Mn)O₃ (CMF–LSFM) into the cathode side as shown in Figure 3.1. The results show 65% CO₂ conversion with 61% CO selectivity are collect and no carbon deposition was evident after the CO₂ reduction with reducing polarization resistance.

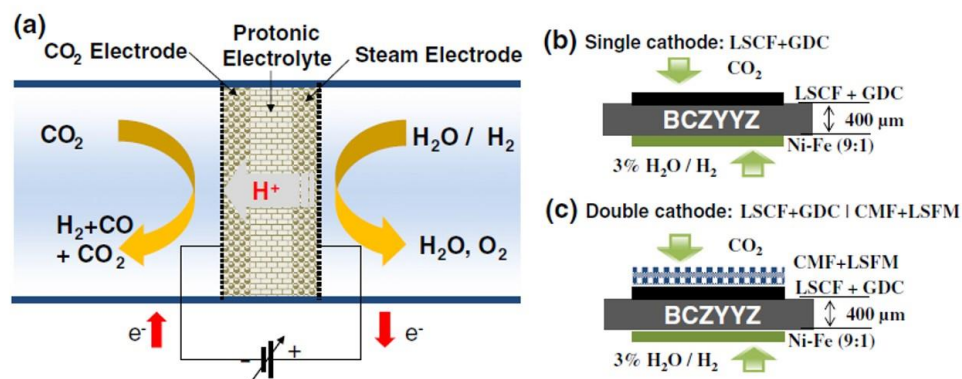


Figure 3.1 (a) Schematic diagram of CO₂ reduction in proton conductor. (b) Cell configuration using a single cathode layer, LSCF+GDC and (c) double cathode layers, LSCF+GDC/CMF+LSFM (Shin et al., 2015).

Moreover, the performance improvement by combined the reforming reaction with SOEC is an attractive way to improve product concentration and CO₂ conversion. Lu et al. (2018) were demonstrated and perform experimental regarding a highly efficient electrochemical reforming of CH₄/CO₂ through dry methane reforming reaction in a perovskite O-SOEC as illustrated in Figure 3.2 with exceptionally high performance and stability. This research used a redox-stable perovskite base-type La_{0.75}Sr_{0.25}Cr_{0.5}Mn_{0.5}O_{3-δ} (LSCM) as both cathode and anode to assemble symmetric cell for electrochemical reforming of CH₄/CO₂. The results indicate exsolved metal/oxide interfaces at nanoscale show strong interactions that deliver enhanced coking resistance and stability. This metal/oxide interface results in an increase of both carbon formation removal performance and high-temperature chemical CO₂ adsorption and activation. In addition, high-temperature stability is obtained for 300 hours, providing the tool to improve and an alternative route for CO₂/CH₄ conversion for energy conversion and storage.

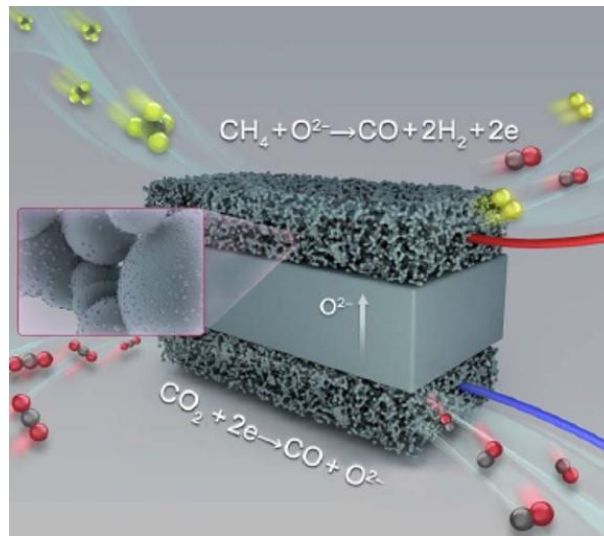


Figure 3.2 The schematic of the CO₂/CH₄ reforming process (Lu et al., 2018).

For a proton-conducting electrolyte process, the CH₄ co-feeding with CO₂ in order to receive highly syngas production is performed in the H-SOFC process as reported by Chen et al. (2018). This research is designed highly syngas coproduction with electricity through the H-SOFC by adding novel layer catalyst into the anode side of the cell for dry methane reforming reaction as call as DMR-SOFC system. Figure 3.3 shown a design of the DMR-SOFC system that SSC/BCZY, BCZY, and Ni-BCZY are used as air-electrode, electrolyte, and hydrogen-electrode, respectively and NiCo-CeO₂/ZrO₂ is used as novel layer catalyst to perform dry methane reforming reaction. The results showed a higher 4.8% improvement for CO₂ conversion and 21.6% for CH₄ conversion with higher electrical output. In addition, this process achieves the CO₂ conversion that higher more than 90% with the CH₄ conversion higher of 80% at 800 °C. Moreover, syngas selectivity is increased by removing water due to the steam methane reforming reaction, which presents s side reaction of this process.

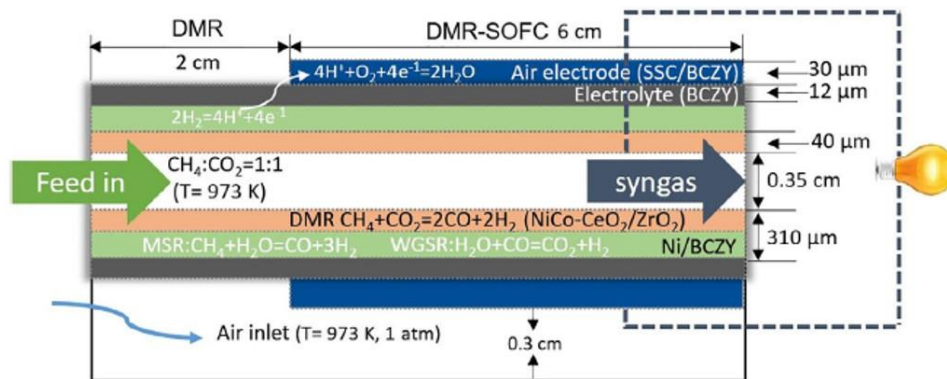


Figure 3.3 The geometrical parameters of the designed reactor with SOFC and dry methane reforming layer (Chen et al., 2018).

From the concepts of DMR-SOFC and double layers cathode of H-SOEC, it is interesting to combine H-SOEC with DMR by adding a novel layer catalyst of DMR into the cathode side of H-SOEC in order to improve the CO₂ conversion and syngas selectivity problems of the H-SOEC process.

3.2 Proton-conducting solid oxide electrolysis cell

Currently, several of H-SOEC researches are a report about the configuration, parametric analysis, and modeling by simulation method. Moreover, it has also reported about an improvement of the H-SOEC process aim to achieve the high energy efficiency process (Ni et al., 2008b; Udagawa et al., 2007; Udagawa et al., 2008).

For the structural parametric analysis of H-SOEC, the configuration of the cell can be divided into electrolyte supported, anode supported, and cathode supported. From the design of H-SOEC cell, it is important to know which a support type that has more advantage than the other. Therefore, the three types of support are evaluated in terms of the H-SOEC electrochemical performance by varying the thickness of cells for each support type (Ni et al., 2008a). Namwong et al. (2016) studied the effect of configuration on the electrochemical performance of H-SOEC for syngas production.

In their study, the thickest side was set at 200 μm and the other sides were set at 100 μm . Under the same operating condition, the results show the cathode-supported is the best configuration due to it requires the lowest cell potential. Therefore, the cathode-supported should be selected as the support structure for H-SOEC. Ni et al. (2008a) reported the same results, they studied the effect of supporting structure on the J-V characteristics of H-SOEC. In their results, the cathode-supported exhibits the best performance as it has the lowest electrical energy requirement.

Moreover, the other structural parameters such as pore size, porosity, and tortuosity have a significant effect on electrochemical performance and should be evaluated. Ni et al. (2007b) studied the effect of electrode porosity and pore size on the process performance of SOEC. The results show that increasing the pore size and porosity is reduced the cell potential, which reduces electrical energy demand that can increase the process performance. In addition, Tsai and Schmidt (2011) studied tortuosity in the proton-conducting solid oxide fuel cell (H-SOFC). They found tortuosity is independent of the cell temperature and electrodes thickness, which is consistent with the fact that tortuosity is a geometric factor of electrodes structure and tortuosity is depend on the porosity of electrodes (as reported by Riazat et al. (2015)). Thus, for H-SOEC, the tortuosity of electrodes should be studied regarding the effect on cell performance. Therefore, the structural parameters study in this thesis is the thickness of cell and support-structure, pore size, porosity, and tortuosity.

For evaluate of the operational parameters term, there are many researches that studied regard operational parametric of solid oxide cell. Ni et al. (2007b) studied the effect of operating temperature on the performance of the process. The results show increases in temperature can improve the SOEC performance. Especially, the operating temperature was a significant parameter that affects performance. In addition, Udagawa et al. (2007) studied the effect of operating temperature on SOEC performance. The results are confirmed that their SOEC performance can improve when operated at high operating temperatures (in range of 873 – 1273 K). Moreover, Im-orb et al. (2018) studied the effect of operating temperature on the energy efficiency of SOEC. The results show the operating temperature has an effect on the cell voltage and energy efficiency of the process. The effect of temperature on the syngas production via H-

SOEC was reported by Namwong et al. (2016). The temperature was studied between 550 to 650 °C. The results revealed that an increase in the temperature leads to a decrease in the cell potential due to both the equilibrium voltage and all overpotentials are strongly affected by the operating temperature. Moreover, the operating temperature has an effect on the carbon dioxide conversion of process. It was found that carbon dioxide conversion increased with increasing temperature due to the RWGS reaction, which is the carbon dioxide converse reaction is endothermic.

The pressure is one of the parameters that affect the performance of the process, Namwong et al. (2016) studied regard to the effect of pressure on the performance of H-SOEC for syngas production. The results show that pressure was not effecting the cell voltage. In general, an increase in the pressure leads to an increase in the equilibrium voltage but it reduces the concentration overpotentials because the gases can easily transfer through the electrodes. However, reduce the concentration overpotentials was almost equal to the increase in the equilibrium voltage. In addition, pressure has an impact on the carbon dioxide conversion rate. It was found that carbon dioxide conversion was reduced with the pressure. The carbon dioxide conversion decreased with an increase in pressure lead to the reduction of carbon monoxide products in the outlet stream. In general, the best operating pressure should be 1 atm due to there is no need for a pump or vacuum the pressure during operation. Moreover, they also studied regard steam to carbon ratio (S/C ratio) on the syngas production performance of the H-SOEC process. The S/C molar ratio was varied from 1 to 4, and the other parameters were constantly. The effect on cell voltage shows that no effect from S/C molar ratio on cell voltage when the carbon dioxide stream was varied. In addition, the S/C molar ratio has an effect on a stoichiometric number of syngas production (hydrogen to carbon monoxide molar ratio or H/C molar ratio).

For the effect of a number of the cell on the performance of SOEC, Li et al. (2014) achieve high-efficiency using planar solid-oxide electrolysis stacks. They fabricate SOEC and use it under the condition of 800 °C up to 500 hours. The results show they can be achieved a maximum efficiency of 52.7% when using 30 cell stack of SOEC. Moreover, Ebbesen et al. (2011) studied the durable stack cell of SOEC for both hydrogen production and syngas production. The 6-cells stack of hydrogen

production and a 10-cells stack of syngas production tests a long time at 850 °C. The results revealed cleaning gas feeds (water and carbon dioxide) to the SOEC cell of stack cells resulted in operation without any long-term degradation. In addition, Im-orb et al. (2018) studied the influence of number cell stack on the energy efficiency of SOEC. They varying the number of cells in the range of 100 – 500 cells. The results show the energy efficiency increase with an increase in the number of cells at 1273 K. The maximum energy efficiency of 78.45 % is achieved in the 500-cell stack. Furthermore, they studied the effect of current density on SOEC performance. The current density is investigated by varying in the range of 500 – 2,500 A m⁻² at a constant temperature of 1273 K. They found the current density had an effect on energy efficiency, a maximum energy efficiency of 78.45 % is found when the current density is operated at 2500 A m⁻². In addition, Xiaoyu et al. (2013) analyze the durability of SOEC. The experiment was test under condition, temperature of 800 °C and current density of 0.175 A cm⁻². The result shows that degradation rate was 6.3 kh⁻¹ after 200-hour operation and high degradation was found when it was operated at double of current density. From the effect of operational parameters described above, it indicates that important to evaluate those operational parameters on the performance of H-SOEC for syngas production in this thesis. Therefore, the operational parameters (i.e., temperature, pressure, S/C ratio, number of cells, and current density) are chosen to evaluate the effect on process performance.

In order to simulation and optimization of the H-SOEC process, the electrochemical model and flowsheet model simulation were the favorite tools used to evaluate the performance of the process. The several researches studied the simulation of SOEC using simulation tools such as Matlab, gPROMS Model builder, C+, and FORTRAN language aim to calculate the mathematic model. In addition, a few researches were studied about flowsheet model simulation through the Ansys, Comsol, and Aspen Plus. The Ansys and Comsol is a simulation program, which used the Computational Fluid Dynamic (CFD) method to evaluate flow and thermal distribution of the process. Hawkes et al. (2007) studied simulation of hydrogen production via planar SOEC using a three-dimensional CFD and show the result of operating temperature, current density, and hydrogen production to evaluate the performance of

the process. Moreover, the Aspen software is one tool used to simulate the SOEC system. Im-orb et al. (2018) using the electrochemical model and flowsheet model via the Aspen Plus software in order to study the effect of operational parameters on the performance of SOEC for hydrogen production. In addition, Namwong et al. (2016) simulate the H-SOEC process for syngas production and using the electrochemical model with the flowsheet model via Aspen Plus to evaluate the effect of parameters on the performance of the process. The electrochemical model used to evaluate the performance of the process in the cell voltage term and the flowsheet model used to evaluate the performance of the process in the syngas production term.

Finally, the analysis of the energy efficiency of the H-SOEC system is important. The energy and exergy analysis has been more interesting at this time. These analyses can assist to evaluate and determine the efficiency of energy and maximum useful work that can be achieved from an amount of energy usage (Hajjaji et al., 2012). Mingyi et al. (2008) evaluate the efficiency and thermodynamic analysis of SOEC. The results revealed that increase operating temperature to 1,000 °C, which increases overall efficiency from 33 % to 59 %. Furthermore, Ni et al. (2007a) perform the energy and exergy analysis of the SOEC plant. The result showed that the difference between energy and exergy efficiency was a few at high operating temperatures. Moreover, the result can indicate which part of the SOEC plant is inefficient. Stempien et al. (2013a) revealed the energy and exergy efficiencies of 70 % and 80%, respectively were obtained when using conditions at the operating temperature of 1073 K and a current density of 5,000 A m⁻². In addition, Im-orb et al. (2018) perform electrochemical and flowsheet model analysis of operating parameters (e.g., temperature, current density, and a number of cell) on the energy and exergy efficiencies of SOEC. The results show the operating parameters effect on both energy and exergy efficiencies. The energy and exergy efficiencies of 78.45% and 92.20% were achieved when operation at an operating temperature of 1273 K, operating pressure of 5 atm, current density of 2500 A m⁻², and the number of cell of 500 cells.

The literature reviews described above can be summarizing that both structural and operational parameters are an important parameter that affects the performance of the H-SOEC process. Thus, the analysis of parameters on performance is necessary.

The simulation method using the electrochemical model and flowsheet simulation via Aspen Plus is a suitable choice to predict the effect of parameters on the performance of the process. Moreover, the energy and exergy analysis should be performed in order to evaluate and determine the efficiency of energy and inefficiency part of the process, which can lead to an improvement of the process.

3.3 Dry methane reforming process

The dry methane reforming (DMR) is a chemical process used to convert methane to produce syngas by using carbon dioxide as an oxidizing agent. The use of CH_4 and CO_2 in the DMR reaction can reduce a higher emission of greenhouse gases, when compared to other fuel utilization processes such as the steam methane reforming or partial oxidation of biogas and natural gas. Moreover, landfill gas generally has a promising composition ($\text{CO}_2/\text{CH}_4 = 1$ in volume) for DMR that promotes the potential of DMR in the waste solid treatment process (Muradov and Smith, 2008). However, the DMR process facing some problem that H_2/CO molar ratio of syngas product, which usually equal or below 1, result in a limit usage application of syngas product. Delikonstantis et al. (2017) designed the DMR combined with another process to adjust the H/C molar ratio of syngas product. They tandem combine the DMR reactor with WGS and SMR reactor in order to raise the H/C ratio of more than 2, which usually used as feedstock for FT-process to methanol, long-chain hydrocarbon, and diesel fuel production (Er-rbib et al., 2012). In addition, Stroud et al. (2018) studied dry and bi reforming of methane over various catalysts. They mention that the presence of steam in DMR simultaneously drives SMR that can rise the selectivity of H_2 and CO and the advantage to adjust the stoichiometric of H/C molar ratio above of 2. Moreover, the nickel base catalyst used in their experimental can be driven by both DMR and SMR reactions. Therefore, combine of the DMR with another process that produces steam as a by-product such as H-SOEC for syngas production, result in an advantage of increase the CH_4 conversion and H/C molar ratio of syngas product above of 2.

According to H-SOEC/DMR process, the CO_2/CH_4 stream is feeding into the cathode side. At this side hydrogen, which produced via electrochemical reaction is

considers as co-reactant. Thus, the influence of hydrogen on a DMR has become interested. Herrera Delgado et al. (2015) studied the influence of hydrogen and water on carbon composite of DMR. In their experiment, the fixed-bed reactor was used at atmospheric pressure, temperatures between 373 and 1173 K and inlet mixture of CH₄, CO₂, and H₂ diluted in N₂. The result shown, the hydrogen co-fed led to an increase of water at low temperatures, which produced through the RWGS. Then, as the increase of temperature, the water was consumed with unconverted methane via SMR, which increased the amount of syngas product with high hydrogen content. In addition, hydrogen act as a coke deposition inhibitor that reveals reduce in surface carbon deposition during conditions where hydrogen was represented as co-reactant.

In operation term, CO₂/CH₄ molar ratio of feedstock is an important parameter that effect on the performance of the process. Dinh et al. (2018) studied the effect of the CH₄/CO₂ molar ratio on the conversion and syngas selectivity of the DMR process. The results indicated that an increase in the CH₄/CO₂ molar ratio leads to an increase in CO₂ conversion. A high CO₂ conversion is achieved over a wild range ratio (from 3.7 to 1). In addition, a decrease in the CO₂ conversion was observed at ratios higher than 1, due to an excessive amount of methane, resulting in a larger amount of carbon. For the syngas selectivity, an increase of methane response the selectivity of H₂ increases quickly. A decrease of H₂ selectivity at CH₄/CO₂ molar ratios greater than 1 occurs for the reason as the reduction of CO₂ conversion. Moreover, a lower energy cost production and higher energy efficiency in the range of CH₄/CO₂ molar ratio from 3/7 to 1. In addition, Cao et al. (2017) studied the effect of the CH₄/CO₂ molar ratio on the carbon formation of the DMR process. The results revealed a carbon formation decreased with decreasing of CH₄/CO₂ molar ratio. Thus, the CO₂/CH₄ molar ratio of 1 is the suggested operating condition in this thesis because of it a higher in CO₂ conversion and H₂ selectivity and lower in carbon formation.

For the simulation and parameters analysis terms of the DMR process, Gopaul and Dutta (2015) simulation the dry reforming of multiple biogas types by using the Aspen Plus software and evaluate the effect of temperature and pressure on syngas production performance. The Aspen Plus software used to model the DMR reactor is RGibbs, which is an equilibrium reactor module that calculates its chemical equilibrium

output using the method of Gibbs free energy minimization at the specified temperature, pressure, and component inlet flow rates. The results show syngas molar flow rate increased with increasing temperature but decreased with increasing pressure. Additionally, the optimal operating condition is at 950 °C and 1 atm. In addition, Chein et al. (2015) studied thermodynamic analysis of dry methane reforming focusing on the high-pressure operation. They using the RGibbs reactor provided in the Aspen Plus to predict the chemical equilibrium and vary the temperature in the range of 300 to 1200 °C at high pressure. The CO₂/CH₄ molar ratio is varied in the range of 0.5 to 5. The pressure varies from 1 to 30 bar to examine its effect on DMR performance. The results show higher pressures have a negative effect on DMR and to obtain a suitable H₂/CO ratio at high pressure it is suggested that DMR be carried out at a lower CO₂/CH₄ ratio and high temperature. Moreover, Cao et al. (2017) studied thermodynamic equilibrium analysis of DMR in order to inhibit carbon deposition and adjust of H₂/CO ratio. They simulate process via FactSage software using minimize Gibbs free energy method. From their results, an increase in temperature decrease carbon deposition of the process but a carbon deposition increased with increasing pressure. Moreover, both temperature and pressure effect on H₂/CO molar ratio of syngas product. In addition, Dinh et al. (2018) studied the regard energy efficiency of dry methane reforming. The results revealed a temperature and CO₂/CH₄ effect on the energy efficiency of the DMR process.

The literature reviews in the previous indication that the CO₂/CH₄ molar ratio of 1 is promised for DMR operation. Moreover, the operating parameters such as temperature and pressure are the effect on the performance of the process. The simulation method using the minimum Gibbs free energy method is one of the suitable choices to predict the effect of parameters on performance for syngas production aim to analyze and design process using conditions that receive optimum performance.

CHAPTER IV

MODELING AND VALIDATION

In this chapter, the procedure of H-SOEC/DMR simulation is shown. The major topics of this work are H-SOEC, DMR, and H-SOEC/DMR simulations based on Aspen Plus software simulation. Moreover, the results simulated from simulation model are validated with published experimental results to check the prediction efficiency.

4.1 H-SOEC for syngas production

The simulation of H-SOEC for syngas production is simulated by using Aspen Plus program. The H-SOEC flowsheet illustrates in Figure 4.1, which includes existing unit of Aspen Plus modules (e.g., RStoic, RGibbs, separator, and mixer) and other functions of program (e.g., calculator block and design spec) for simulation. The simulation of each modules are described as below and the italic words are represented the terminology from Aspen Plus flowsheet simulation

4.1.1 MIXER module

The major reactant for electrolysis reaction is steam but hydrogen is usually used as co-reactant, as was reported by several researches (Namwong et al., 2016; Ni et al., 2007a; Ni et al., 2012), in order to prevent oxidation reaction on the anode and reduce partial pressure of steam because the use of pure steam has an effect on the electrical energy demand. According to Figure 4.1, the steam in feed stream (named “STEAM”) is mixed with a hydrogen feed stream (named “HYDROGEN”) at the *Mixer module* (named “MIXER”). The hydrogen feed do not take place in the electrochemical reaction and the flow rate of this stream is adjust by using calculator block function in order to obtained the steam to hydrogen ratio of 95% in stream STEAMH (Namwong et al., 2016).

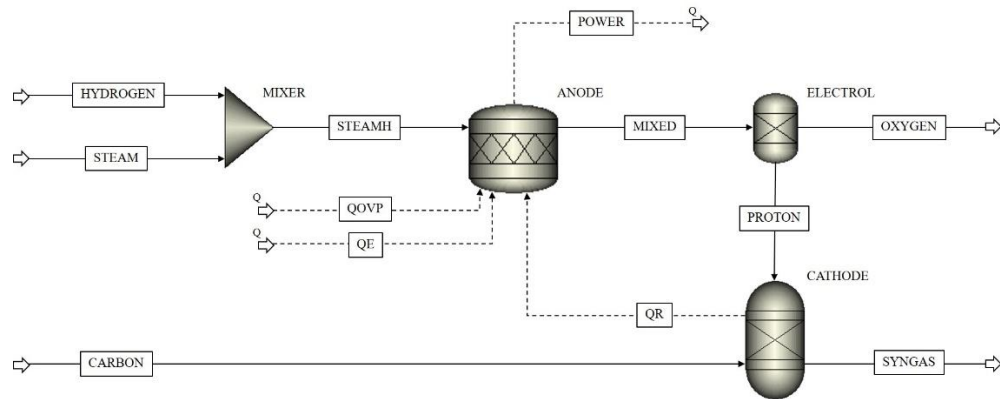


Figure 4.1 Process flowsheet of the H-SOEC for syngas production.

4.1.2 Electrochemical reaction in ANODE module

The steam and hydrogen mixture (Stream “STEAMH”) are flowed into the anode, which the electrochemical reaction occurs in order to produce hydrogen and oxygen. The anode channel is simulated by using the *RStoic module* (named “ANODE”) because of the irreversible and non-spontaneous reaction. In addition, the conversion (X) of this module can be defined by the steam utilization factor (U_s), which depends on inlet steam molar flow rate and current density as shown in Eq. 4.1. In this thesis, the utilization factor of 80% was selected in order to reduce the investment cost of the process (Namwong et al., 2016; Udagawa et al., 2007).

$$X = U_s = \frac{JAN_{\text{cell}}}{2FN_{\text{H}_2\text{O},\text{in}}} \quad (4.1)$$

The electrochemical reaction use both thermal and electrical energies to perform the reaction. In this simulation, the electrical energy used in this reaction can be calculated by using electrochemical model. The electrical energy is calculated in the calculator block function of Aspen Plus and represent as the stream “POWER” supplied to the system. For the thermal energy, it can be provided from the external heat stream (named “QE”) and the heat of overpotential stream (named “QOVP”). For the

simulation, the ANODE block can be specified temperature for any operating condition, which the energy demand of system are change. The thermal energy can be adjusted by design-spec function in order to receive the POWER stream value as calculated by electrochemical model according to overall energy balance of system.

4.1.3 Proton and oxygen separation in ELECTROL module

According to the electrochemical reaction, proton and oxygen are produced. In terms of simulation, the proton produced is represent by the hydrogen product from the ANODE block. For H-SOEC, the proton-conducting electrolyte is simulated by *Sep module* (named “ELECTROL”) and aims to separate proton, oxygen, and unreacted steam. The unreacted steam and oxygen are flowed out of the system (Stream “OXYGEN”) and the separated hydrogen will permeate to cathode channel. For the simulation, the hydrogen split fraction of ELECTROL module is specified as 1 in order to split only hydrogen (Stream “PROTON”) and represents the proton-conducting electrolyte.

4.1.4 Chemical reaction in CATHODE module

At the cathode channel, protons are reacted with electrons and converted into hydrogen, then hydrogen interaction with carbon dioxide, which feed into cathode side through the reversible water gas shift reaction (RWGS) and is converted to syngas. For the simulation, the *RGibbs module* (named “CATHODE”) represents the cathode channel, which is simulated based on a chemical equilibrium. The carbon dioxide feed is represented by stream “CARBON”. The molar flow rate of this stream is adjust following the steam/carbon ratio and the syngas product is represented by stream “SYNGAS”. The RWGS is endothermic reaction, which needs the thermal energy to carry out reaction. The stream “QR” is represented the consumed energy at any conditions of the CATHODE module. This stream is transferred to the ANODE module and shown as the total energy demand of system. Then, the external heat energy is adjusted to provide the total energy demand of system.

4.1.5 Cell voltage, power, and overpotentials calculation

The cell voltage and overpotentials used for H-SOEC operation can be calculated according to Table 4.1. The cell voltage can be calculated by the Nernst equation, the activation overpotential can be calculated by the Butler-Volmer equation, the ohmic overpotential can be calculated by the Ohm's law, and the concentration overpotential can be calculated by Fick's model and Permeation's model of hydrogen permeates in cathode channel based on the hydrogen permeates through the porous ceramic electrode as illustrates by Figure 4.2 and the partial pressure used in the model were estimated by Aspen Plus simulation (Stempien et al., 2013b).

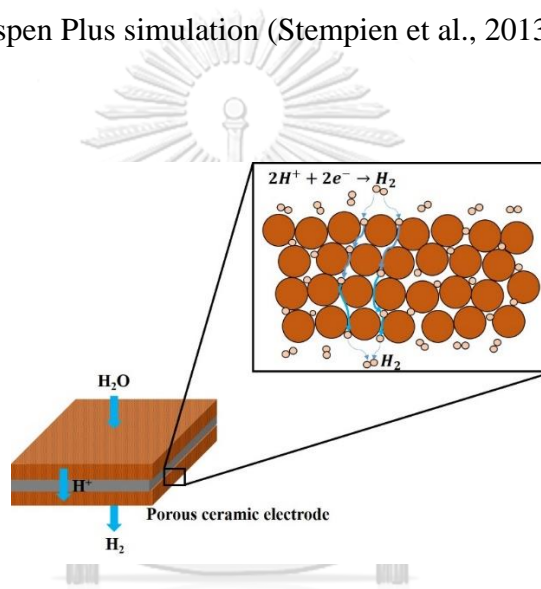


Figure 4.2 A schematic of the hydrogen permeation through the porous ceramic electrode (C. Reid et al., 1959).

Table 4.1 Cell voltage and overpotentials calculation equations

Type	Equation	Eqn. NO.
Cell voltage	$V = E + \eta_{act,a} + \eta_{act,c} + \eta_{ohm} + \eta_{conc,a} + \eta_{conc,c}$	(2.19)
Equilibrium voltage	$E = E^0 + \frac{RT}{2F} \ln \left(\frac{P_{H_2} P_{O_2}^{1/2}}{P_{H_2O}} \right)$	(2.27)
	$E^0 = 1.253 - 0.0002451(T)$	(2.28)
Activation overpotential	$\eta_{act,i} = \frac{RT}{F} \ln \left[\frac{J}{zJ_{0,i}} + \sqrt{\left(\frac{J}{zJ_{0,i}} \right)^2 + 1} \right]$	(2.31)
	$J_{0,i} = \frac{RT}{2F} k_i \exp \left(-\frac{E_{act,i}}{RT} \right)$	(2.32)
Ohmic overpotential	$\eta_{ohm} = J \cdot R_e = J \cdot \frac{l_e}{\rho_e}$	(2.34)
	$\rho_e = \rho_0 \cdot T^{-1} \cdot \exp \left(-\frac{E_{elec}}{RT} \right)$	(2.35)
Concentration overpotential	$\eta_{conc,a} = \frac{RT}{2F} \ln \left[\left(\frac{P_{H_2O}}{P_{H_2O}^{TPB}} \right) \left(\frac{P_{O_2}^{TPB}}{P_{O_2}} \right)^{1/2} \right]$	(2.36)
	$\eta_{conc,c} = \frac{RT}{2F} \ln \left[\left(\frac{P_{H_2}^{TPB}}{P_{H_2}} \right) \right]$	(2.37)

Moreover, the other equations that are used to calculate the inlet steam molar flow rate, electrical power, current, and heat of overpotential and calculate for the operation and evaluation of system are summarized in Table 4.2

Table 4.2 Calculation equation for system operation and evaluation

Type	Equations	Eqn. NO.
Inlet steam molar flow rate	$\dot{N}_{\text{H}_2\text{O},\text{in}} = \frac{JAN_{\text{cell}}}{2FU_s}$	(2.57)
Electrical current	$I = JA$	(2.58)
Electrical power	$W = IVN_{\text{cell}}$	(2.59)
Heat of overpotential	$Q_{\text{ovp}} = (\eta_{\text{act},a} + \eta_{\text{act},c} + \eta_{\text{ohm}} + \eta_{\text{conc},a} + \eta_{\text{conc},c})JAN_{\text{cell}}$	(2.61)

4.1.6 Energy balance

The electrical energy used in system can be calculated by using electrochemical model and the calculator block function of Aspen Plus program. For the electrochemical system, both electrical and thermal energies must be used to provide the total energy demand of system in which thermal energy increases and electrical energy will be decreased following the thermodynamic relationship. Thus, the energy balance of system is required for simulation. The total energy for system operation (Q_T) can be calculated by Eq. 4.2, which included heat for the reaction, heat of overpotential, and external heat. These thermal energies are represented the energy used to carry out the reactions and keep the cell temperature at a stable point because the electrochemical reaction is a highly endothermic reaction. Hence, the energy balance equation can be derived into Eq. 4.3. In this thesis, the heat loss term is assumed to be negligible. Then, the energy balance can be derived into Eq. 4.4, which uses for energy balance of system and uses design spec function to adjust Q_E (Im-orb et al., 2018; Zhang, 2004).

$$Q_T = Q_r - Q_E - Q_{ovp} \quad (4.2)$$

$$Q_T - Q_{loss} + W_{elec} = 0 \quad (4.3)$$

$$Q_T + W_{elec} = 0 \quad (4.4)$$

where Q_r is the energy for all of the reactions in system (W), Q_E is the external heat (W), Q_{ovp} is the heat of overpotential (W), Q_{loss} is the energy losses of system (W), and W_{elec} is the power used of system (W).

4.1.7 H-SOEC validation

To estimate the prediction efficient of simulation model, the J-V characteristics results from simulation model are validated with the experimental data reported by Ruiz-Trejo and Irvine (2012), which investigated the J-V characteristics of syngas production via planar H-SOEC. In their experiment, the electrolysis cell consists of 2 electrodes and electrolyte, and made from 2 electrode 100 μm thick porous Pt layers and 200 μm thick dense BCZY electrolyte. The inlet gas introduced at the anode side used steam to hydrogen ratio of 95 to 5. The experiment is operated at a constant pressure of 1 atm and operating temperature of 550, 600, and 650 $^{\circ}\text{C}$. The model input parameters are summarized in Table 4.3. For the activation overpotentials calculation, the kinetic parameters are used following Table 4.4. In addition, the parameters of effective diffusion coefficient calculation are used according to Table 4.5. The results show that it is a good agreement with the experimental data as shown in Figure 4.3. The results indicate that carbon dioxide is not involved in the electrochemical for syngas production. It is assumed the RWGS reaction is the reaction that carbon dioxide converted into carbon monoxide (Namwong et al., 2016).

Table 4.3 Input parameters and operating conditions.

Operating temperature, T (°C)	550, 600, and 650
Operating pressure, P (atm)	1
Anode stream inlet composition	95 mol% H ₂ O/5 mol% H ₂
Cathode stream inlet composition	100 mol% CO ₂
Steam utilization factor, U _s (%)	80
Electrolyte conductivity, ρ_e (S m ⁻¹)	$3.14 \times 10^4 / T \times \exp(-3.86 \times 10^3 / T)$
Active cell area, A (m ²)	0.04
Number of cell, N _{cell} (cell)	500
Electrode pore radius, r (μm)	0.5
Electrode porosity, n	0.3
Electrode tortuosity, ξ	$(1.5 - 0.5n)^{1/2}$
Cell thickness	
Anode thickness, d _a (μm)	100
Cathode thickness, d _c (μm)	100
Electrolyte thickness, l _e (μm)	200

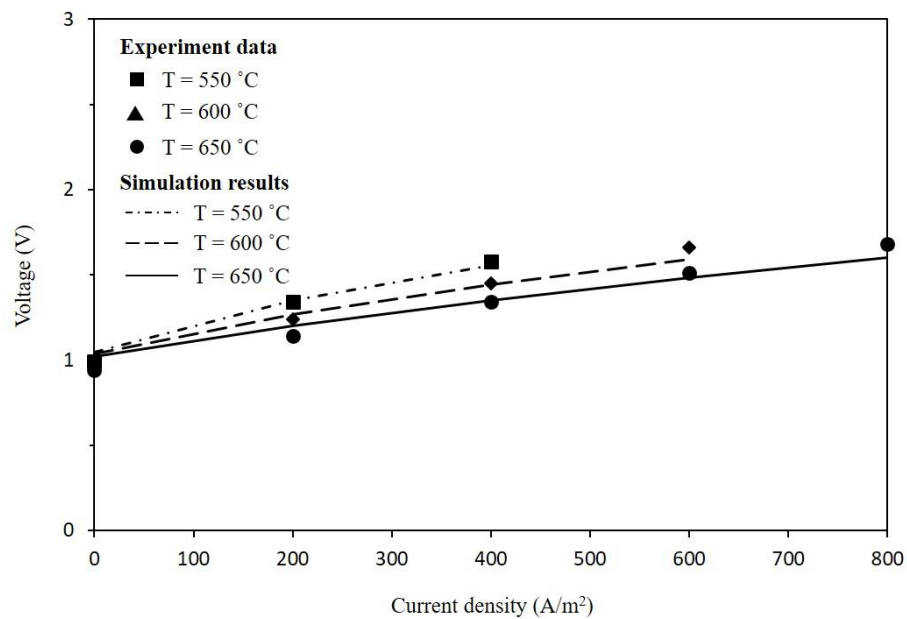
**Figure 4.3** Comparison between the experimental data and simulation results.

Table 4.4 Pre-exponential factor and activation energy values.

k_a ($\Omega^{-1} \text{ m}^{-2}$)	2.802×10^6	$E_{\text{act},a}$ (J mol^{-1})	53,123
k_c ($\Omega^{-1} \text{ m}^{-2}$)	8.569×10^6	$E_{\text{act},c}$ (J mol^{-1})	56,739

Table 4.5 Parameters for effective diffusion coefficient calculations (C. Reid et al., 1959).

	H ₂ O	H ₂	O ₂	CO	CO ₂
σ_i (Å)	2.641	2.827	3.467	3.690	3.941
ε_i/k_B (K)	809.1	59.7	106.7	91.7	195.2

4.2 Dry methane reforming catalyst layer

A dry methane reforming can be simulated through Aspen Plus software via *RGibbs module* (named “DMR”) as shows in Figure 4.4. The *RGibbs* reactor can calculate phase equilibrium and chemical equilibrium composition of each temperature based on Gibbs free energy minimization method. For experiment data validation, the chemical composition reported by Herrera Delgado et al. (2015) was used. They studied regarding syngas production through catalytic dry methane reforming reaction with hydrogen co-reactant over Ni-based catalysts using fixed-bed reactor.

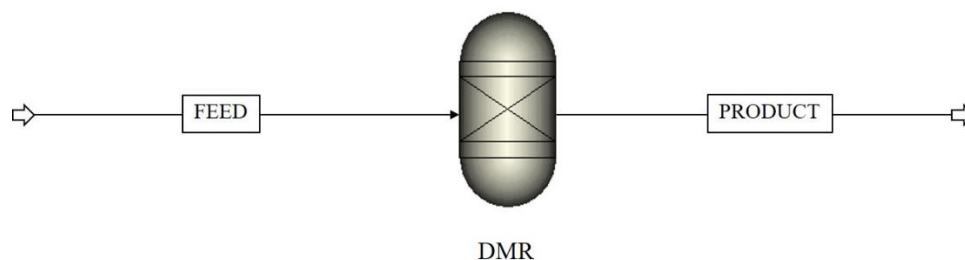
**Figure 4.4** Dry methane reforming flowsheet simulation.

Figure 4.5 shows a schematic drawing of their reactor, the reactor consists of a quartz tube with an inner diameter of 10 mm filled with 20 mg of a Ni-based catalyst with a reaction zone of 27 mm length surrounded by a quartz frit and glass wool. The experiments were carried out at 1 bar total pressure, 4 slpm inlet flow rate (standard liters per minute, $T = 298.15$ K, and 1 bar), residence time of 0.013 s, reaction temperature between 373 and 1173 K at a rate of 15 K/min, and inlet mixture of 1.6% CH_4 , 2.1% CO_2 , and 1.8% H_2 dilute in N_2 .

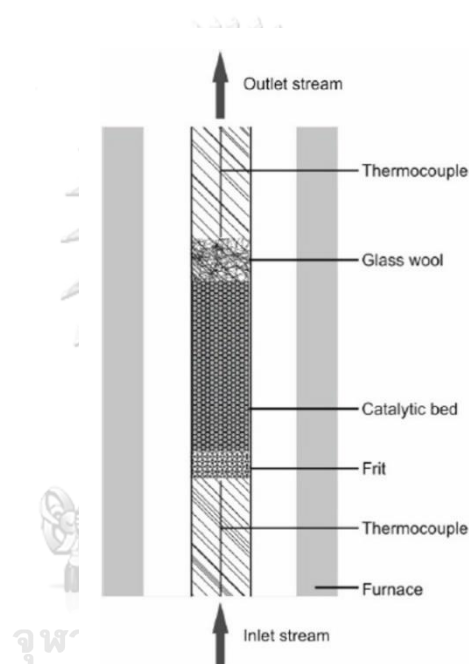
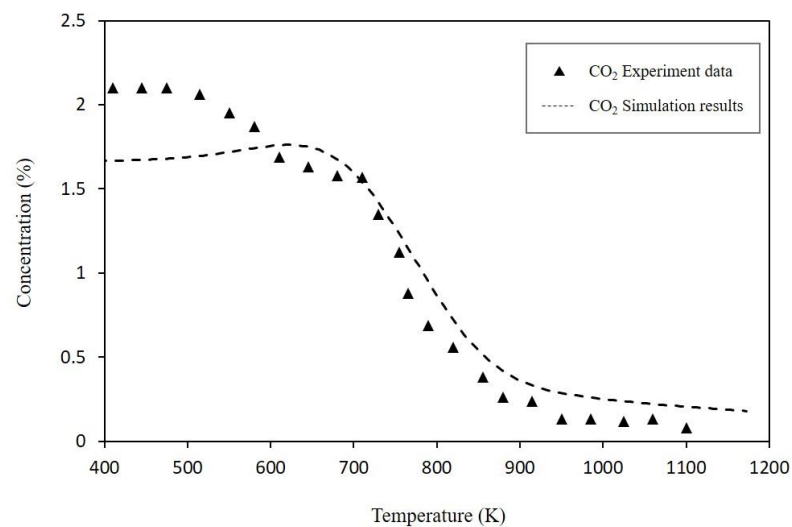


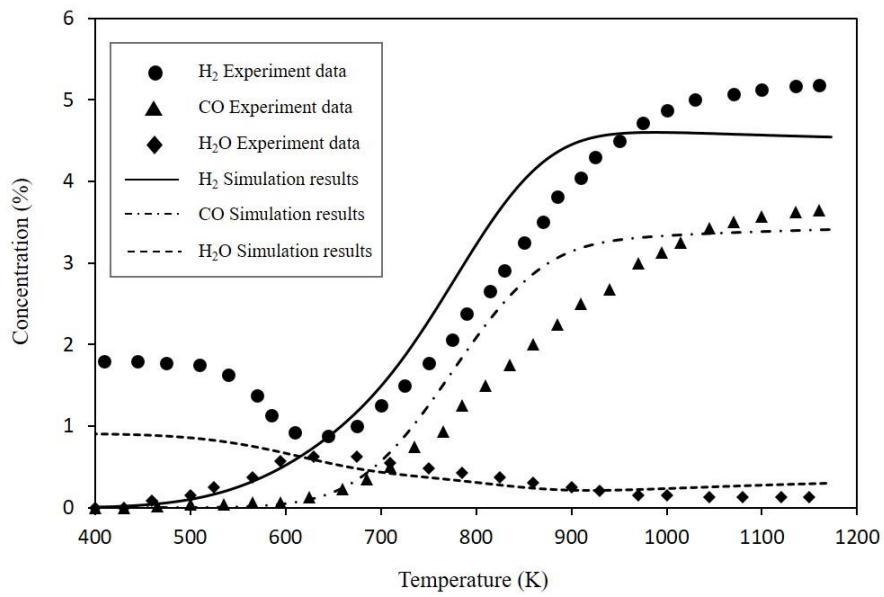
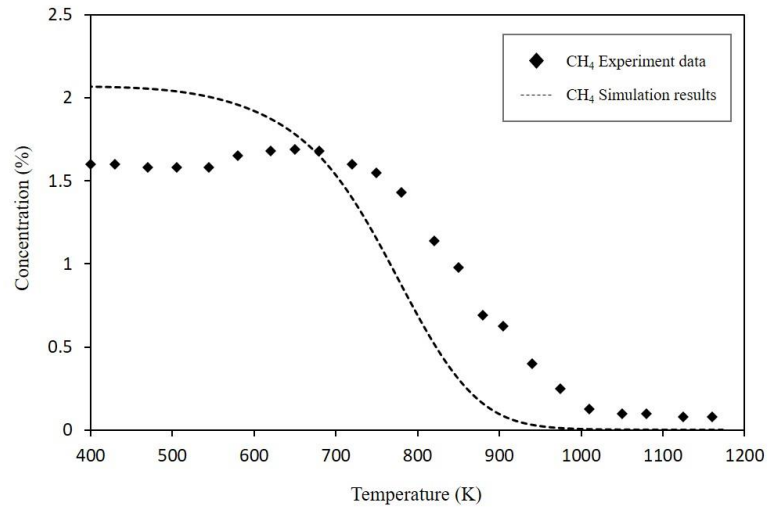
Figure 4.5 Schematic drawing of the packed-bed reactor (Herrera Delgado et al., 2015).

The validation result between experimental data and simulation is shown in Figure 4.6. The experimental data were found good correspond with simulation results in the high temperature regimes. For both experimental and simulation results, CO_2 and CH_4 were suddenly decreased between 700 and 1000 K for the steady state operation of the system, while H_2 and CO show opposite trends. The experimental results show that the water was produced through RWGS and received a maximum water concentration at 400 °C (673 K). The water was used with unconverted methane via

SMR reaction (Eq. 2.17) with an increasing of temperature influence increase of syngas product (Abdullah et al., 2017; Herrera Delgado et al., 2015). For the simulation results, the water and methane are found to increase at low temperature due to present of RWGS and reversible of SMR. At low operating temperatures, the simulation result has more deviation compared to high operating temperatures due to low temperature, low residence time, and limited time of experiment led to kinetic limitations. The operating temperature is observed to be a controlling factor leading to kinetic limitation, as can be seen, at low temperatures the concentration approach to equilibrium condition is much deviate compared to higher temperatures which shows that the process is kinetically limited. In general, kinetic limitations are always present to effect at low temperatures typically below 500°C (Challiwala et al., 2017; Chein et al., 2015).



(a)



(c)

Figure 4.6 Comparison between the simulation results and experiment data of (a) carbon dioxide, (b) methane, and (c) hydrogen, carbon monoxide, and water concentration.

4.3 H-SOEC/DMR for syngas production

The H-SOEC/DMR simulation can be performed by substitute the DMR simulation (Figure 4.4) into a cathode side of the H-SOEC simulation (Figure 4.1). The H-SOEC/DMR flowsheet simulation is shown in Figure 4.7. The component in “CARBON” feed stream was changed from only CO₂ to CH₄ and CO₂ mixture and the “QR” heat stream was represented the heat energy used to sufficient the energy consumed by DMR, SMR, and RWGS reactions occur in the process.

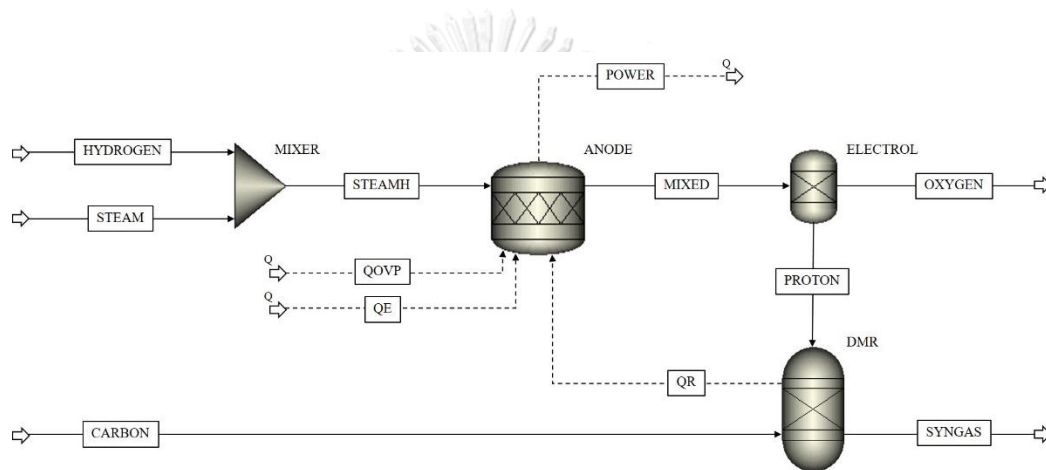


Figure 4.7 Process flowsheet of the H-SOEC/DMR for syngas production.

4.4 Other units in H-SOEC/DMR

The steam generator (SG) and syngas compressor (SC) are perform and connect with the H-SOEC/DMR process in order to evaluate the efficiency of process since water liquid feed until receive compressed syngas product.

4.4.1 Steam generator

Steam generator unit is used to produce a steam from liquid water. The simulation of this unit is shown in Figure 4.8 that include of *Pump module* (named “PUMP”) and *Heater module* (named “HEATER1”) in order to pressurizing and

heating water feed. This unit uses both thermal and electrical energies for steam production. According to steam table, the temperature increases with an increasing of pressure that at the pressure of 5 bar, water has a boiling point of 425 K. In this thesis, the water feed is pressurized at 5 bar and boiled at 427 K, which is higher temperature than boiling point, and aims to change all of water into steam.

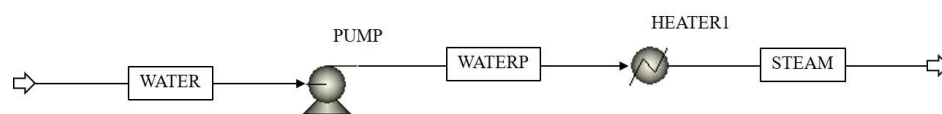


Figure 4.8 Flowsheet simulation of the steam generator unit.

4.4.2 Syngas compressor

Syngas product from the H-SOEC/DMR process always has high temperature due to a high of operating temperature, which needs high capacity to storage this product because gas has high expansion at a high temperature,. In order to reduce the storage capacity, the syngas compressor unit is perform to pressurize and cool syngas product. In this thesis, the 2 stages compressor is used as a syngas compressor. The 2 stages compressor simulation can be performed as shown in Figure 4.9 that the 2 *compressor module* (named “COMP1” and “COMP2”) are connected in series with *cooler module* (named “COOLER2”) between them. The pre and after coolers are simulation via *cooler module* (named “COOLER1” and “COOLER3”, respectively) and the flash separators are simulation via *flash drum module* (named “FLASH1”, “FLASH2”, and “FLASH3”). In order to minimum work done for multiple stages compressor, pressure drop between stages is negligible, the syngas compressor unit should be operated following conditions: (i) the work at each stages are equal (ii) the pressure ratio between stages are equal and (iii) the syngas temperature in the intercooler is cooled equal to the first compressor inlet temperature (also known as

“Perfect intercooler”). To receive the equal work and pressure ratio at each stages, the intermediate pressure can be calculated by Eq. 4.5.

$$P_{\text{inter}} = \sqrt{P_{\text{in}} \times P_{\text{out}}} \quad (4.5)$$

when P_{inter} is the intermediate pressure (atm), P_{in} is the syngas compressor inlet pressure (atm), and P_{out} is the syngas compressor outlet pressure (atm).

In this thesis, the condition of syngas compressor operation is pressure of 30 atm and temperature of 318 K with the isentropic type compressor. The isentropic is performed to be negligible the heat loss of process. For pressure, it has no effects on the syngas composition when storage (Yang et al., 2009), but it has effects on the volumetric. The volumetric is reduced with an increasing of pressure. The pressure of 30 atm is chosen because it is high pressure that reduces the high storage volume and it is an operating pressure for methanol synthesis process. The H/C molar ratio of syngas product from H-SOEC/DMR process is suitable to be feedstock for methanol synthesis process (H/C molar ratio ≥ 2). Syngas storage at the same pressure as methanol synthesis condition influent reduced of energy demand because no further compressor need to compress syngas, when storage syngas used as feed for methanol synthesis process. For temperature, it has no effects on the syngas composition when storage in range of 258 K to 318 K (Yang et al., 2009), but it has effects on the volumetric. The volumetric is reduced with a decreasing of temperature. The temperature of 318 K is chosen because it in the range that recommend. The highest temperature of recommendation range is chosen in order to minimize the cold utility requirement. In addition, it is not a temperature value that is too high to make a high volumetric of syngas storage tank and too low to make a high tar formation on surface of syngas storage tank.

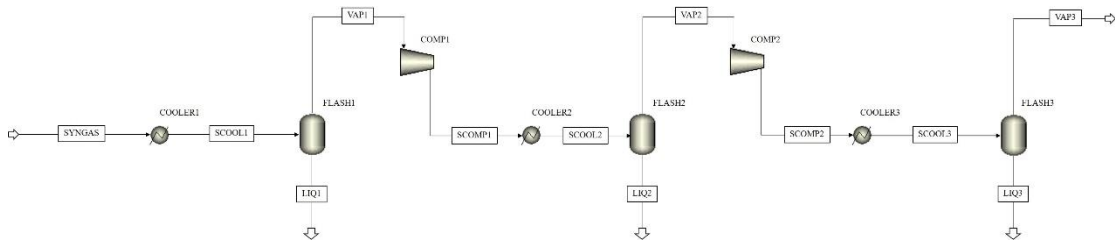


Figure 4.9 Flowsheet simulation of the 2 stages syngas compressor unit.

4.5 Performance analysis

The steam generator (Figure 4.8) and the syngas compressor (Figure 4.9) are connected with the H-SOEC/DMR process (Figure 4.7) and become the overall process as shown in Figure 4.10 under the main assumptions that are described as below:

1. Steady state calculation
2. Zero dimension calculation
3. All of the gases follow ideal gas behavior
4. No heat loss and pressure drop
5. The exchange current density does not depend on electrolyte materials

For energy efficiency calculation of overall H-SOEC/DMR process that is used as performance indicator in this thesis, it can be calculated according to Eq. 2.70. To evaluate performance of overall H-SOEC/DMR process, S/C molar ratio, H/C molar ratio, %CO₂ conversion, %CH₄ conversion, and %Syngas in product can be calculated following Eqs 4.6 – 4.10.

$$\text{S/C molar ratio} = \left(\frac{\dot{N}_{\text{H}_2\text{O},\text{in}}}{\dot{N}_{\text{CO}_2,\text{in}} + \dot{N}_{\text{CH}_4,\text{in}}} \right) \quad (4.6)$$

$$\text{H/C molar ratio} = \left(\frac{\dot{N}_{\text{H}_2}}{\dot{N}_{\text{CO}}} \right) \quad (4.7)$$

$$\% \text{CO}_2 \text{ conversion} = \left(\frac{\dot{N}_{\text{CO}_2, \text{in}} - \dot{N}_{\text{CO}_2}}{\dot{N}_{\text{CO}_2, \text{in}}} \right) \times 100 \quad (4.8)$$

$$\% \text{CH}_4 \text{ conversion} = \left(\frac{\dot{N}_{\text{CH}_4, \text{in}} - \dot{N}_{\text{CH}_4}}{\dot{N}_{\text{CH}_4, \text{in}}} \right) \times 100 \quad (4.9)$$

$$\% \text{Syngas in product} = \left(\frac{\dot{N}_{\text{H}_2} + \dot{N}_{\text{CO}}}{\dot{N}_{\text{H}_2} + \dot{N}_{\text{CO}} + \dot{N}_{\text{CO}_2} + \dot{N}_{\text{CH}_4} + \dot{N}_{\text{H}_2\text{O}}} \right) \times 100 \quad (4.10)$$

when \dot{N}_{CO_2} , \dot{N}_{CH_4} , and $\dot{N}_{\text{H}_2\text{O}}$ are the molar flow rates of CO_2 , CH_4 , and H_2O in product stream, respectively (mol s^{-1}) and $\dot{N}_{\text{CO}_2, \text{in}}$ is the molar flow rate of CO_2 in feed stream (mol s^{-1}).

CHAPTER V

SENSITIVITY ANALYSIS

This chapter presents the effect of parameters on the performance of the H-SOEC/DMR process. The structural parameters analyzed in this work are thickness of cell, support structure, electrode pore size, electrode porosity, and tortuosity. The operational parameters analyzed in this work are temperature, pressure, current density, steam to carbon ratio, and number of cell. In terms of electrochemical performance, it is analyzed with cell voltage, equilibrium voltage, and overpotentials. Additionally, the performance will be analyzed with electrical power, external heat, and heat of overpotential. Syngas production term is analyzed by product molar flow rates, hydrogen to carbon ratio, carbon dioxide and methane conversion, and amount of syngas in products.

5.1 Effect of structural parameters

The structural parameters effect will be investigated only electrochemical term, under the operating conditions (i.e., temperature of 1273 K, pressure of 1 atm, steam to carbon ratio of 1, and number of cell of 500 cells), to find the structural value that receives the minimum of the electrical energy required for the system. In this section, the key parameters are thickness of cell, support structure, electrode pore size, electrode porosity, and tortuosity. The sensitivity analysis and cell voltage calculation are performed in order to find the structural value that minimize the electrical energy demand. The indicator of this section is cell voltage. At current density constant, if cell voltage reduces, it means that decreasing in the required electrical energy is obtained following Eq. 2.59. Additionally, the effective structural value will be used as constant parameters for the operational parameters analysis section.

5.1.1 Effect of thickness of cell and support structure

The effect of thickness of cell (anode, cathode, and electrolyte) is studied in range of 50 to 500 μm . The analyzed side was varied, while the other sides were set at 50 μm , under the operating conditions (i.e., temperature of 1273 K, pressure of 1 atm, current density of 11000 A m^{-2} , steam to carbon ratio of 1, and number of cell of 500 cells). Figure 5.1 shows the result of calculated cell voltage when varying the thickness of each side of cell. The cell voltage increases with increasing of anode, cathode, and electrolyte sides because the increase of transfer length in each side increases the ohmic overpotential for electrolyte side and also increases the concentration overpotential for anode and cathode sides. It can be seen that the thickness of electrolyte gives the most cell voltage while the thickness of cathode gives the lowest value. From results, the thickness of electrolyte should be low in order to minimize the electrical energy demand of system but it has covenant that the electrolyte must be wide enough to prevent the recombination of hydrogen and oxygen, but it must not be too wide in order to minimize an ohmic overpotential.

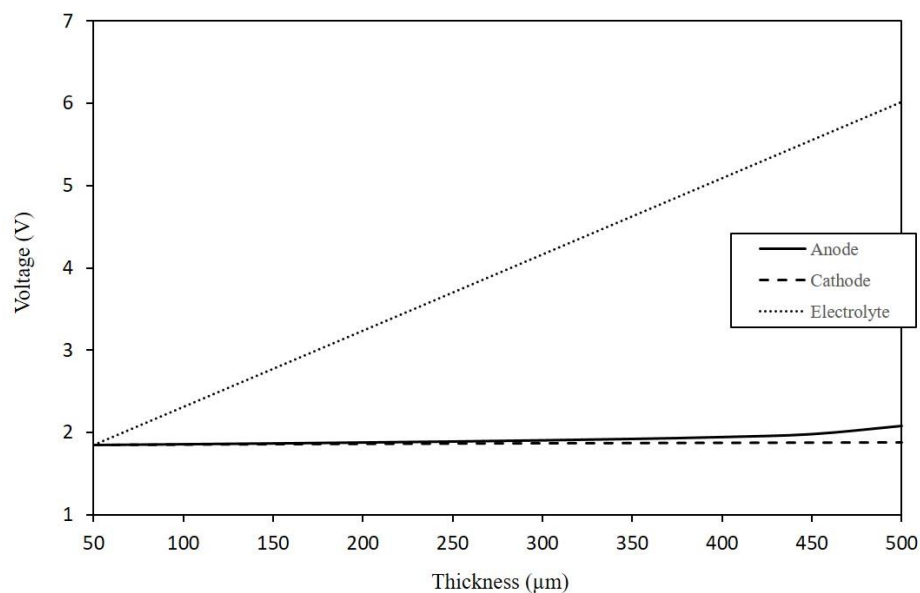
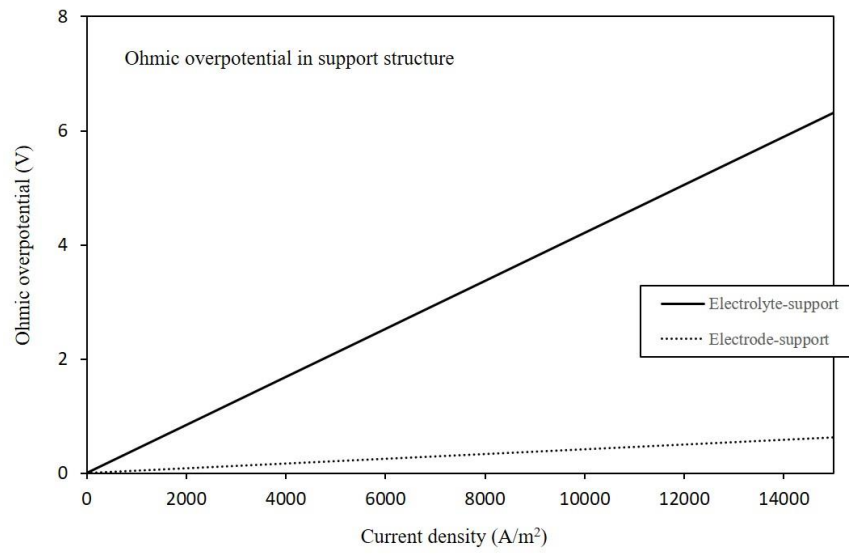
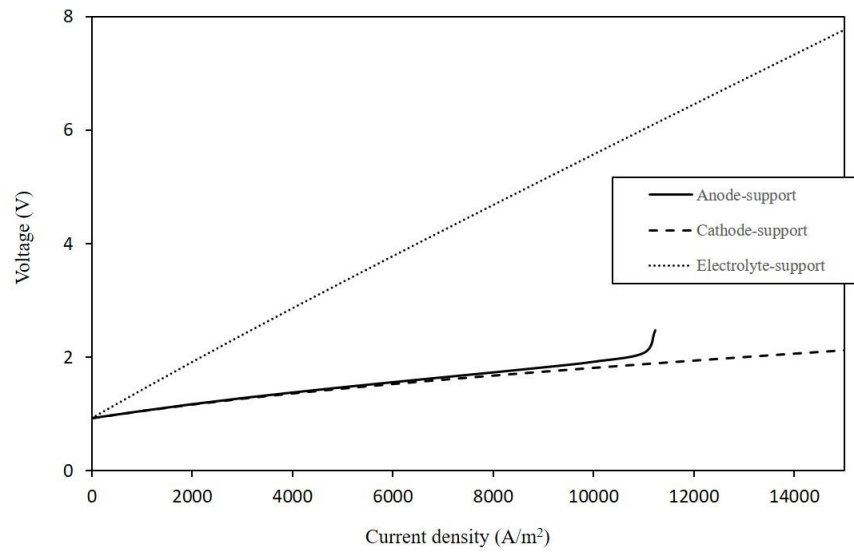


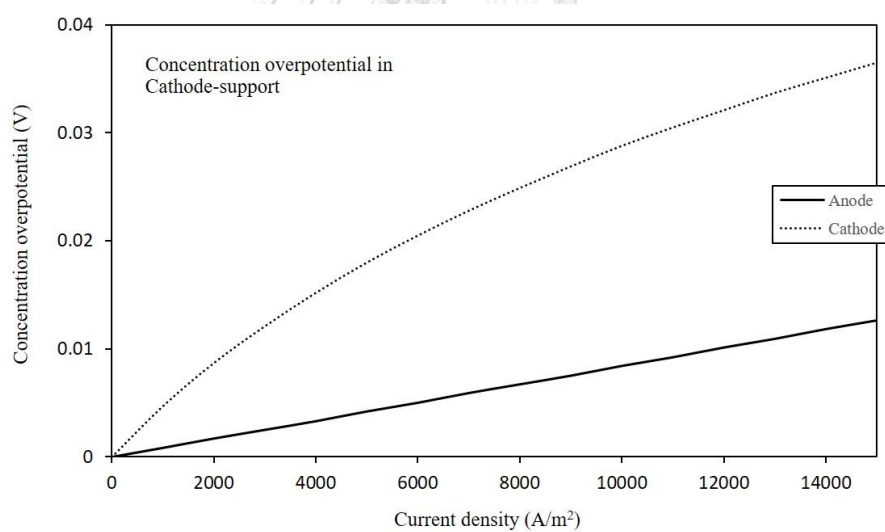
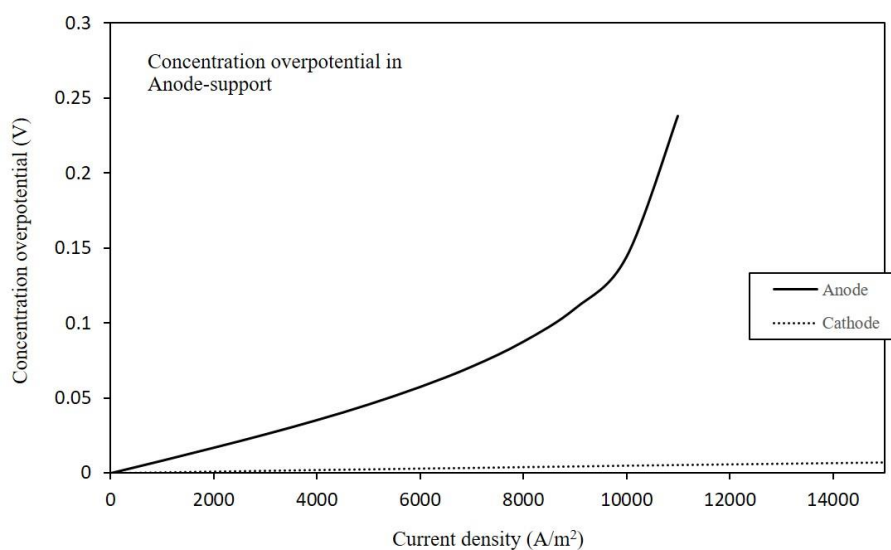
Figure 5.1 Effect of thickness of anode, cathode, and electrolyte on the performance of system.

For the support structure, it can be either anode supported, cathode supported, or electrolyte supported. From the design point of view, it is important to know that a particular support type is more helpful than the others. In this part, the three types of support are analyzed in terms of electrochemical performance. The thickness of supported side was set at 500 μm and the other sides were set at 50 μm .

The J-V characteristics of system with different support structures are shown in Figure 5.2. The best performance is the cathode-supported as it has the lowest electrical energy requirement (Figure 5.2a). At the cathode side, the transport of proton (H^+) is not limited by the porous media structure. Thus, there is no limiting current for the cathode, even the cathode has large thickness. Additionally, the small molecular weight of the product (H_2) promotes its transport. As a result, the resistance of the porous cathode to the gas transport is very low, and influent low concentration overpotential (Figure 5.2d). Same to the cathode-supported configuration, the anode-supported has extremely lower voltage than the electrolyte-supported due to the reduction of ohmic overpotential (Figure 5.2b). However, the cell voltage of the anode-supported increases sharply at a current density of about 11000 A m^{-2} , which is the limiting current density for the thick anode (Figure 5.2a). The limit of thick anode due to the transport of the reactant at the anode (H_2O) has reached the anode-concentration overpotential that its limit (Figure 5.2c). Unlike the cathode, the steam reactant at the anode is transported through the pores; thus, its transport depends on the porous structure of the electrode. The consumption of H_2O can result in a lower pressure inside the porous anode than the anode surface (pressure gradient). This pressure gradient increases with increasing current density and promotes the transport of steam from the anode surface to the anode-electrolyte interface. However, the transport of oxygen (product) from the anode-electrolyte interface to the anode surface is resisted by this pressure gradient. Regarding the small pressure difference between the anode-electrolyte interface and anode surface (less than 10%) at low current density, the effect of pressure gradient on the transport of steam and oxygen is small. The high molecular weights of steam and oxygen result in low effective diffusion coefficient of steam ($D_{\text{H}_2\text{O}}^{\text{eff}}$), lead to high concentration overpotential.



(b)



(d)

Figure 5.2 Evaluation of anode-supported, cathode-supported, and electrolyte-supported for system (a) J-V characteristics, (b) ohmic overpotential of electrolyte-supported and electrode-supported, (c) concentration overpotentials in an anode-supported, and (d) concentration overpotentials in a cathode-supported.

5.1.2 Effect of electrode pore size

A pore size is the one of an important parameter for the gas transport characteristics in the porous media electrode layer. The J-V curves of a system with electrode pore radius of 0.3, 0.4, and 0.5 μm are shown in Figure 5.3. The pore size increases with decreasing of the cell voltage. As increase of pore size, the gas transport within porous media structures becomes easier, lead to lower concentration overpotentials as well as higher anode limiting current density. The pore size effect would be more pronounced for an anode-supported configuration because the resistance to gas transport in the porous anode is the dominant factor of overpotential. However, the pore size value should not be too much because the increase in pore size has effect on the reducing in active area of electrodes.

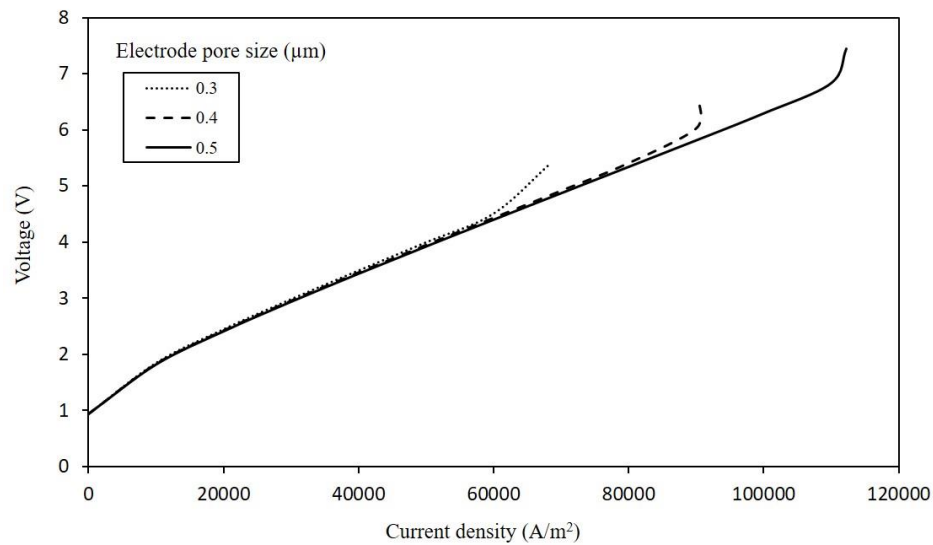


Figure 5.3 Effect of electrode pore size on J-V characteristics of cathode-supported configuration.

5.1.3 Effect of electrode porosity

The electrode porosity effect on anode and cathode concentration overpotentials were combined, the porosity effect on J-V curve was shown as Figure 5.4. A high porosity is advantageous, as more space is available for gas transport, lead to smaller concentration overpotential and higher anode limiting current density. However, recent experimental research have revealed that too high porosity (around 0.76) is harmful as the electrolyte becomes non-gas tight, led to reducing of Nernst potential (Zhao and Virkar, 2005). In addition, as a porosity of 0.57 did not reveal any reducing of Nernst potential in Zhao and Virkar's experiments, thus a recommend optimal porosity is between 0.5 and 0.6. Additionally, the current paper assumes that electrochemical reaction performed only at the electrode-electrolyte interface. However, in an advance composite electrode, a reaction area is extended from the interface to inside of electrode. The increase in porosity reduces concentration overpotential, but it can increase activation overpotential because of less active surface area available (Chan et al., 2004; Chan and Xia, 2001). Thus, the system performance cannot be further increased when the porosity exceeds a certain value.

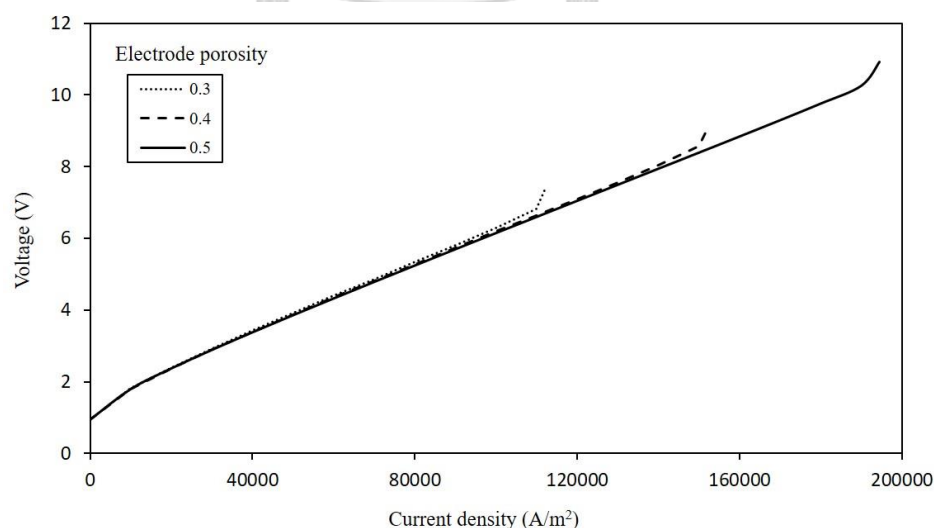


Figure 5.4 Effect of electrode porosity on J-V characteristics of cathode-supported configuration.

5.1.4 Effect of electrode tortuosity

In geometrical terms, tortuosity is defined as the fraction of the shortest pathway flow through a porous structure and the Euclidean distance between the starting and end point of that pathway, thus the tortuosity value is always equal to or greater than unity. For a porous structure, there only one shortest pathway and one tortuosity value are exist. The tortuosity plays as an essential role in the transport of mass and charge in electrochemical devices to determine the concentration overpotential losses at high current densities due to mass transport limitations. As tortuosity is notoriously difficult to ascertain, a many of method has been developed to find the tortuosity of a structure. The tortuosity-porosity relationship is one of the most fundamental and simply to derive a tortuosity. The Maxwell and Bruggeman relation (Eq. 5.1) is used as the tortuosity-porosity relation to calculated tortuosity (Matyka et al., 2008). When the increase in porosity (n) decreases the tortuosity (ξ).

$$\xi = (1.5 - 0.5n)^{\frac{1}{2}} \quad (5.1)$$

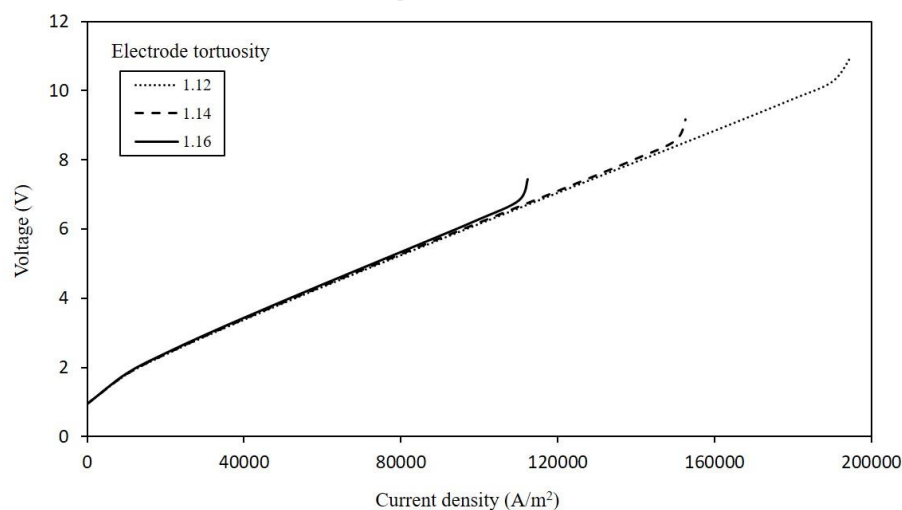


Figure 5.5 Effect of electrode tortuosity on J-V characteristics of cathode-supported configuration.

Figure 5.5 shows J-V characteristics of tortuosity effect that contrast with the results from porosity effect (Figure 5.4), which follow the porosity-tortuosity relation. A high tortuosity is disadvantageous, as less space is available for gas transport, lead to larger concentration overpotential and lower anode limiting current density.

The structural parametric analysis indicates that the ohmic overpotential and the anode concentration overpotential are sensitive to the electrolyte and the anode thicknesses, respectively. As a result, the cathode-supported cell configuration is most favorable for H-SOEC/DMR in order to achieve the lowest overpotentials. For the cathode-supported configuration, the thickest side is cathode and is set of 500 μm thick, when other sides are set of 50 μm thick. Furthermore, to improve the performance, thin anode and electrolyte should be used. Although, the typical thicknesses of anode and electrolyte of a cathode-supported cell are 50 μm , thinner layers around 10 μm thick are possible (Zhao and Virkar, 2005). However, it is noteworthy that the thermal and mechanical stresses should be carefully considered when very thin cell thicknesses are used. Additionally, it is found that large electrode pore size and porosity are desirable to reduce resistance of gas transport. In this thesis, the pore size of 0.5 μm and porosity of 0.5 are selected. Moreover, the tortuosity analysis indicates that it has effect on cell performance and it depends on porosity-tortuosity relation. From the structural analyze, all of favorable parameter values are used as constant parameters in the operational analyze section to achieve the most performance process.

5.2 Effect of operational parameters

The operational parameters effect will be investigated both electrochemical and syngas production terms, aims to evaluate the influent of operational parameters change on the cell performance. In this section, the key parameters are S/C ratio, current density, temperature, pressure, and number of cell. The sensitivity analysis and cell voltage calculation are performed in order to indicate the effect of parameters on cell performance. The performance of the process is expressed in terms of cell voltage, heat and electrical energies demand, CO_2 and CH_4 conversions, and amount of syngas in

products. Additionally, the effective structural value from the previous section will be used as constant parameters for the operational parameters analysis and the input parameters of this section are summary in Table 5.1 based on simulation flowsheet as Figure 4.10.

Table 5.1 Input parameters and operating conditions for operational parameters analysis.

Operating temperature, T (K)	1073 to 1273
Operating pressure, P (atm)	1 to 5
Current density, J ($A\ m^{-2}$)	500 to 2500
S/C ratio	0.5 to 2
Number of cell, N_{cell} (cell)	100 to 500
Anode stream inlet composition	95 mol% H_2O /5 mol% H_2
Cathode stream inlet composition	50 mol% CO_2 /50 mol% CH_4
Steam utilization factor, U_s (%)	80
Electrolyte conductivity, ρ_e ($S\ m^{-1}$)	$3.14 \times 10^4 / T \times \exp(-3.86 \times 10^3 / T)$
Active cell area, A (m^2)	0.04
Electrode pore radius, r (μm)	0.5
Electrode porosity, n	0.5
Electrode tortuosity, ξ	$(1.5 - 0.5n)^{1/2}$
Cell thickness	
Anode thickness, d_a (μm)	50
Cathode thickness, d_c (μm)	500
Electrolyte thickness, l_e (μm)	50

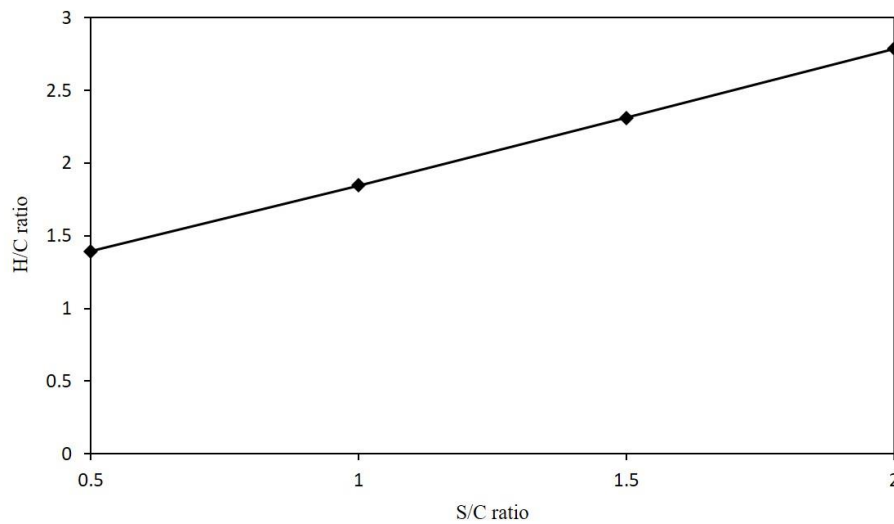
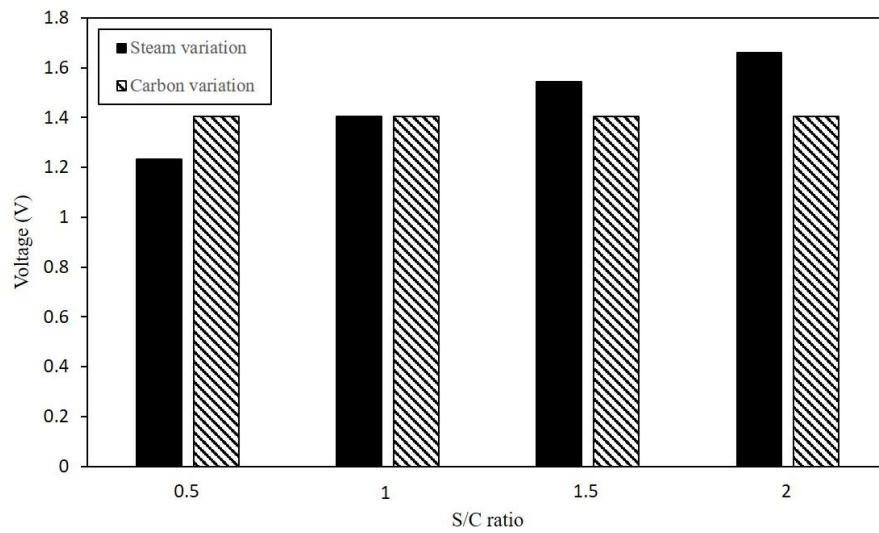
5.2.1 Effect of S/C molar ratio

This section have focused the influence of the S/C molar ratio on the cell voltage and the H/C molar ratio of syngas product stream. The S/C molar ratio was varied from 0.5 to 2, under the operating conditions (temperature of 1073 K, pressure of 1 atm, and number of cell of 500 cells). To determine the variations in S/C ratio, the 2 methods are used in this study: (i) the steam molar flow rate is specified in order to find the carbon stream molar flow rate, and (ii) the carbon stream molar flow rate is specified in order to find the steam molar flow rate. For simulation term, the steam (or carbon stream) molar flow rate is set at 1 kmol hr⁻¹ and varied the carbon stream (or steam) until reached the desired S/C molar ratio.

The effect of S/C molar ratio on cell voltage is shown in Figure 5.6a. The results indicates that the S/C molar ratio do not affect the cell voltage when the carbon stream molar flow rate is varied. In contrast, the increase in steam molar flow rate increases the cell voltage. According the Eq. 4.1, only the steam molar flow rate has a significant effect on the current density calculation for a given steam utilization load, result in a current density constant, when the carbon stream molar flow rate is varied. Additionally, it can be explained that the carbon stream molar flow rate do not have an effect on the cell voltage because the conversion of carbon dioxide and methane are not involve in the electrochemical reaction. This is in contrast to increasing the steam molar flow rate that the current density is increased for achieving 80% of steam utilization. Moreover, a higher of current density has effect on a higher in cell voltage and electrical power.

For the H/C molar ratio term, the result shows that the H/C molar ratio increases with an increasing steam flow rate or a decreasing carbon stream flow rate, as shown in Figure 5.6b. At high S/C molar ratio, less in the carbon stream molar flow rate that is appearance as carbon source decreases amount of carbon monoxide produce, result in a higher of H/C molar ratio. In this study, the favorable H/C molar ratio is molar ratio that equal to or higher than 2, which is suitable for methanol and long-chain hydrocarbon synthesis applications. In conclusion, the S/C molar ratio of 2 is selected

because it shows the highest of H/C molar ratio and higher than 2. In order to adjust the S/C molar ratio, the carbon stream is varied to minimize the cell voltage of system.



(b)

Figure 5.6 Effect of the S/C molar ratio (a) on the cell voltage and (b) on the H/C molar ratio.

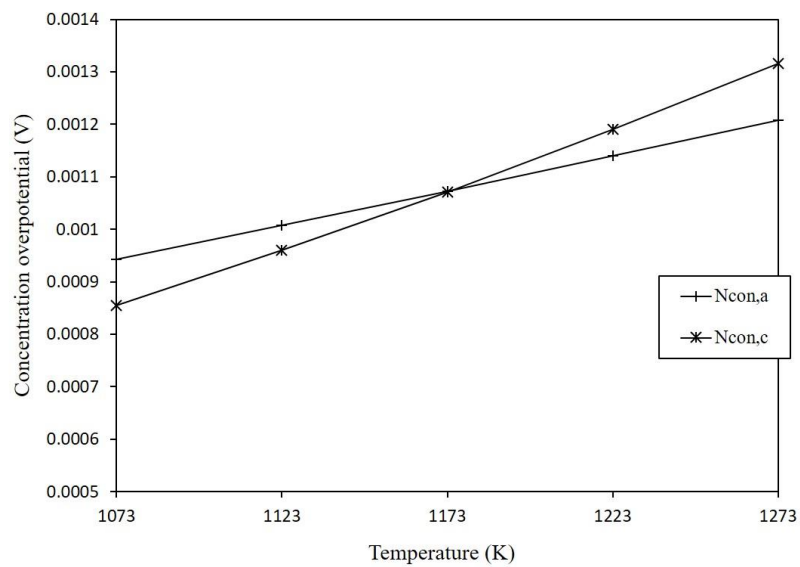
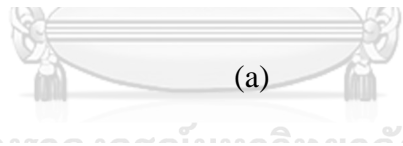
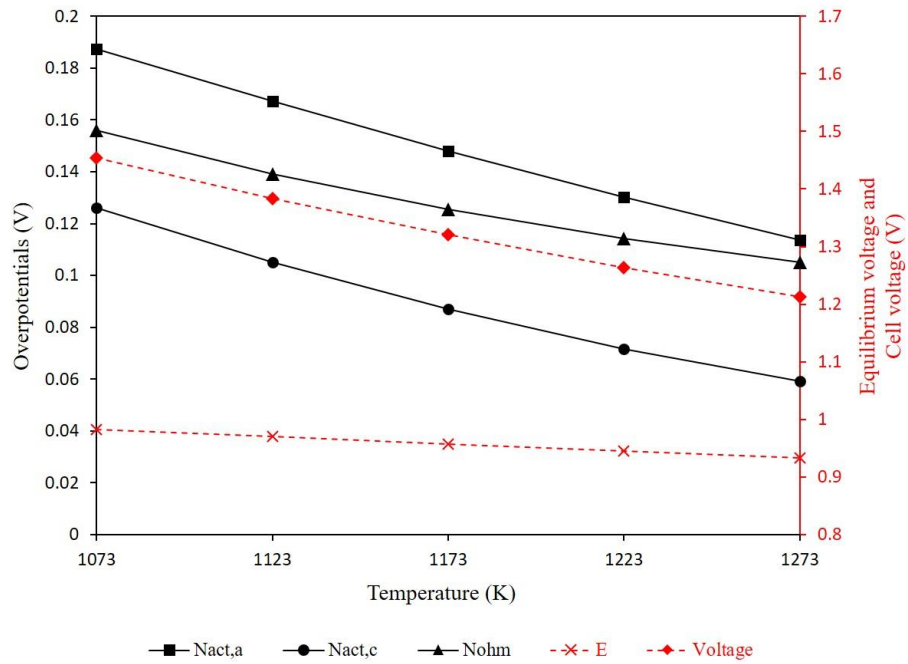
5.2.2 Effect of temperature

The effect of operating temperature on the cell performance is investigated in both electrochemical and syngas production terms by varying the temperature in the range of 1073 to 1273 K because it is the operating temperature of both H-SOEC and DMR processes, under operating conditions (pressure of 1 atm, S/C ratio of 2, current density of 2500 A m⁻², and number of cell of 500 cells). The variations in cell voltage, equilibrium voltage, and overpotentials are shown in Figures 5.7a and 5.7b.

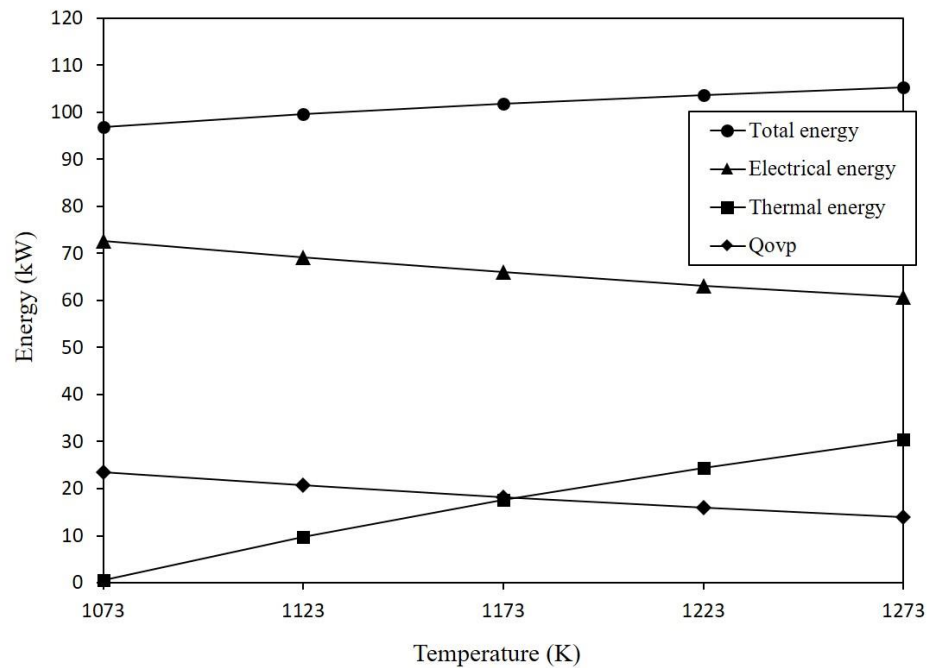
The simulation results indicates that an increase in the temperature decreases the equilibrium voltage and cell voltage. For the equilibrium voltage, according to the thermodynamic relation that increasing of temperature can reduce electrical energy demand, but it increases the thermal energy demand of system. When the operating temperature increases, the increase in electrochemical kinetic energy of steam electrochemical reaction increases the electrochemical rate in both electrodes and decreases the activation overpotentials in both anode and cathode sides. For the ohmic overpotential, the resistance of ionic conductivity in the electrolyte layer, it is reduced by increasing temperature because the increase in conductivity of electrolyte decreases the resistance of ionic conductivity. On the other hand, the concentration overpotentials has opposite result with other overpotentials, it increases with the operating temperature because the increase in steam effective diffusion coefficient, which decrease molar diffusion rate, lead to the increase in the mass transfer resistance between the electrodes and electrolyte. The value of activation and ohmic overpotentials is more significant than concentration overpotentials. Thus, the results of the effect of temperature on the cell voltage show the same trend as the activation and ohmic overpotentials that increasing temperature can be reduce the cell voltage of system.

Figure 5.7c, shows the results regarding the energy demand. For the total energy demand, overall energy for all of the reactions, slightly increases with the operating temperature due to the system need more energy to sufficient the electrochemical and chemical reactions when temperature increased. At the current density constant, reduced in cell voltage when increases temperature result decreased electrical energy demand of system, while the thermal energy demand increased in order to sufficient the

total energy demand of system. Additionally, the heat of overpotential, heat generated from overpotential, which depend on value of the overpotential, was decreases with an increasing of temperature. The heat of overpotential is a heat that can be supplied to system that decreases in it led to increases the thermal energy demand.



(b)

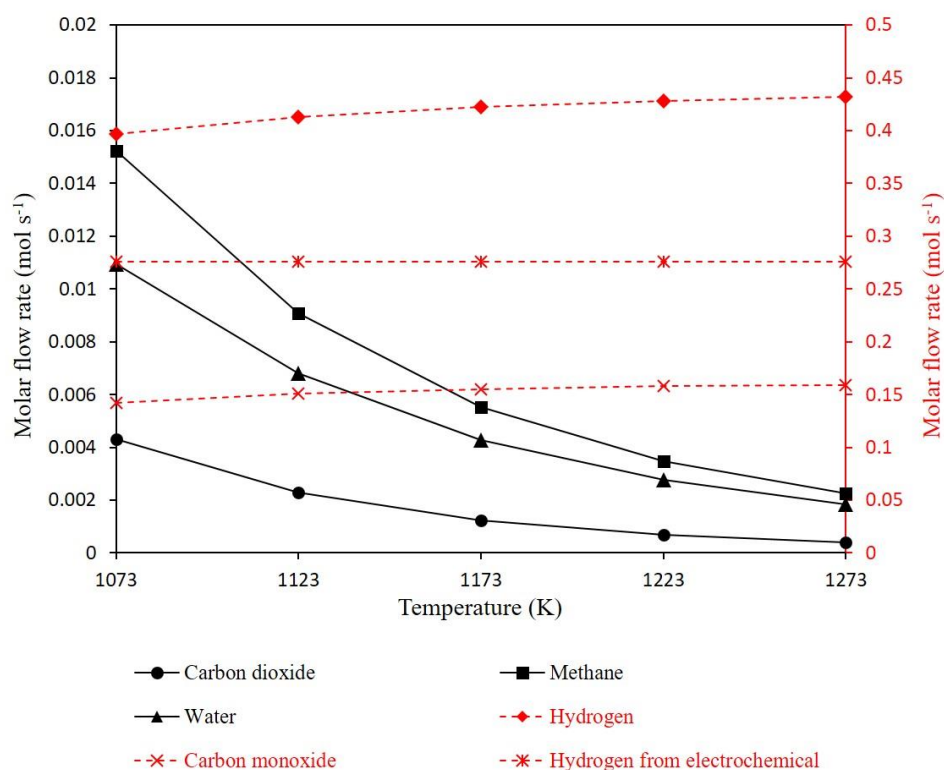


(c)

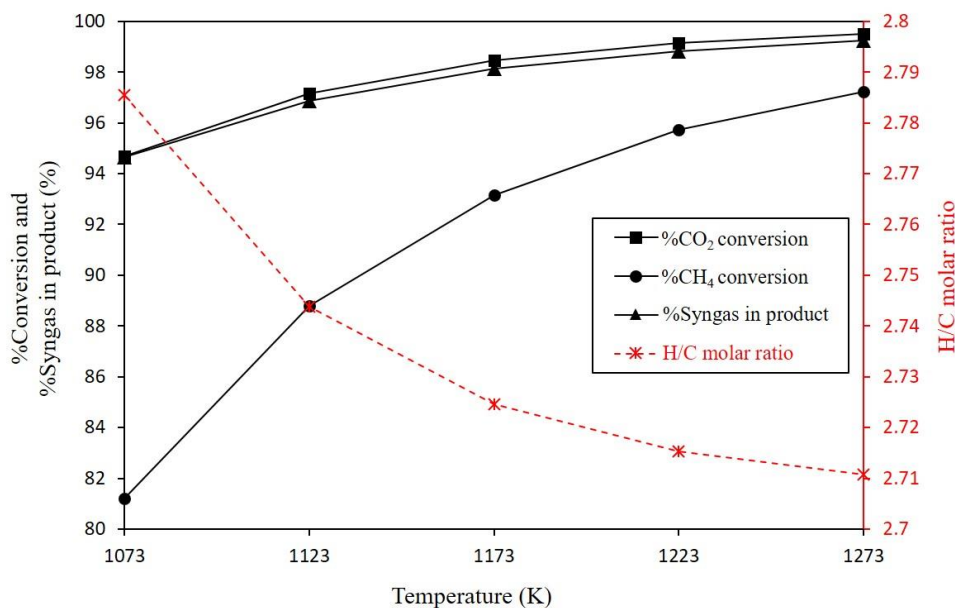
Figure 5.7 Effect of operating temperature on (a) the cell voltage, equilibrium voltage, activation and ohmic overpotentials, (b) the concentration overpotentials, and (c) the energy demand of system.

For the syngas production term, Figures 5.8a and 5.8b indicates that changing in operating temperature has effect on syngas production. The molar flow rate of H₂ and CO in product stream are found to increase with increasing of operating temperature because of the endothermic reactions that produced syngas are favorable at the high temperature. The content of H₂ shows higher value than CO in every single point of temperature because the further constant H₂ is produced via electrolysis reaction, result in the H/C ratio of syngas in product stream always higher than 2 that is favorable value. On the other hand, the molar flow rates of CO₂, CH₄, and water in product stream are found to decrease with increasing of operating temperature due to increase of reforming reaction rates at high temperature, lead to increase of CO₂, CH₄, and water consumption. For the CO₂, %CO₂ conversion increases with increasing temperature because CO₂ is consumed with both CH₄ and H₂ via DMR (Eq. 2.15) and

RWGS (Eq. 2.16) reactions, respectively, which are the endothermic reactions that are favorable at the high temperature. The presence of RWGS results in generated of water in product stream. For the CH_4 , as the temperature increases, the CH_4 is consumed with both CO_2 and water via DMR and SMR, respectively, result in the increase of the % CH_4 conversion. The presence of SMR decreases water molar flow rate in product stream with increasing temperature. As the operating temperature increases, the CO_2 , CH_4 , and water consumption are increased, lead to higher %Syngas in product. However, the H/C ratio of syngas in product stream seems to be slightly decreased with increasing temperature because higher of carbon content consumption leads to higher in CO molar flow rate.



(a)



(b)

Figure 5.8 Effect of operating temperature on (a) product stream molar flow rate and (b) %CO₂ and CH₄ conversions, %Syngas in product, and H/C molar ratio.

In conclusion, the operating temperature has significant effect on both electrochemical and syngas production terms. For the electrochemical term, as the temperature increases, the cell voltage was decreased result in a decreasing of electrical energy demand of system, which is the major cost in electrolysis process. As decrease in electrical energy demand and heat of overpotential, the thermal energy demand of increases and is advantageous as it provides more opportunities to utilize industrial waste heat or to utilize alternative heat sources. For syngas production term, as temperature increases, higher consumptions of CO₂, CH₄, and water are achieved and results in higher of %CO₂ (higher than 90%) and %CH₄ conversions (higher than 80%), %Syngas in product, and H₂ and CO productions. Additionally, the H/C ratio was higher than 2 due to a constant H₂ further produced from electrochemical, which is not affect by temperature.

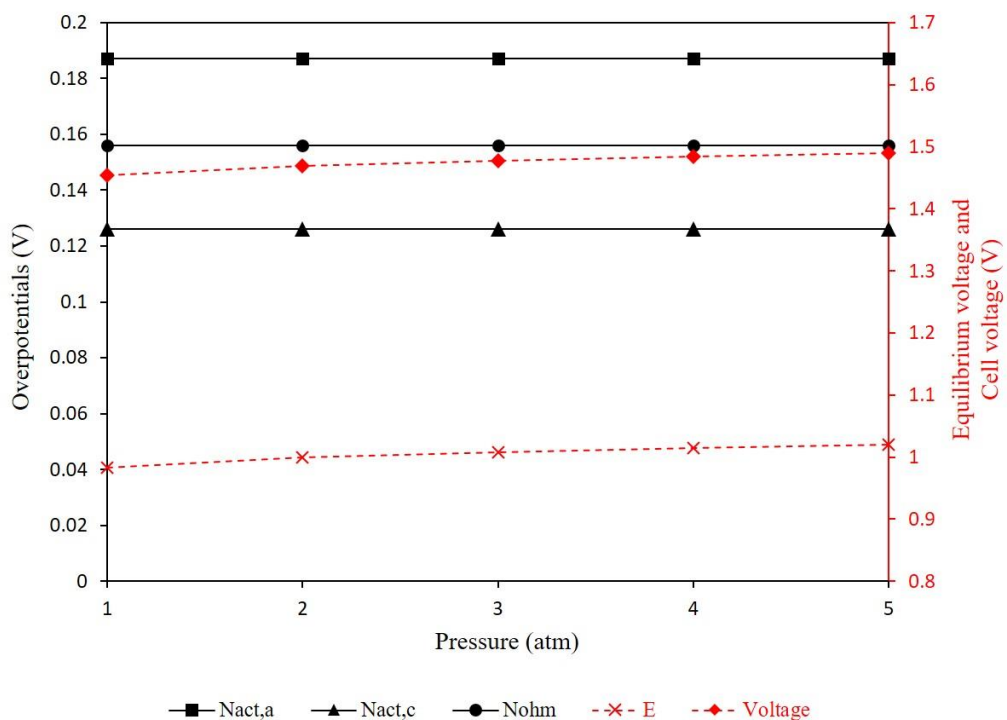
5.2.3 Effect of pressure

Pressure is the one of operating parameter that has effect on both H-SOEC and DMR processes. For this reason, the H-SOEC/DMR process should be performed the pressure analysis on performance of system. The effect of operating pressure is investigated by varying the temperature in the range of 1 to 5 atm in order to find the effect of pressure change on process performance, under the operating conditions (temperature of 1073 K, current density of 2500 A m⁻², number of cell of 500 cells, and S/C molar ratio of 2). The simulation results are discuss as below.

Figure 5.9a and 5.9b show the effect of pressure on the electrochemical value of process. The pressure has not effect on the activation and ohmic overpotentials because pressure has not effect on the electrochemical kinetic energy and ionic conductivity of system, respectively, thus the activation and ohmic overpotentials are constant in every single point of pressure values. For the equilibrium voltage term, increasing the operating pressure slightly increases the equilibrium voltage; as a result, the Nernst equation depends on the partial pressure. For the concentration overpotentials, both anode and cathode concentration overpotentials decrease with increasing of operating pressure. According to previous research, the molecular diffusion coefficient ($D_{H_2O-O_2}$), was inversely proportional to the pressure, but the Knudsen diffusion coefficient ($D_{H_2O,k}$) was not depend on pressure. Therefore, the effective diffusion coefficient ($D_{H_2O}^{eff}$), was less sensitivity to pressure. On the other hand, the gas density increased with pressure (Ni et al., 2007b). The combined effect results in an increase in molar diffusion rate and a decrease in concentration overpotentials at high pressure. The increase of equilibrium voltage increase is higher than the decrease of concentration overpotentials, lead to an increase of cell voltage.

For the energy term, the simulation results are shown in Figure 5.9c. An increase in operating pressure results in the total energy demand decreases because the chemical reaction rates in cathode are reduced and that makes the process needs a lower energy to sufficient. At the current density constant, the electrical energy demand slightly increases because of an increasing of cell voltage. In contrast, the heat of overpotential

slightly decreases due to a decrease in concentration overpotentials. At a higher operating pressure, the process is operated as an exothermal system that results in the process does not need the external thermal energy demand. For the exothermal operation, it is achieved at a higher operating pressure because of a decrease in total energy demand of process and an increase in electrical energy of process. Additionally, the electrical energy is combined with heat of overpotential, which represents a heat energy produced from overpotential and supplied to process. The energy supply value is higher than the total energy demand of process and that makes the process is operated in the exothermal system. Although, the heat of overpotential supplied decreases with an increasing of operating pressure, but it is smaller than a decreasing in total energy demand, result in an increase of the exothermal energy of process.



(a)

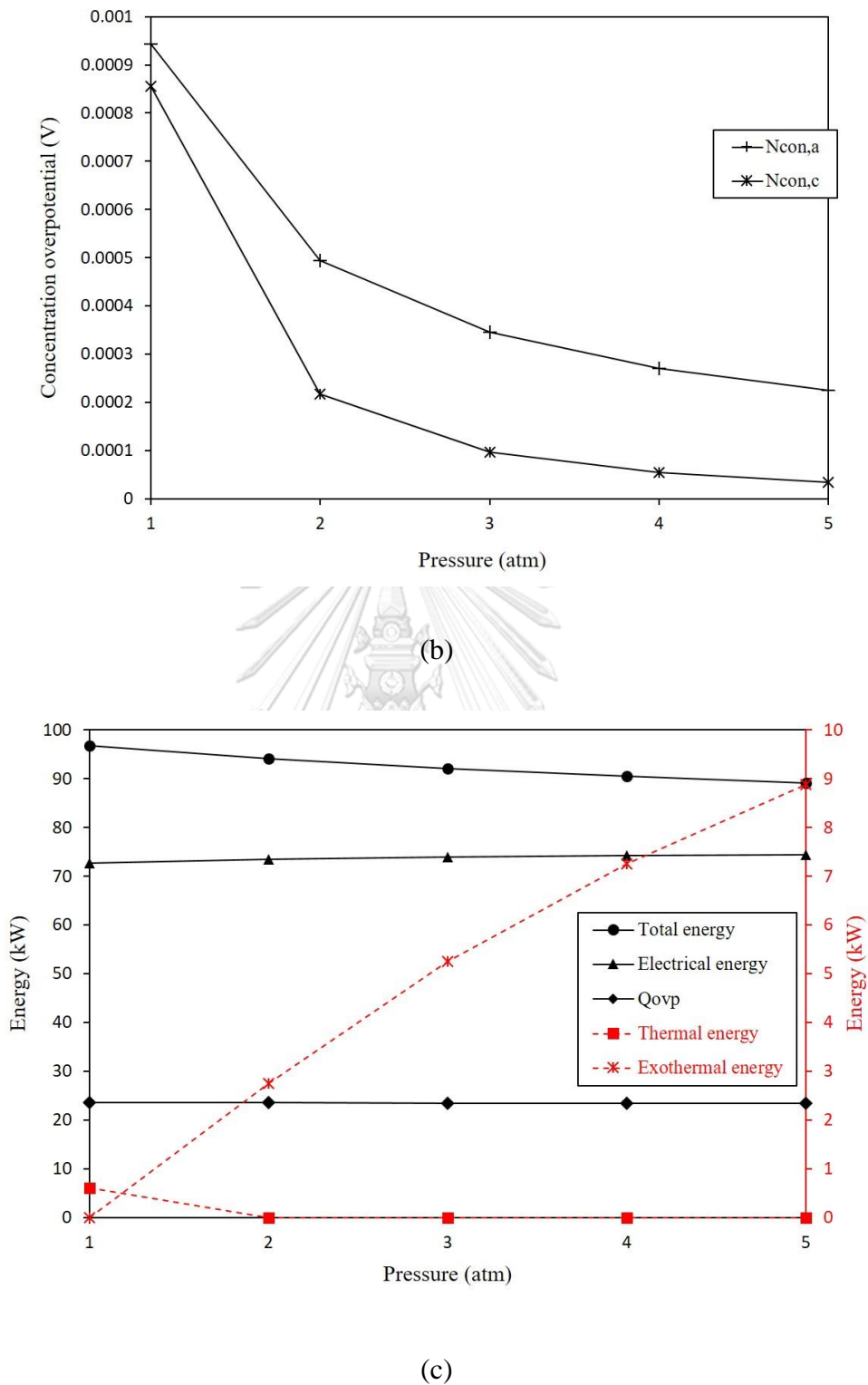
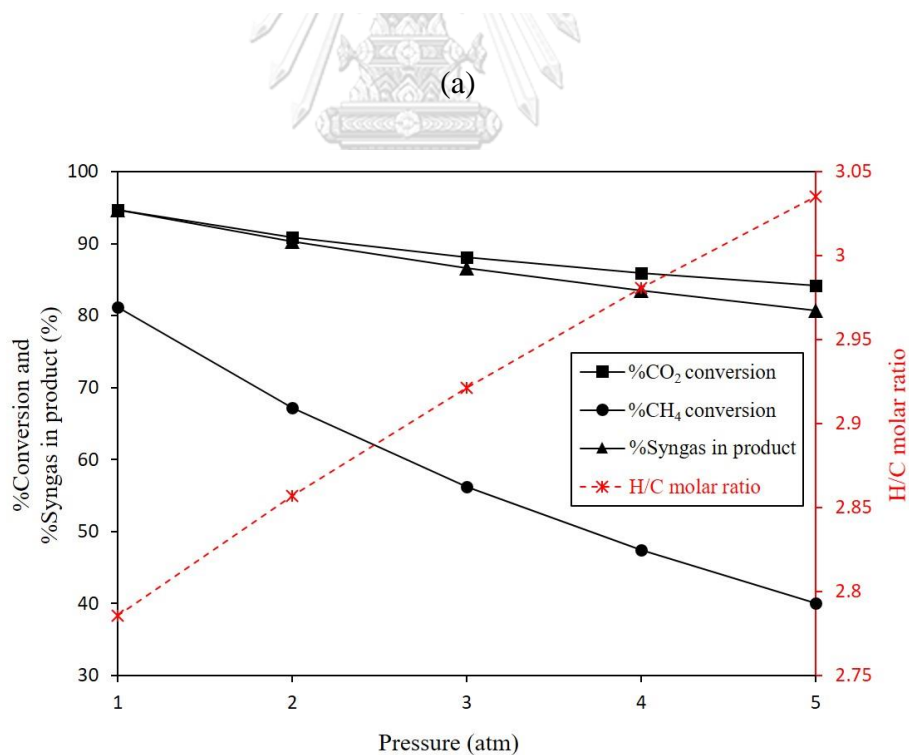
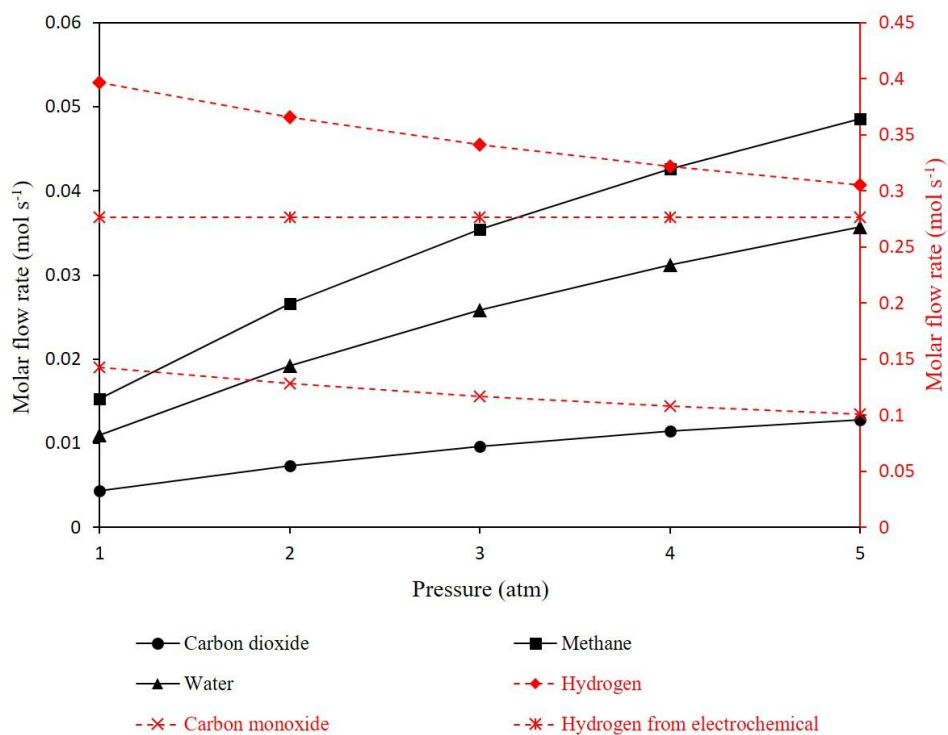


Figure 5.9 Effect of operating pressure on (a) the cell voltage, equilibrium voltage, activation and ohmic overpotentials, (b) the concentration overpotentials, and (c) the energy demand of system.

For the syngas production term, the simulation result of pressure changed are shown in Figure 5.10a and 5.10b. As the operating pressure increase, the amounts of CO_2 and CH_4 in the product stream are found to increase, result in the calculated % CO_2 and % CH_4 conversions are found to decrease. For the CO_2 , it can be consumed with CH_4 and H_2 via the DMR and RWGS, respectively, thus the conversion of CO_2 was higher than CH_4 . The presence of RWGS result in part of the H_2 , which was produced, was being consumed to produce water, result in appearance of water in product stream. For the CH_4 , it can be further consumed with water through the SMR. As reported from previous research (Gopaul and Dutta, 2015), the suitable operating pressure of DMR and SMR was the atmospheric pressure and when the increase in pressure increased reduced the CO_2 , CH_4 , and water consumptions and increased the amount of those in product stream. The H_2 and CO are found to decrease with increasing of operating pressure because of decrease in DMR and SMR. As H_2 and CO reduce with increase of CO_2 , CH_4 , and water in product stream, result in reducing of %Syngas in product, when operating pressure is increased. However, the H/C ratio is still higher than 2 due to the further H_2 produced from electrolysis reaction. The H_2 produced from electrolysis is constant with increasing of the operating pressure, it indicates that operating pressure has not effect on the production term of electrolysis reaction. Additionally, H/C ratio slightly increases because of reducing in carbon content consumption.

In conclusion, the operating pressure has effect on performance of H-SOEC/DMR process. For electrochemical term, the operating pressure has not affect the activation and ohmic overpotentials. As the operating pressure increases, the cell voltage increases because of an increasing of equilibrium voltage, while the concentration overpotentials decreases. For energy term, process should be operated as exothermal system at a high pressure operation due to a decrease of total energy demand and increase of electrical energy. For syngas production term, an increase of pressure results in a decreasing of % CO_2 and % CH_4 conversions and %Syngas in product and that makes decreasing of H_2 and CO in product stream. However, the H/C ratio is higher than 2 because further H_2 produced from electrolysis, which does not affect by pressure change.



(b)

Figure 5.10 Effect of operating pressure on (a) product stream molar flow rate and (b) %CO₂ and CH₄ conversions, %Syngas in product, and H/C molar ratio.

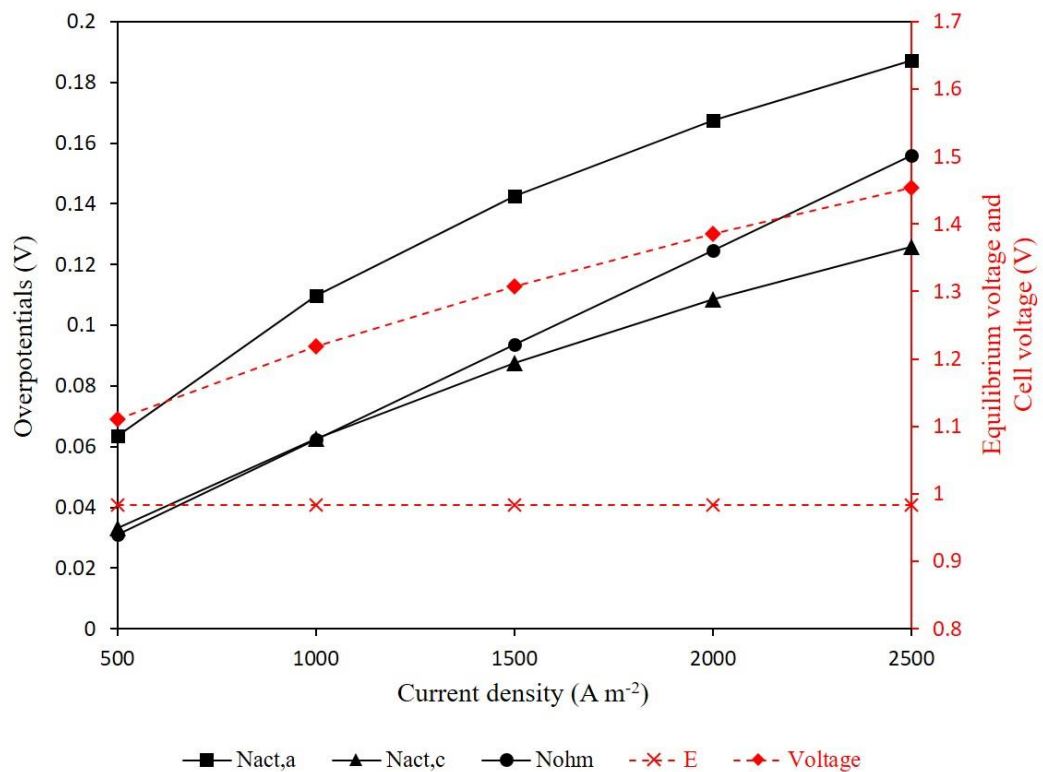
5.2.4 Effect of current density

Current density is operating parameter that has effect on the process performance. According to previous research (Im-orb et al., 2018), the current density should be controlled in the range of 1000 to 3000 A m⁻² to prevent SOEC electrode deterioration. In this study, the effect of current density is investigated in the range of 500 to 2500 A m⁻² in order to analyze effect of lower and in the range that recommendation, under the operating conditions (temperature of 1073 K, pressure of 1 atm, S/C ratio of 2, and number of cell of 500 cells).

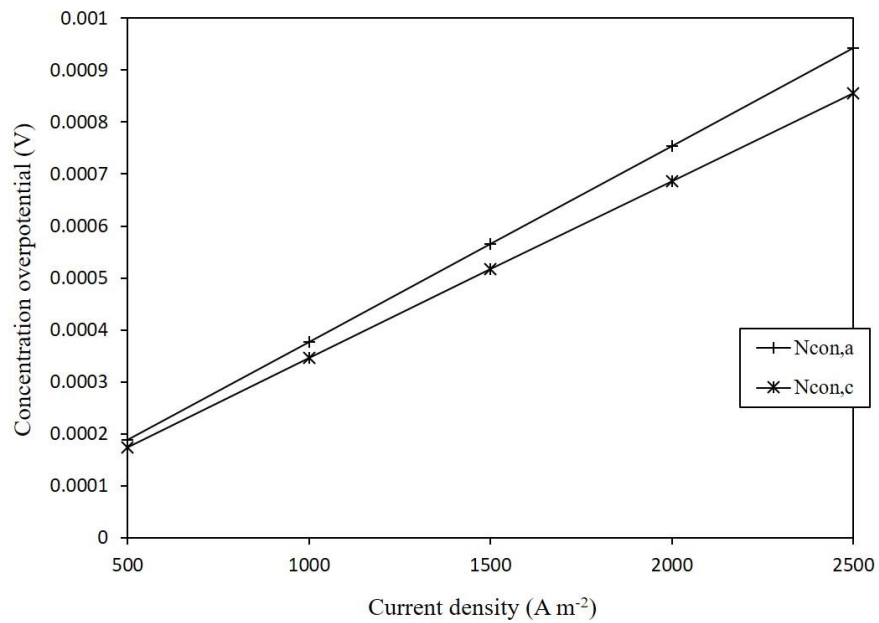
The effect of current density on the electrochemical value are shown in Figure 5.11a and 5.11b. As the current density increases, the equilibrium voltage is constant, while all of the overpotentials increase. The equilibrium voltage does not depend on current density because it is based on the Nernst equation, which depends on temperature and pressure. The equilibrium voltage is the minimum electrical voltage and used to split water. A presence of current density in process results in the voltage loss (overpotential) of process. For the overpotentials, the ohmic and concentration overpotentials are steadily increased with an increasing of current density, while the activation overpotentials have reduced in an increase rate at higher current density. The cell voltage increases with current density due to an increasing of overpotentials and it has a same trend as activation overpotential, which shows the highest overpotential.

For the energy term, the simulation results are shown in Figure 5.11c. The total energy demand steadily increase with an increasing of current density. The total energy demand depends on amount of water, CO₂, and CH₄ consumed. As current density increases, the amount of water, CO₂, and CH₄ feeds are increased in order to reach the 80% steam utilization factor. A rate of current density steadily increases, resulting in increasing of total energy demand. For the electrical energy demand, it depends on cell voltage, current density, and number of cell. At the constant number of cell condition and current density increase, the electrical energy shows an opposite increase rate with cell voltage, it indicates that the electrical energy is sensitive with current density more than cell voltage. In addition, the heat of overpotential increases with an increasing of current density because of an increase in overpotential and it also has a same trend as

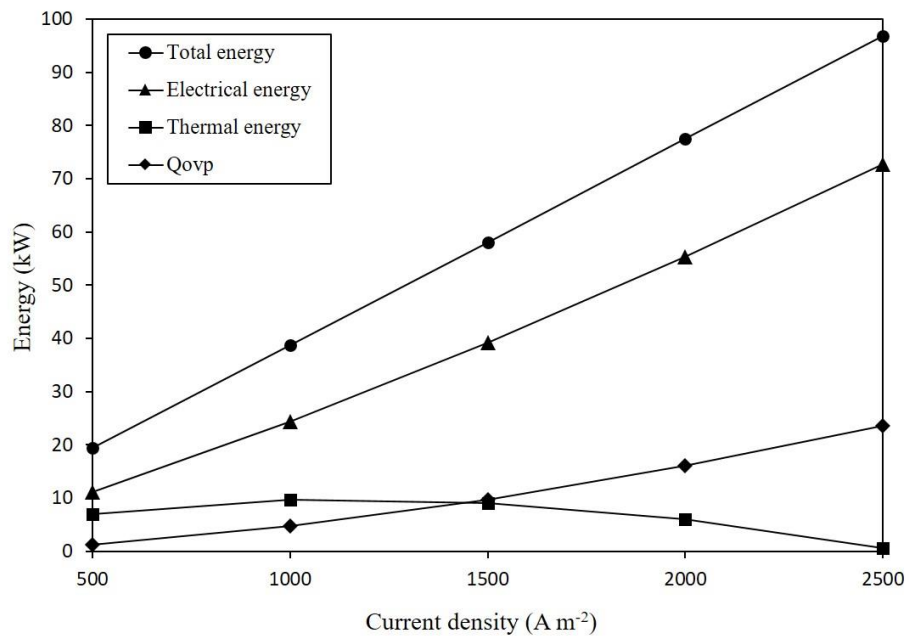
electrical energy. For the thermal energy, at current density of 500 to 1000 A m^{-2} , thermal energy increases because of a low in electrical energy and heat of overpotential. Inversely, at current density of 1000 to 2500 A m^{-2} , thermal energy reduces because of a high in electrical energy and heat of overpotential and it indicates that the system should be operated with reducing a deterioration.



(a)



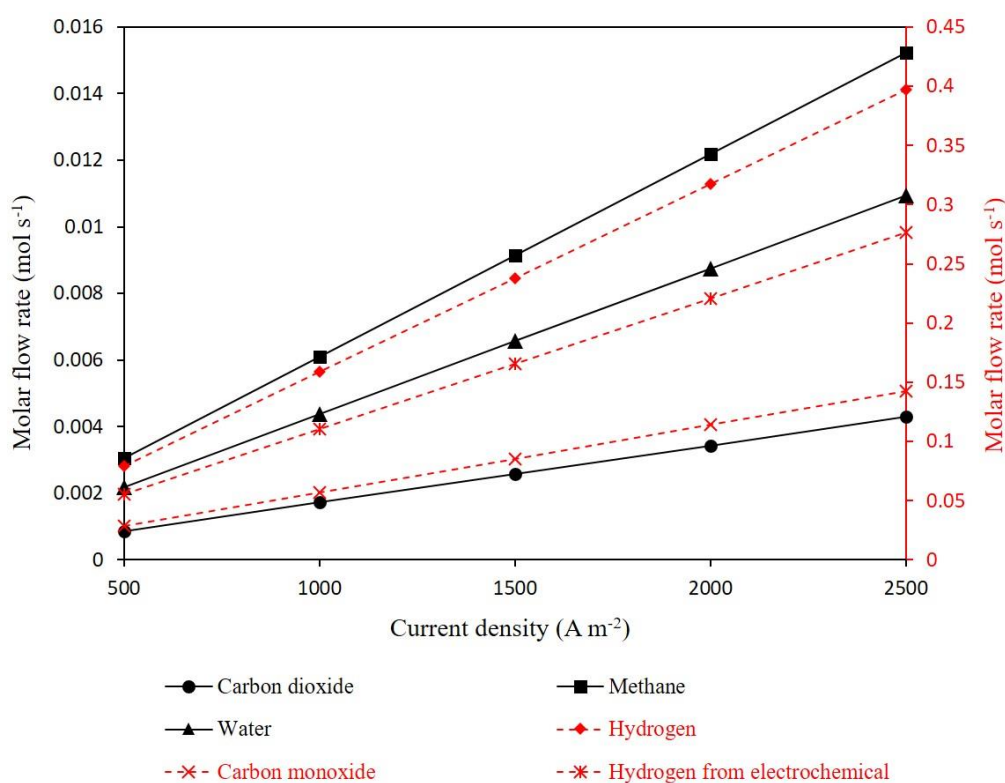
(b)



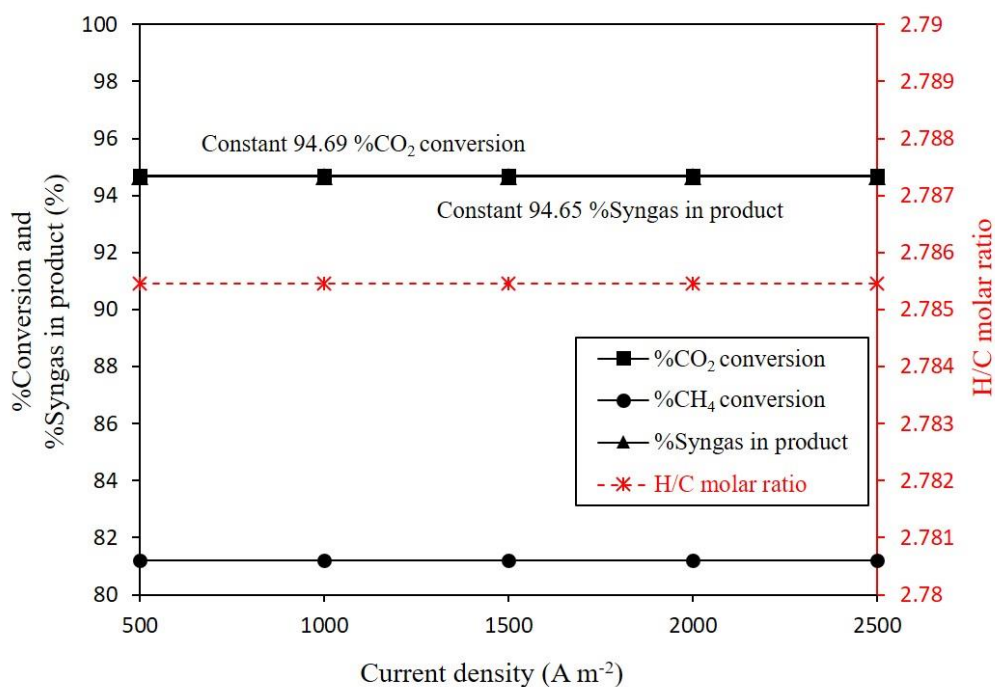
(c)

Figure 5.11 Effect of current density on (a) the cell voltage, equilibrium voltage, activation and ohmic overpotentials, (b) the concentration overpotentials, and (c) the energy demand of system.

For the syngas production term, the influence of current density are shown in Figure 5.12a and 5.12b. As the current density steadily increases, all components in product stream increase steady too. It is the same reason that is described for total energy demand, according to Eq. 2.57, an increase of current density, resulting in an increase of water, CO₂, and CH₄ feed streams in order to achieve 80% steam utilization factor. While, the %CO₂ and %CH₄ conversions are constant with an increasing of current density because those did not depend on current density, resulting in the same ratio of components in every single point of current density. According previous reason, %Syngas in product and H/C molar ratio are constant. From all results, it indicates that the current density has effect on the quantity term, but it has not effect on the quality term of syngas production.



(a)



(b)

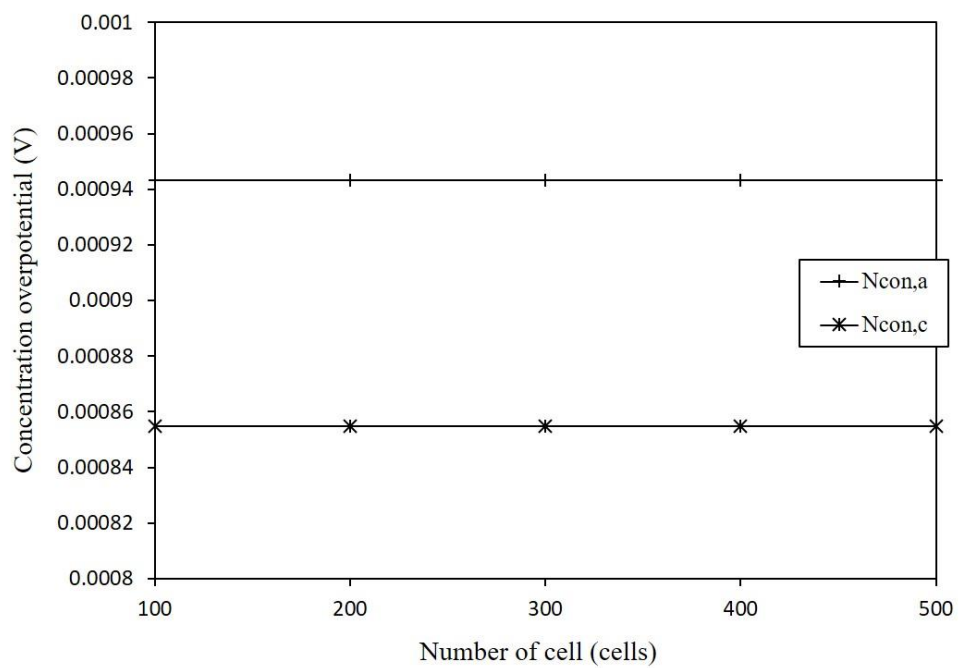
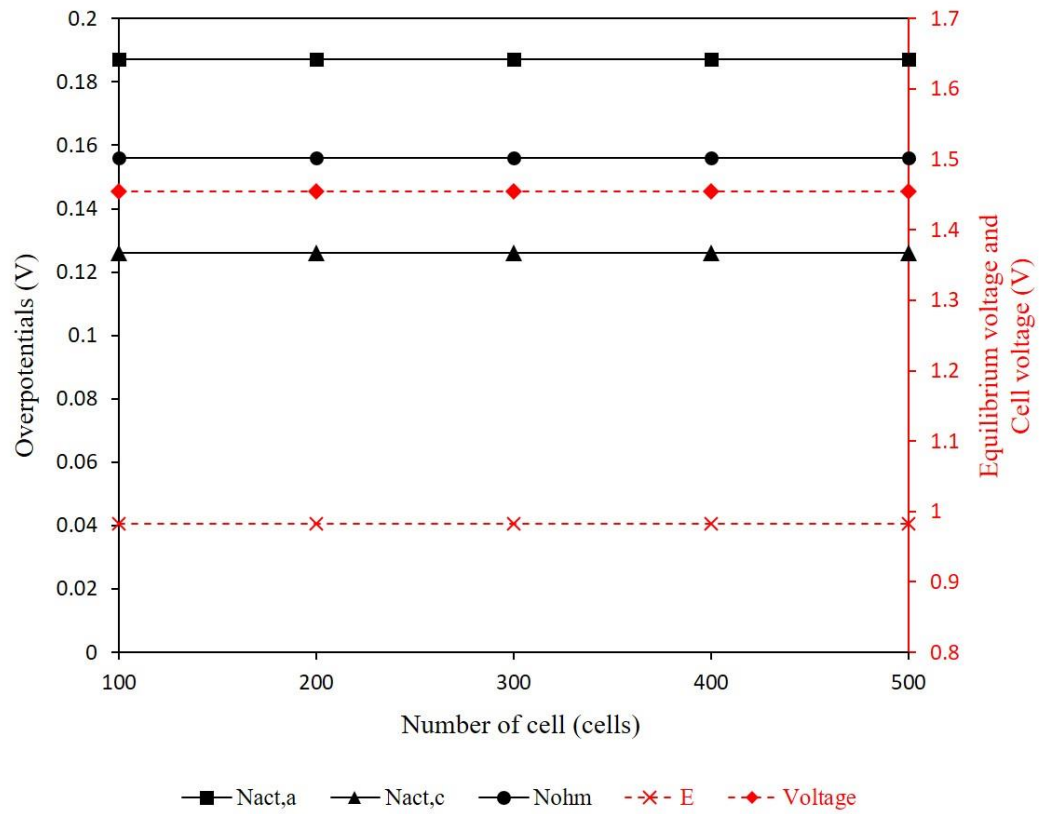
Figure 5.12 Effect of current density on (a) product stream molar flow rate and (b) %CO₂ and CH₄ conversions, %Syngas in product, and H/C molar ratio.

In conclusion, the current density has effect on the H-SOEC/DMR process. For the electrochemical term, the equilibrium voltage is constant but all the overpotentials increase with an increasing of current density, resulting in an increase of cell voltage. In energy term, total energy, electrical energy, and heat of overpotential increase with current density. At current density of 500 to 1000 A m⁻², thermal energy increases, but it decreases at current density of 1000 to 2500 A m⁻². For the syngas production term, current density has effect on the quantity term, but it has not effect on the quality term.

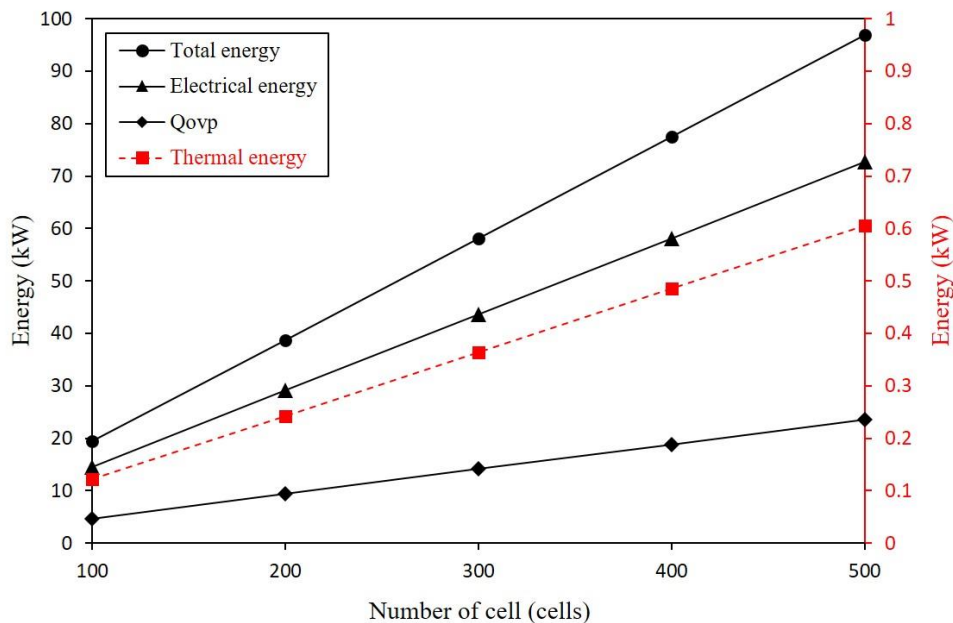
5.2.5 Effect of number of cell

The effect of number of cell stack on the performance of process is investigated in order to find that how scale up is effect on the process performance. In this study, the number of cell is varied in the range of 100 to 500 cells, under conditions (temperature of 1073 K, pressure of 1 atm, current density of 2500 A m⁻², and S/C ratio of 2). The simulation results of number of cell effect are discussed as below.

In electrochemical value term, an increasing of number of cell has not effect on the cell voltage, equilibrium voltage, and all overpotentials, as shown in Figure 5.13a and 5.13b. Those electrochemical values are the values that are calculated for each cell at any condition. At the constant condition, the increase number of cell does not affect those values, thus those values are constant. For energy term, result of the number of cell effect is shown in Figure 5.13c. As the number of cell increases, all energies steadily increase. As the same reason as current density, the total energy demand depends on amount of water, CO₂, and CH₄ consumed and when number of cell increases, the amount of water, CO₂, and CH₄ feeds are increase in order to reach the 80% steam utilization factor. A rate of number of cell steadily increases, resulting in a steadily increase rate of water, CO₂, and CH₄ feeds and total energy demand. For the electrical energy, it can be calculated by Joule's law (Eq. 2.59), which is calculated for 1 cell that when the number of cell increases, resulting in an increasing of electrical energy. The heat of overpotential increases with number of cell, as the same reason as electrical energy. The total energy demand increases with an increasing of number of cell, resulting in an increasing of thermal energy demand in order to sufficient the total energy demand of process.



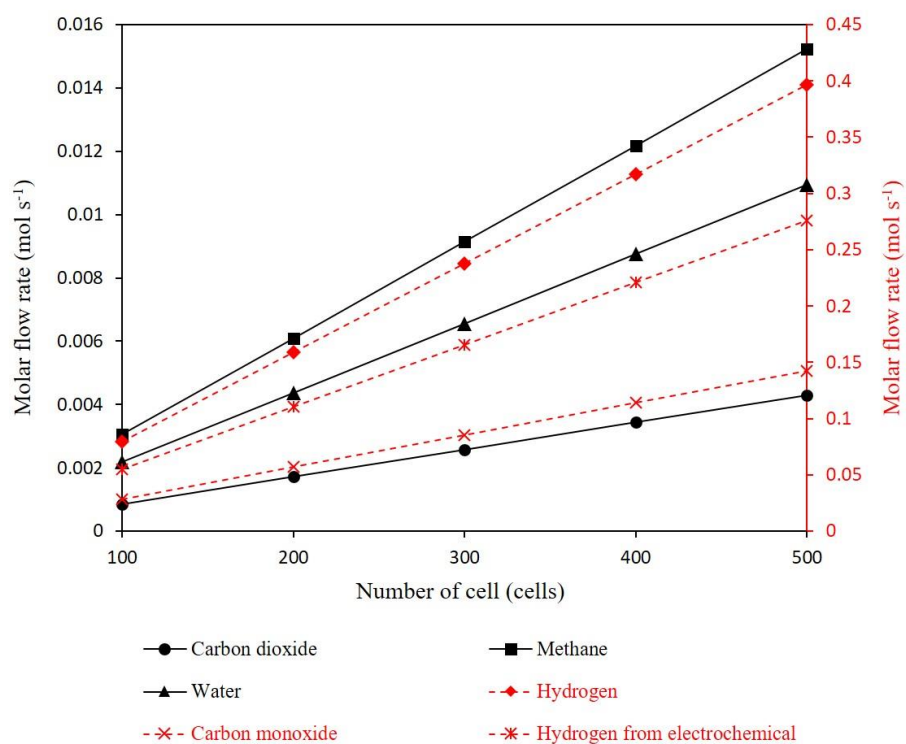
(b)



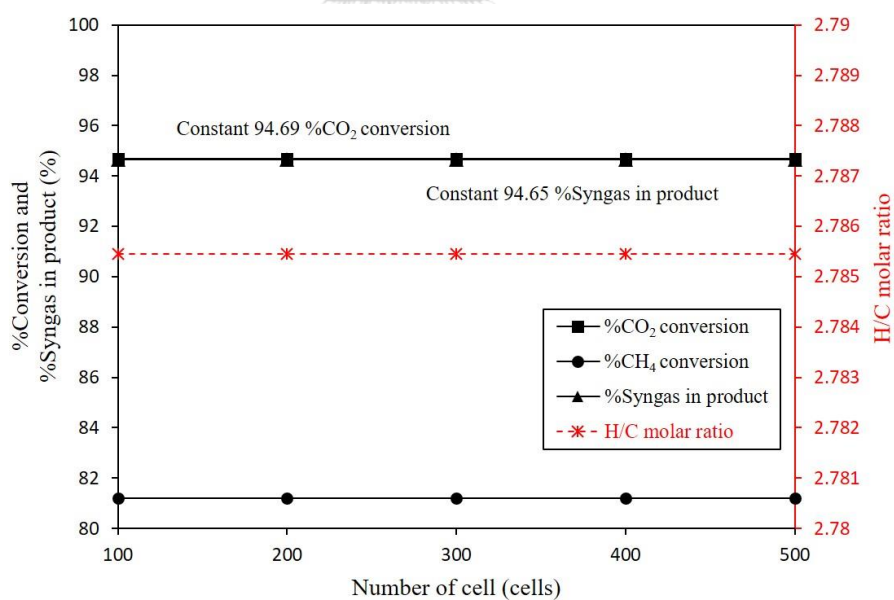
(c)

Figure 5.13 Effect of number of cell on (a) the cell voltage, equilibrium voltage, activation and ohmic overpotentials, (b) the concentration overpotentials, and (c) the energy demand of system.

For the syngas production term, the number of cell has effect on the quantity term, but it has not effect on the quality term of syngas production as same as current density effect (see Figure 5.14a and 5.14b). As the number of cell steadily increases, all components in product stream increase steady too. It is the same reason that is described for current density section, an increase of number of cell results in an increase of water, CO₂, and CH₄ feed streams in order to achieve 80% steam utilization factor. Additionally, an increase of number of cell has not effect on the %CO₂ and %CH₄ conversions because those do not depend on number of cell, resulting in the same ratio of components in every single point of number of cell. According previous reason, %Syngas in product and H/C molar ratio are constant.



(a)



(b)

Figure 5.14 Effect of number of cell on (a) product stream molar flow rate and (b) %CO₂ and CH₄ conversions, %Syngas in product, and H/C molar ratio.

In conclusion, the number of cell has effect on the H-SOEC/DMR process. For electrochemical value term, the number of cell has not effect on those values. However, in the energy term, an increase of number of cell results in an increasing of all energy values. For the syngas production and energy terms, the number of cell has effect on the quantity term, but it has not effect on the quality term.



CHAPTER VI

ENERGY ANALYSIS AND OPTIMUM CONDITION

In this chapter, the effect of the operating parameters on the energy efficiency of H-SOEC/DMR process are present. The key operating parameters analyzed in this chapter consist of temperature, pressure, current density, and number of cell. In order to evaluate the energy efficiency, the results of both energy demand and syngas production terms are presented when changing the operating parameters. In terms of energy demand, it is analyzed with total, electrical, and thermal energies demand and heat of overpotential of H-SOEC/DMR unit, power (SG power) and hot utility (SG hot utility) demands of steam generator unit, and power (SC power) and cold utility (SC cold utility) demands of syngas compressor unit. For syngas production term, it is analyzed by molar flow rate of hydrogen and carbon monoxide products and carbon dioxide, methane, and hydrogen feeds. Additionally, the optimum condition that give the highest energy efficiency is find to obtain the suitable operating condition of the H-SOEC/DMR process.

6.1 Energy analysis

The energy efficiency, which is performance indicator in this thesis, is analyzed based on thermal efficiency of H-SOEC/DMR process. The energy efficiency can be calculated following Eq. 2.70 based on flowsheet simulation of the overall H-SOEC/DMR process, as shown in Figure 4.10. According to energy efficiency calculation from Eq. 2.70, Q_{total} includes the external heat demand of H-SOEC/DMR unit, hot utility demand of SG unit, and cold utility demand of SC unit and W_{total} includes the electrical demand of H-SOEC/DMR, SG, and SC units and the lower heating value (LHV) of H_2 , CO , and CH_4 are 244, 283.24, and 802.34 MJ/kmol, respectively (Perry and Green, 2008), which is also popularly used for calculation of thermal energy efficiency in previous studies.

6.1.1 Effect of temperature on energy efficiency

Temperature is an important operating parameter that has effect on performance of H-SOEC/DMR process both electrochemical and syngas production terms. For energy efficiency analysis, temperature is varied in the range of 1073 to 1273 K, under operating conditions (pressure of 1 atm, S/C ratio of 2, current density of 2500 A m⁻², and number of cell of 500 cells). The influence of temperature change on the energy efficiency are described as below.

Figure 6.1 shows the effect of temperature on the energy efficiency of process. The energy efficiency increases when increasing temperature from 1073 to 1123 K, then it decreases when temperature is increased in range of 1123 to 1273 K. The highest energy efficiency is received at 1123 K. The results of energy flow are shown in Figure 6.2a and 6.2b. The total energy demand of H-SOEC/DMR unit increases with an increasing of temperature. As temperature increases, the electrical energy demand and heat of overpotential decrease, while the thermal energy demand increases in order to sufficient the total energy demand of H-SOEC/DMR unit. For the SG unit, the power and hot utility demand are constant with an increasing of temperature because temperature has not effect on the inlet molar flow rate of water that made amount of water feed into SG unit was constant. For the SC unit, the cold utility steadily increases with a steadily increase of temperature because a higher of heat at a high temperature needs a higher of cold utility to cool down. For the SC power, it has the same trend with product molar flow rate (see Figure 6.3) that indicates the power demand of SC unit depends on the amount of product. The effect of temperature on the syngas production are show in Figure 6.3. As temperature increases, the molar flow rate of CO₂, CH₄, and H₂ feeds are constant because temperature has not effect on the inlet flow rate of feed. For H₂ and CO products, those increase with an increasing of temperature. An increase rate of product in temperature range of 1073 to 1123 K is higher than range of 1123 to 1273 K. As total energy demand steadily increases, the molar flow rate of products in range of 1123 to 1273 K are not worth and reduces the energy efficiency of the system.

In conclusion, the energy efficiency increases in the temperature range of 1073 to 1123 K, but it decreases in the range of 1123 to 1273 K. For H-SOEC/DMR unit, the

total energy increase with an increasing of temperature. The electrical demand and heat of overpotential decrease with an increasing temperature, while the thermal energy demand increases in order to sufficient the total energy demand. For SG unit, the power and hot utility demand are constant with an increasing of temperature. For SC unit, the cold utility demand increases with increasing temperature. As temperature increases, the power demand of SC unit increases and has the same trend as product molar flow rates. For syngas production term, the molar flow rate of feeds are constant with an increasing of temperature, while the molar flow rates of products increase. The rate of product molar flow rates increase in range of 1073 to 1123 K and show higher than range of 1123 to 1273 K. The highest energy efficiency is achieved at 1123 K.

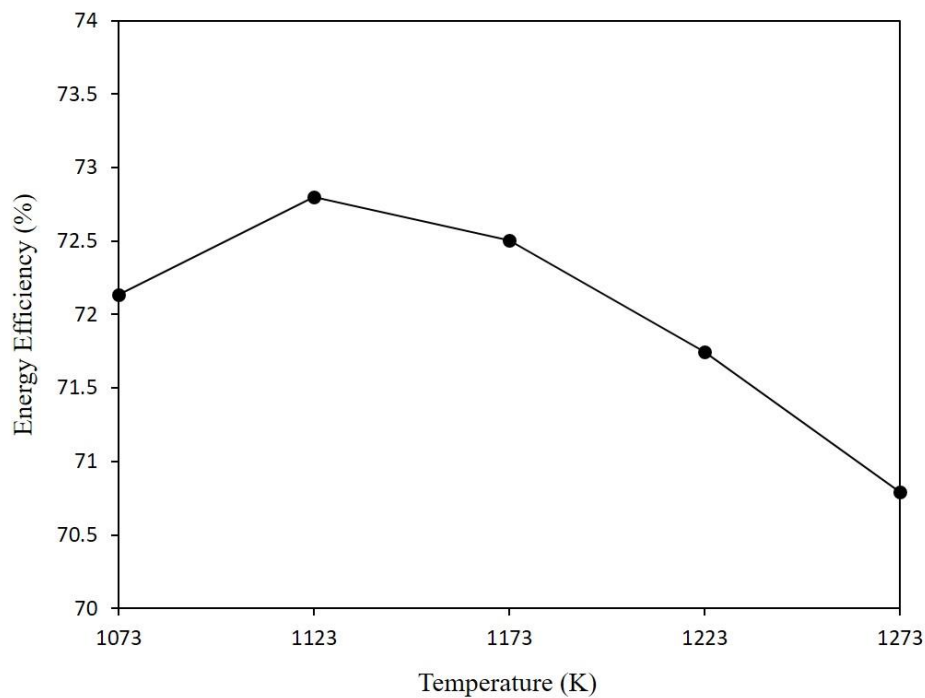
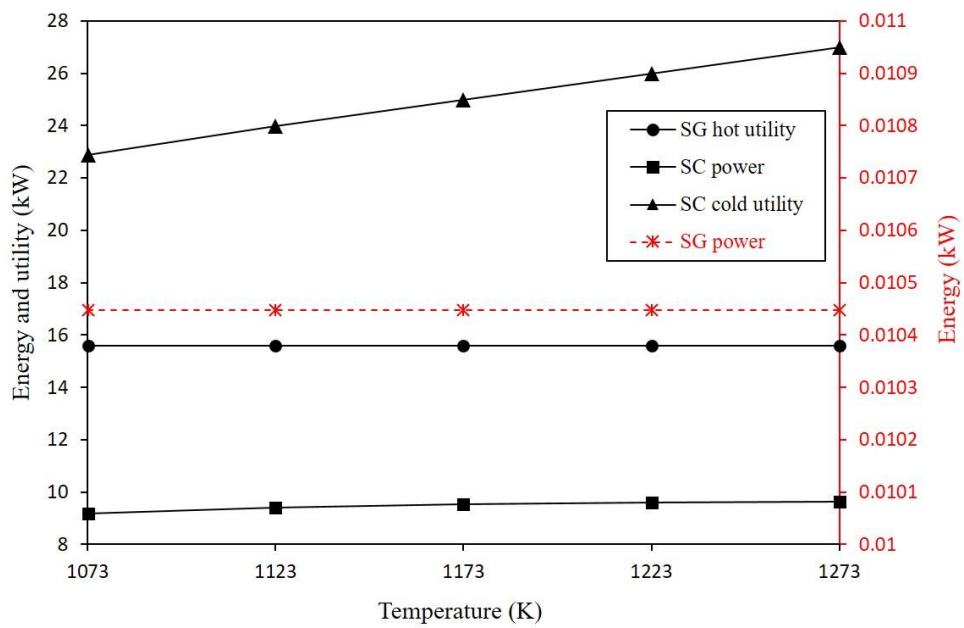
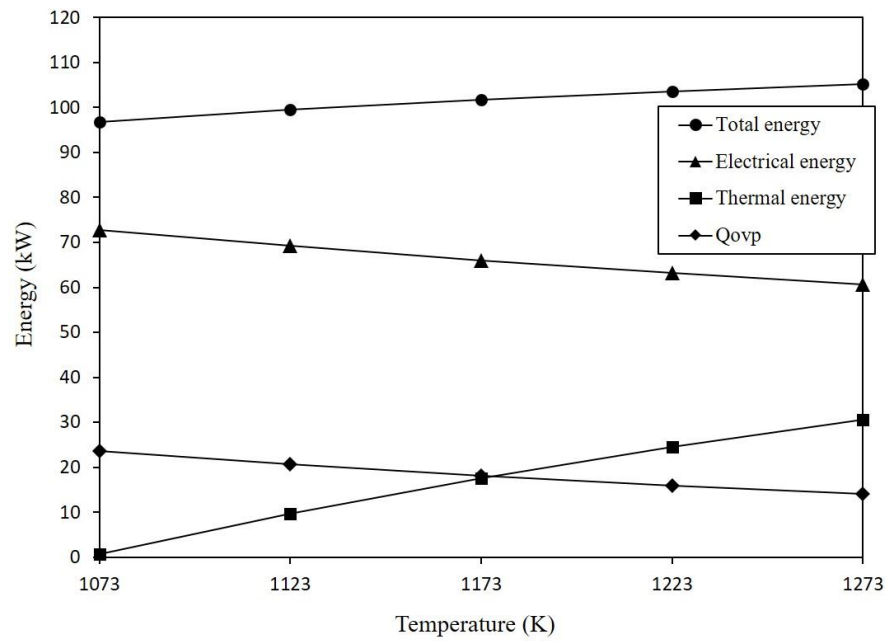


Figure 6.1 Effect of temperature on energy efficiency of process.



(b)

Figure 6.2 Effect of temperature on (a) energy demand of H-SOEC/DMR unit and (b) energy demand of SG and SC units.

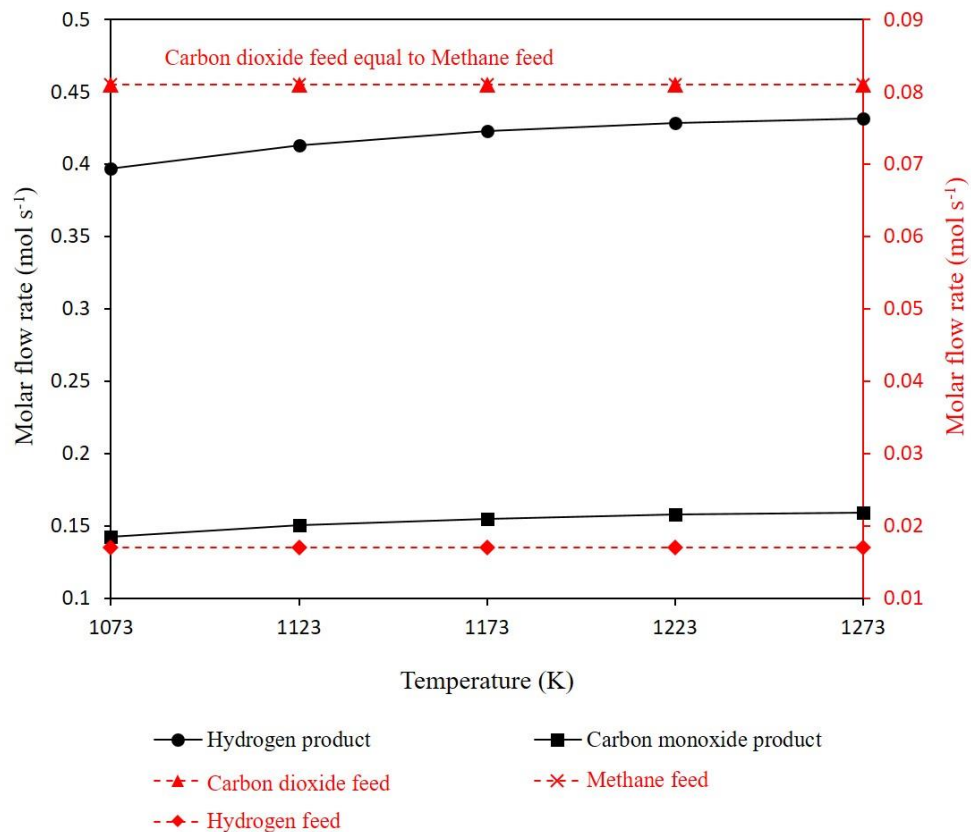


Figure 6.3 Effect of temperature on syngas production term.

6.1.2 Effect of pressure on energy efficiency

According to previous chapter, pressure is the major parameter that has effect on performance of H-SOEC/DMR process. In term of energy efficiency analysis, pressure is varying in range of 1 to 5 atm, under operating conditions (temperature of 1073 K, S/C molar ratio of 2, current density of 2500 A m⁻², and number of cell of 500 cells). The simulation results are discuss as below.

As operating pressure increases, the energy efficiency decreases as shown in Figure 6.4. The highest energy efficiency is achieved at the atmospheric pressure (1 atm). In the energy term, the energy demand simulation results of overall H-SOEC/DMR process are shown in Figures 6.5a and 6.5b. For H-SOEC/DMR unit, the total energy demand decreases with an increasing of pressure because the decrease in

chemical reactions in cathode side leads to a lower need of energy. As the pressure increases, the electrical energy demand slightly increases, while the heat of overpotential slightly decreases. At higher pressure more than 2, process should be operated in the exothermal system because of a lower in total energy demand of process. The electrical energy and heat of overpotential are combined and supplied to process. The supply energy is higher than total energy demand and that makes the system has energy excess and does not need the external heat demand at high operating pressure. The exothermal energy increases with an increasing of pressure because of a decrease of total energy demand. For SG unit, the power and hot utility demands are constant with an increasing of pressure because pressure has not effect on the molar flow rate of water feed and that makes the amount of input water feed into the SG unit is constant. For SC unit, the power and cold utility demands decrease with an increasing of pressure. As operating pressure increases, the molar flow rate of product decreases (Figure 6.6) and that makes the compressors of SC unit needs lower power to compress product stream. In addition, at the temperature of SC unit (318 K), an increase of pressure leads to part of product is condensed to liquid phase, and then it can be separated by flash drum and has effect on product stream molar flow rates. A decrease of product stream molar flow rates results in a decreasing in power demand of compressor and cold utility demand of cooler in SC unit. For syngas production term, the simulation results are shown in Figure 6.6. The CO₂, CH₄, and H₂ molar ratio feeds are constant with an increasing of pressure because pressure has not effect on the inlet molar flow rate of process. As the operating pressure increases, the H₂ and CO molar flow rates are increased because of the decrease of chemical reactions in cathode side. Although, the total energy demand of H-SOEC/DMR and SC units decrease with an increasing of pressure but syngas product decreases, leading to a decreasing in energy efficiency of process.

In conclusion, the increase in operating pressure, resulting in a decreasing of energy efficiency of process. For energy term, the total energy of H-SOEC/DMR unit decreases with an increasing pressure. The H-SOEC/DMR unit should be operated as exothermal system when operating pressure higher than 2. The power and hot utility demand of SG unit are constant with increasing pressure, while power and cold utility

demand of SC unit decrease. For syngas production term, all of the feed molar flow rates are constant with an increasing of pressure, while the syngas product molar flow rate decrease. As operating pressure increases, the molar flow rate of syngas product decrease, leading to a decreasing in energy efficiency of process. The highest energy efficiency is achieved at operating pressure of 1 atm.

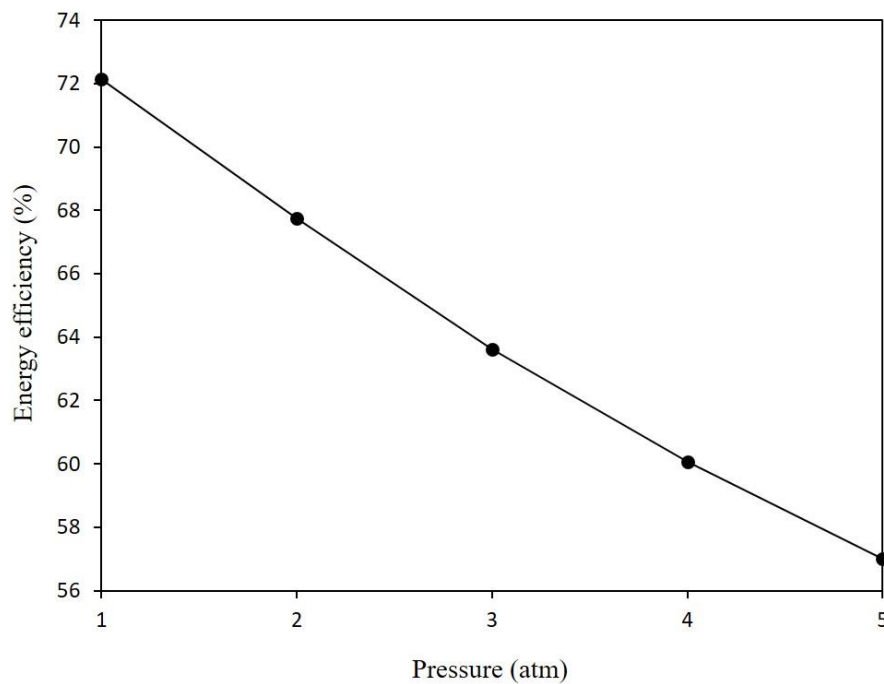
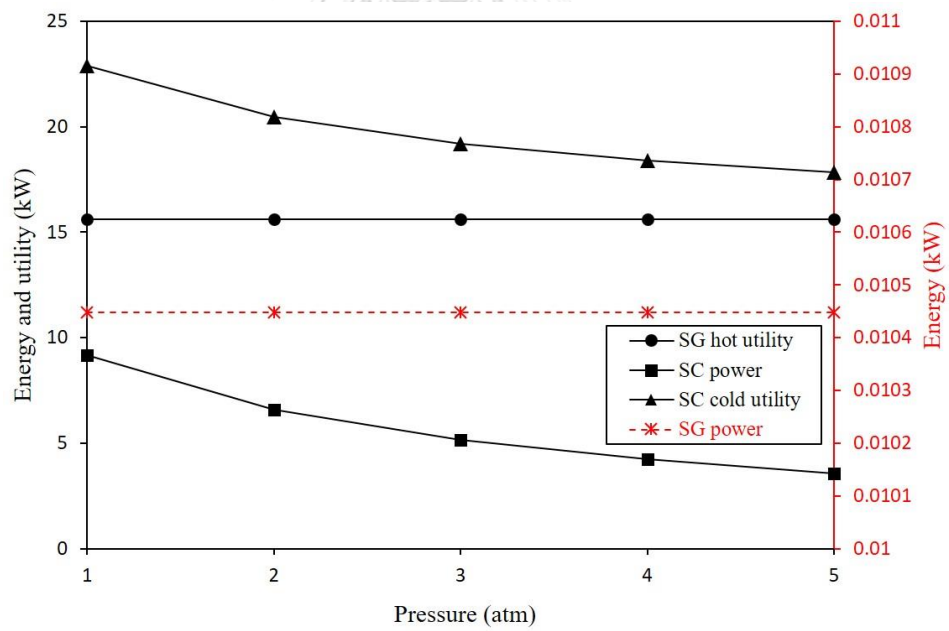
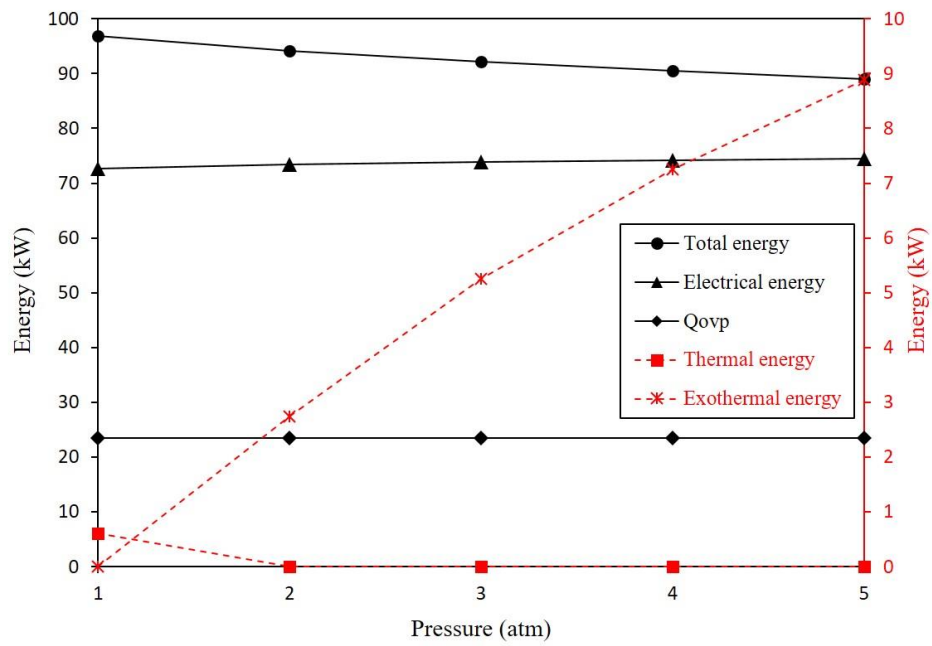


Figure 6.4 Effect of pressure on energy efficiency of process.



(b)

Figure 6.5 Effect of pressure on (a) energy demand of H-SOEC/DMR unit and (b) energy demand of SG and SC units.

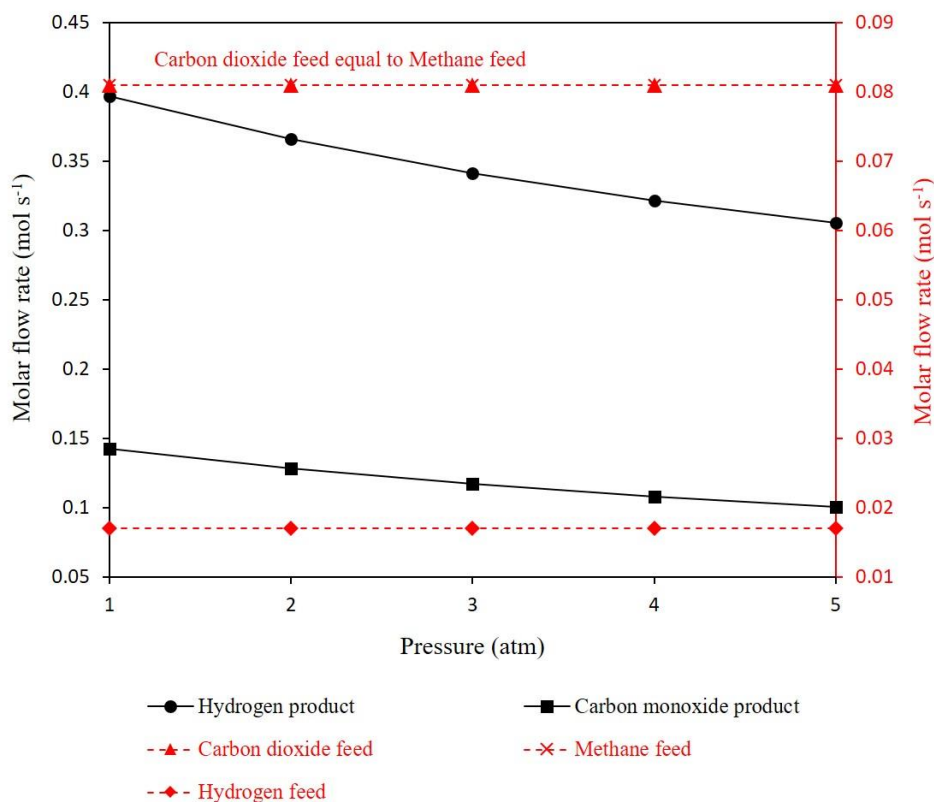


Figure 6.6 Effect of pressure on syngas production term.

6.1.3 Effect of current density on energy efficiency

Current density has effect on the energy demand and syngas production quantity of H-SOEC/DMR process as described in previous chapter. In this chapter, the current density effect is analyzed in range of 500 to 2500 A m⁻², under operating conditions (temperature of 1073 K, pressure of 1 atm, S/C molar ratio of 2, and number of cell of 500 cells). The influence of current density on the energy efficiency of overall H-SOEC/DMR process are described as below.

Figure 6.7 shows the effect of current density on the energy efficiency. It is found that energy efficiency increases with an increasing of current density. The operation under the current density of 2500 A m⁻² gives the highest energy efficiency. For energy term, effect of current density are shown in Figures 6.8a and 6.8b. For H-

SOEC/DMR unit, the total energy demand increases with an increasing of current density because of an increase of water and carbon feeds, resulting in need of higher energy to sufficient. As current density increases, the electrical energy demand and heat of overpotential increase, while the thermal energy demand decreases. The heat of overpotential increases with an increasing current density and can be sufficient the total energy demand of process, resulting in the decreasing of thermal energy demand. For SG and SC units, the energy demand of both units steadily increase with a steadily increasing of current density. According to previous chapter, current density has effect on quantity term of feeds and products, resulting in an increasing of feed and product molar flow rates. From this reason, as the current density increases, the SG and SC energy demand increase. For syngas production term, the simulation results are shown in Figure 6.9. As the current density steadily increases, the steam molar flow rate is steadily increased in order to achieve 80% steam utilization factor. The CO₂ and CH₄ molar flow rates increase with an increasing of steam molar flow rate in order to achieve the S/C molar ratio of 2. As the steam molar flow rate increases, the H₂ feed molar flow rate is increased in order to achieve the steam feed concentration of 95%. The current density has effect on the quantity term of syngas production, but it has not effect on the quality term. Thus, the H₂ and CO product molar flow rates steadily increase when the current density steadily increases. As the current density increases, the heat of overpotential and syngas molar flow rate increase, while the thermal energy demand decreases, resulting in an increase of energy efficiency of process.

In conclusion, the energy efficiency increases with an increasing of current density. In term of energy, the energy demand of SG and SC units steadily increase with a steadily increase of current density. For H-SOEC/DMR unit, the total and electrical energy demand and heat of overpotential increase with an increasing of current density, while the thermal energy demand decreases. In term of syngas production, the current density has effect on quantity term, but it has not effect on quality term. The highest energy efficiency is achieved at current density of 2500 A m⁻².

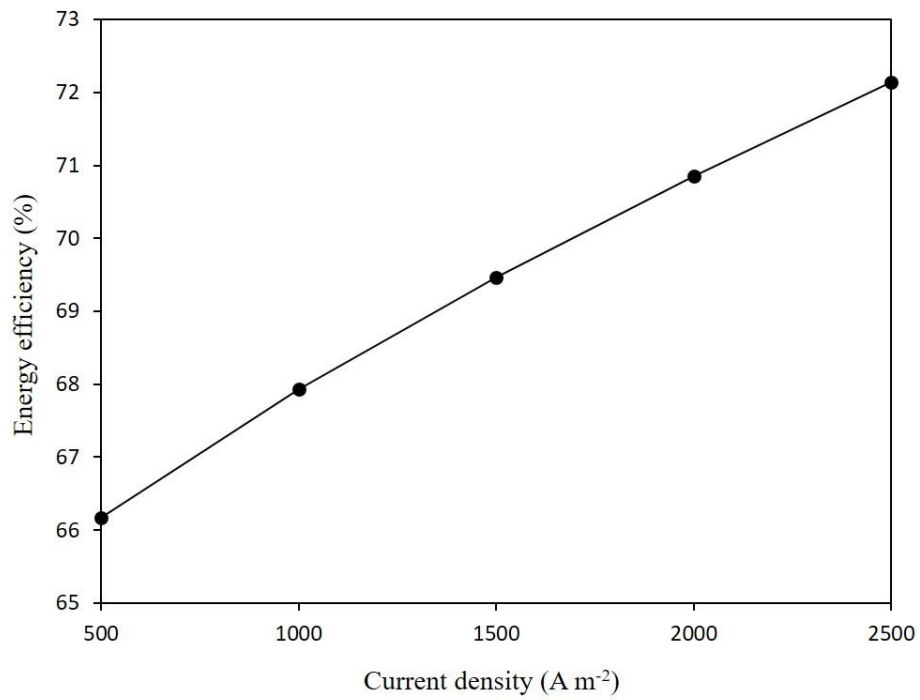
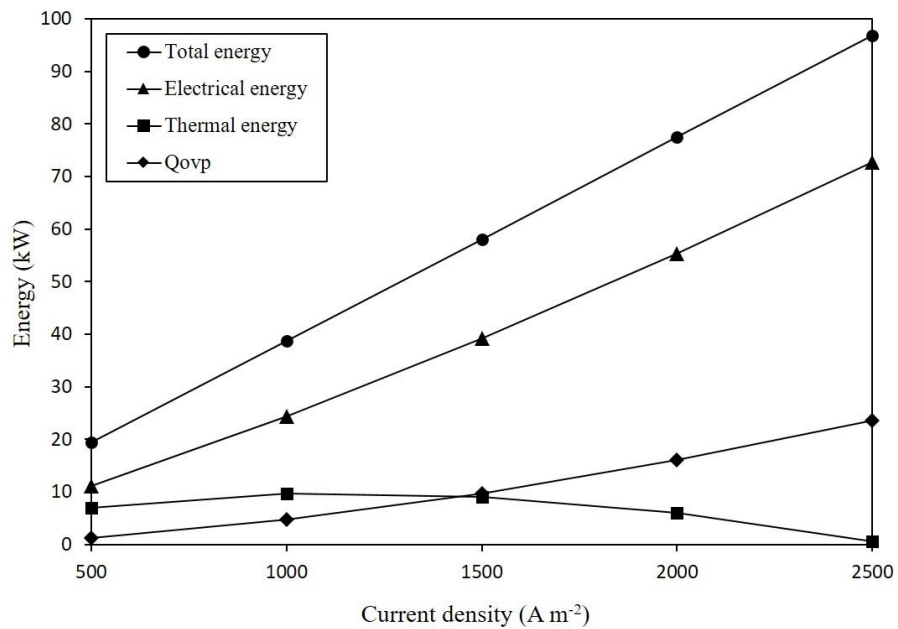
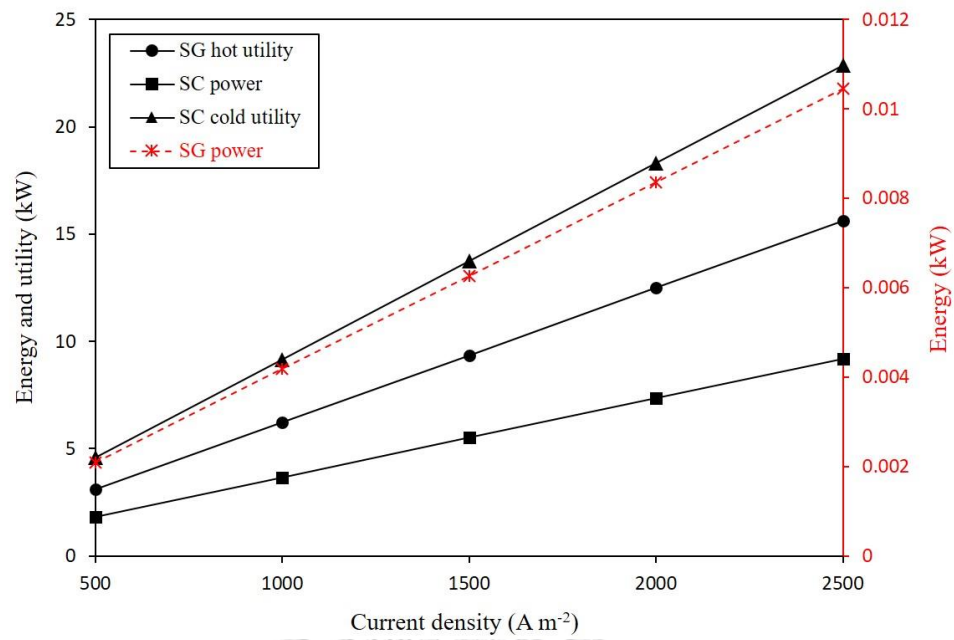


Figure 6.7 Effect of current density on energy efficiency of process.



(a)



(b)

Figure 6.8 Effect of current density on (a) energy demand of H-SOEC/DMR unit and (b) energy demand of SG and SC units.

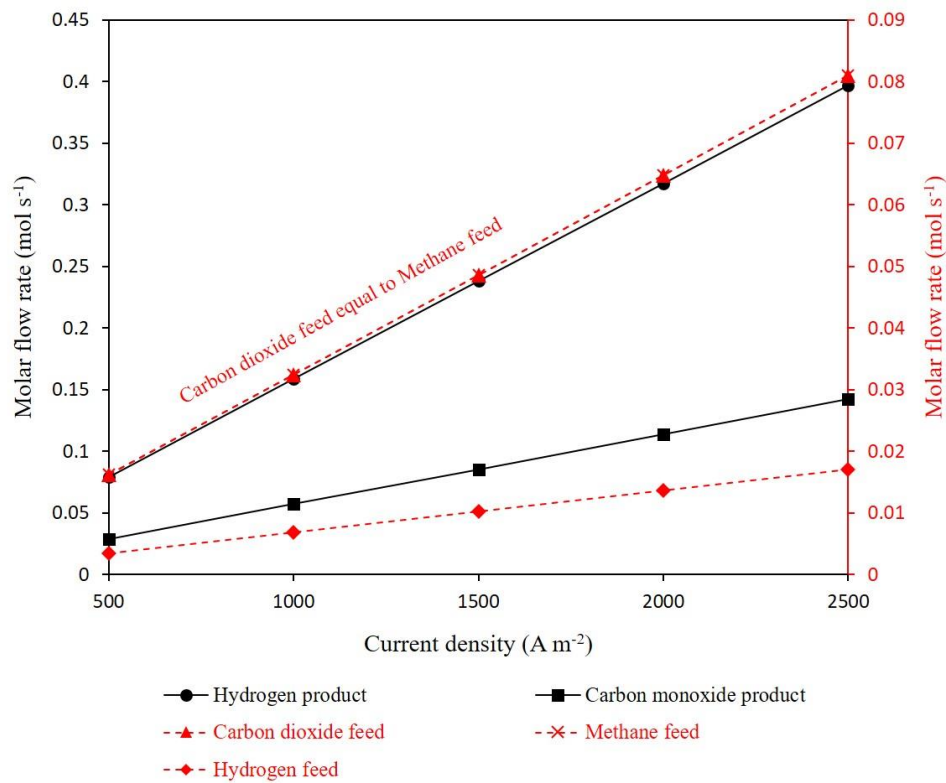


Figure 6.9 Effect of current density on syngas production term.

6.1.4 Effect of number of cell on energy efficiency

According to previous chapter, the results indicate that the number of cell has only effect on quantity term of process performance. In this chapter, the effect of number of cell on energy efficiency is investigated in range of 100 to 500 cells, under operating conditions (temperature of 1073 K, pressure of 1 atm, S/C molar ratio of 2, and current density of 2500 A m⁻²). The simulation results are discussed as below.

The effect of number of cell on the energy efficiency of overall H-SOEC/DMR process is shown in Figure 6.10. The energy efficiency are constant with an increasing of number of cell. It indicates that the number of cell has not effect on the energy efficiency. For energy demand term, the effect of number of cell on energy demand are shown in Figure 6.11a and 6.11b. For H-SOEC/DMR unit, all of energy demand steadily increases with a steadily increasing of number of cell and the same results are

shown for the SG and SC units. As the result reported in previous chapter, the number of cell has only effect on quantity term of both electrochemical and syngas production terms, when the number of cell is steadily increased, resulting in a steadily increasing of water, CO₂, CH₄, and H₂ inlet molar flow rates in order to reach the 80% steam utilization factor, S/C molar ratio of 2, and steam concentration feed of 95%, respectively. As the all of inlet molar flow rates are steadily increased, the all product molar flow rates steadily increase, resulting in an increase of energy demand of H-SOEC/DMR, SG, and SC units in order to sufficient an operating energy for each units. For the syngas production term, the effect of number of cell on energy efficiency is shown in Figure 6.12. All feed and product molar flow rates steadily increase with a steadily increasing of number of cell, it indicates that the number of cell has only effect on quantity term, but it has not effect on quality term of syngas production. As the energy demands and the syngas molar flow rate steadily increase with a steadily increasing of number of cell, resulting in a constant of energy efficiency value in every single point of number of cell.

In conclusion, the energy efficiency is constant with an increasing of number of cell. All of energy demands and component molar flow rates steadily increase with a steadily increasing of number of cell, it indicates that the number of cell has only effect on quantity term of energy and syngas production terms. Although, the energy efficiency is constant with an increasing number of cell but the amount of syngas product increases. However, the number of cell is increased, leading to an increasing in syngas product, but it increases the initial and maintain costs too.

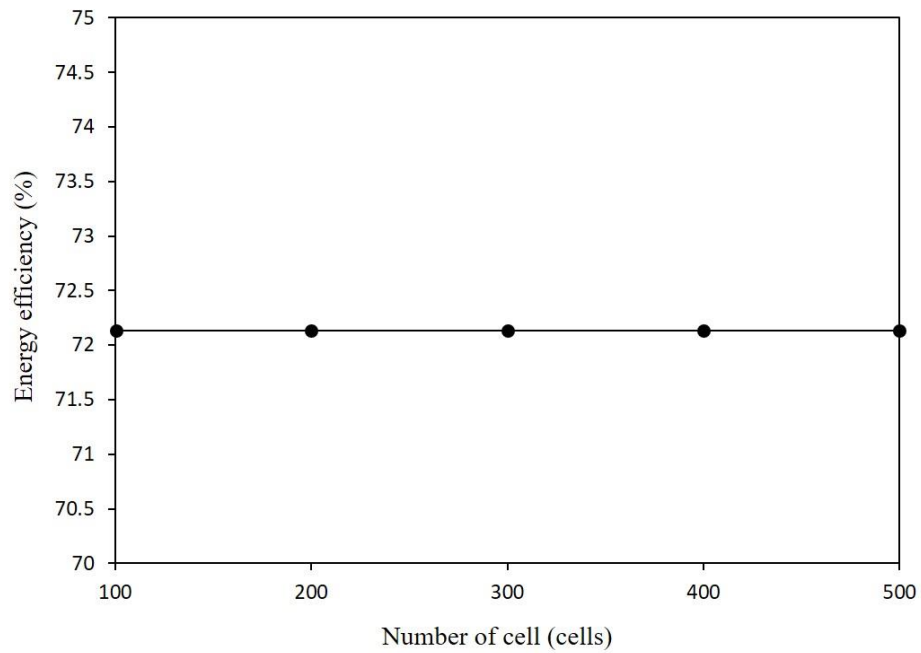
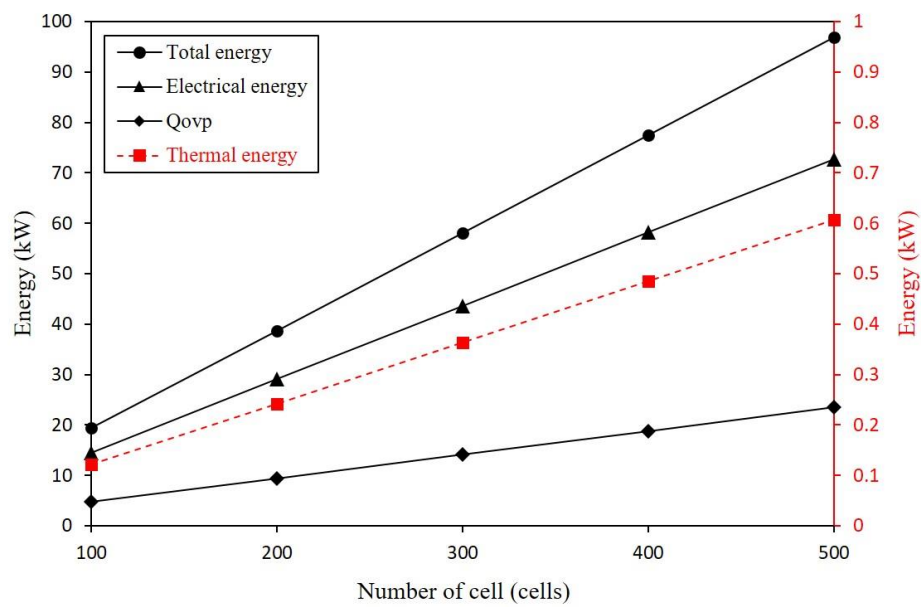
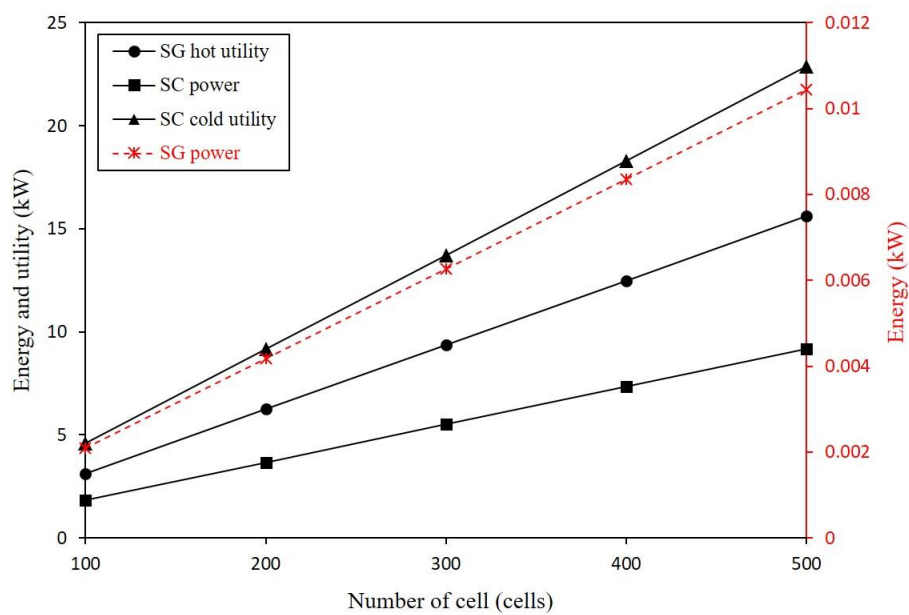


Figure 6.10 Effect of number of cell on energy efficiency of process.



(a)



(b)

Figure 6.11 Effect of number of cell on (a) energy demand of H-SOEC/DMR unit and (b) energy demand of SG and SC units.

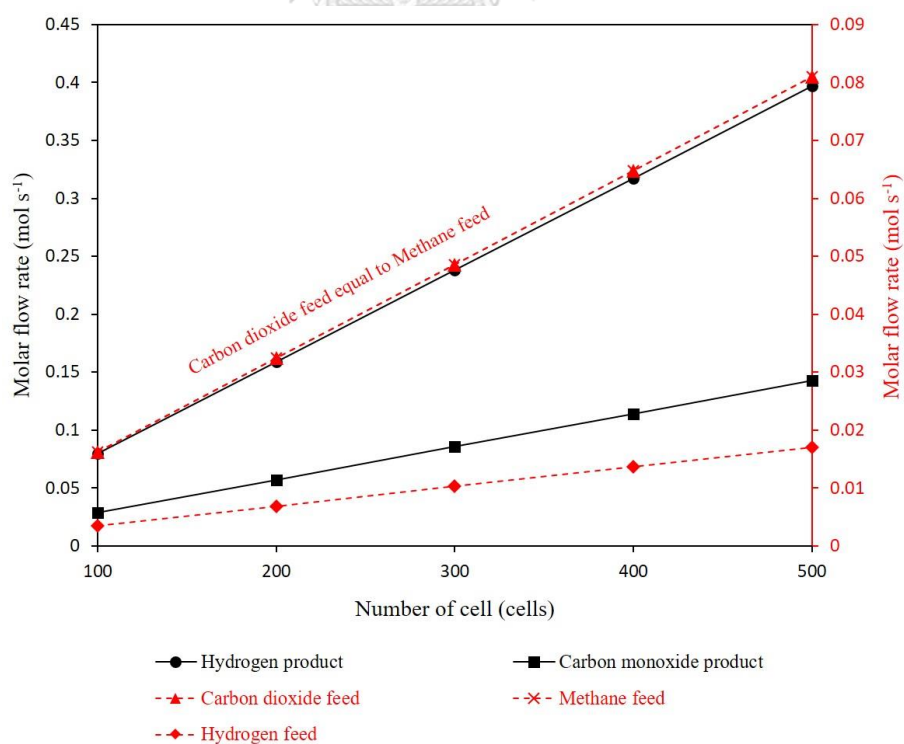


Figure 6.12 Effect of number of cell on syngas production term.

6.2 Optimum condition

In order to choose condition to perform the heat exchanger network design, the optimum condition that gives high energy efficiency is suitable because it indicates that the energy efficiency is improved or not improved after performing heat exchanger network and how much the most energy efficiency of this process is found. In this thesis, the simple method is used to find the optimum condition by measuring the energy efficiency of each parameter. The value of previous parameter that gives the highest energy efficiency is used to be the condition for the next parameter analysis. Based on each point of parameter values, the values of parameters are used in sensitivity and energy efficiency analysis sections. Temperature is used as the main parameter on this section.

For temperature analysis, the values of temperature used are 1073, 1123, 1173, 1223, and 1273 K, under operating conditions (pressure of 1 atm, current density of 2500 A m⁻², and number of cell of 500 cells). The summary of the energy efficiency results are shown in Table 6.1. The energy efficiency does not depend on temperature. The highest energy efficiency is received at temperature of 1123 K, which is value that will used as optimal condition for next parameter analysis. For pressure analysis, the values used are 1, 2, 3, 4, and 5 atm, under operating conditions (temperature of 1123 K, current density of 2500 A m⁻², and number of cell of 500 cells). The results indicate that the energy efficiency has inverse variation with pressure. The energy efficiency decreases with an increasing of pressure because of the decreasing of syngas production. The highest energy efficiency is obtained at pressure of 1 atm. For current density, the analysis is perform by using the values of 500, 1000, 1500, 2000, and 2500 A m⁻², under operating conditions (temperature of 1123 K, pressure of 1 atm, and number of cell of 500 cells). According to the energy analysis section, current density has only effect quantity term for syngas production term. However, for energy term, the heat of overpotential increases with an increasing of current density, resulting in an increasing of energy efficiency. Current density of 2500 A m⁻² is given for the highest energy efficiency. For number of cell analysis, the values used are 100, 200, 300, 400, and 500 cells, under operating conditions (temperature of 1123 K, pressure of 1 atm, and current density of 2500 A m⁻²). The energy efficiency is constant with an increasing

of number of cell, as shown in Table 6.1. According to the results in energy efficiency analysis section, number of cell has only effect on quantity term for both energy and syngas production terms, resulting in a constant of energy efficiency when number of cell was increased. The number of cell of 500 cells is chosen because this condition gives higher amount of syngas production and carbon usage.

Table 6.1 Summary of effect of parameters on the energy efficiency.

Temperature (K)	1073	1123	1173	1223	1273
η_{en} (%)	72.14	72.80	72.50	71.74	70.79
Pressure (atm)	1	2	3	4	5
η_{en} (%)	72.80	71.24	69.24	67.27	65.37
Current density (A m ⁻²)	500	1000	1500	2000	2500
η_{en} (%)	67.50	69.00	70.37	71.63	72.80
Number of cell (cells)	100	200	300	400	500
η_{en} (%)	72.80	72.80	72.80	72.80	72.80

In conclusion, based on the operating temperature of 1123 K of the H-SOEC/DMR process, a pressure of 1 atm, current density of 2500 A m^{-2} , and number of cell of 500 cells are used as optimum conditions in order to achieve the highest energy efficiency of 72.80% and highest amount of syngas production and carbon usage. These conditions are selected as the optimum conditions in this thesis, even it may not be the real optimum condition of this process. Furthermore, these conditions are used as optimum conditions for this thesis, to perform heat exchanger network design and exergy analysis in the next chapters.



CHAPTER VII

HEAT EXCHANGER NETWORK DESIGN

Previous chapter, the energy efficiency of the H-SOEC/DMR process is analyzed in order to evaluate effect of operating parameters on the energy efficiency and selects the optimum conditions based on the highest energy efficiency. In addition, the energy efficiency of the H-SOEC/DMR process can be improved through the heat exchanger network design method by using heat recovery of process, to achieved higher energy efficiency. In this chapter, the heat exchanger network design is performed based on a pinch analysis method in order to improve the energy efficiency of the H-SOEC/DMR process. The aim of this method is to minimize energy requirement (hot and cold utilities requirement) by maximizing energy recovery in the process.

7.1 Data extraction

In order to perform heat exchanger network design, the first step is to select the hot and cold streams from process under the optimum operating conditions. The optimum operating conditions and the design of process flowsheet simulation for this chapter are shown in Table 7.1 and Figure 7.1, respectively. According to Figure 7.1, a liquid water that represents by WATER stream is vaporized to become a steam through the steam generator unit by using HEATER1. The steam (“STEAM” stream) is mixed with hydrogen feed (“HYDROGEN” stream) and becomes a mixing stream feed (“STEAMH” stream), then it is heated into 1103 K by HEATER2 and fed into anode side of the H-SOEC/DMR. For carbon feed stream (“CARBON” stream), it is heated from 298 K into 1103 K by HEATER3, then is fed into cathode side of the H-SOEC/DMR. The syngas product stream (“SYNGAS” stream) is cooled from 1123 K into 318 K by COOLER1 and fed into syngas compressor unit. The syngas product is compressed by COMP1, resulting in an increases of pressure and temperature of product stream and represents by SCOMP1 stream. The SCOMP1 stream is cooled into 318 K by intercooler (named “COOLER2”) and compressed by COMP2 for a higher

pressure and temperature stream (“SCOMP2” stream). The SCOMP2 stream is cooled into 318 K by after cooler (named “COOLER3”) and sent to the storage.

The cold streams, which want to increase temperature of this process, are WATERP, STEAMH, and CARBON streams. The hot streams, which want to decrease temperature of this process, are SYNGAS, SCOMP1, and SCOMP2 streams. The WATERP and SCOMP1 streams are not considered for heat recovery. The WATERP stream is not considered because it is steam that has a phase change and high energetic potential stream that not suitable for heat recovery method. For the SCOMP1 stream, it is not considered because of a limitation of instrument. The process streams information from energy and mass balance by simulation using Aspen Plus software are summarize in Table 7.2. The heat capacity flow rate (CP) of each stream can be calculated according to Eq. 2.71 ($\Delta H = \dot{m} C_p (T_t - T_s) = CP(T_t - T_s)$).

Table 7.1 Input parameters and operating conditions for heat exchanger network design.

Operating temperature, T (K)	1123
Operating pressure, P (atm)	1
Current density, J (A m ⁻²)	2500
S/C ratio	2
Number of cell, N _{cell} (cell)	500
Anode stream inlet composition	95 mol% H ₂ O/5 mol% H ₂
Cathode stream inlet composition	50 mol% CO ₂ /50 mol% CH ₄
Steam utilization factor, U _s (%)	80
Electrolyte conductivity, ρ _e (S m ⁻¹)	$3.14 \times 10^4 / T \times \exp(-3.86 \times 10^3 / T)$
Active cell area, A (m ²)	0.04
Electrode pore radius, r (μm)	0.5
Electrode porosity, n	0.5
Electrode tortuosity, ξ	$(1.5 - 0.5n)^{1/2}$

Cell thickness

Anode thickness, d_a (μm)	50
Cathode thickness, d_c (μm)	500
Electrolyte thickness, l_e (μm)	50

Table 7.2 The information data of process streams.

Stream	Type of stream	Heat capacity flow rate (W K^{-1})	Supply temperature, T_s (K)	Target temperature, T_t (K)	Enthalpy change (W)
1. STEAMH	cold	12.93	415.12	1103	8897.31
2. CARBON	cold	8.57	298	1103	6902.51
3. SYNGAS	hot	17.86	1123	318	-14376.09
4. SCOMP2	hot	18.16	588.52	318	-4911.41

7.2 Pinch and energy target calculation

In this section, the pinch point and minimum energy target are calculated. This thesis, the problem table algorithm method is performed in order to calculate minimum energy target or maximum heat recovery, under the assumptions (i.e., (i) heat capacity (C_p) of each stream are constant (ii) no heat loss and (iii) no pressure drop). In the first step, the minimum temperature approach (ΔT_{\min}), which represents as driving force of energy exchange, is selected. It is noted that the hot stream temperature must be equal to or higher than the cold stream temperature in order to perform heat exchange. The ΔT_{\min} of 10 to 20 K are recommended for petrochemical process. In this thesis, the ΔT_{\min} of 20 K is selected to perform the minimum energy target calculation. In the next step, the temperature shifted of streams data from Table 7.2 are performed by setting the shifted temperature at $1/2\Delta T_{\min}$ below hot stream temperatures and $1/2\Delta T_{\min}$ above cold stream temperature. The aim of temperature shifted is to ensure that within any interval, hot streams and cold streams are apart at least ΔT_{\min} . The shifted temperatures of stream data from Table 7.2 are showed in Table 7.3.

Table 7.3 The information data of process streams with shifted temperature.

Stream and type	CP (W K ⁻¹)	Actual temperature		Shifted temperature	
		T _s (K)	T _t (K)	S _s (K)	S _t (K)
STEAMH (cold)	12.93	415.12	1103	425.12	1113
CARBON (cold)	8.57	298	1103	308	1113
SYNGAS (hot)	17.86	1123	318	1113	308
SCOMP2 (hot)	18.16	588.52	318	578.52	308

Then, the temperature interval diagram is performed as shows in Figure 7.2. The streams in a diagram represent with a vertical scale and interval boundaries superimposed (as shifted temperatures). For example in interval number 2, streams 1 and 2 (cold streams) run from 415.12 K to 568.52 K, and streams 3 and 4 (hot streams) run from 588.52 K to 435.12 K in the shifted temperatures range between 425.12 K and 578.52 K. It is noticed that the temperature difference between hot and cold streams are equal to ΔT_{\min} of 20 K. In order to guarantees that full heat interchange within any intervals was possible, the temperature interval was setting up. In the next step, the net enthalpy of each temperature intervals are performed. Each interval will have either a net surplus or net deficit of heat as dictated by enthalpy balance. The energy balances of each interval can be calculated according to Eq. 2.72 ($\Delta H_i = (S_i - S_{i+1})(\sum CP_H - \sum CP_C)_i$). The results of any interval are shown in Table 7.4. The results indicates that an interval is in heat surplus or heat deficit. Thus, it would be possible to produce a feasible network design based on the assumption that all surplus interval rejects heat to cold utility, and all deficit intervals need heat from hot utility. The next step, in order to evaluate the minimum energy target, the cascade diagram was performed. This step was carry out under the condition that any heat available in interval i is hot enough to supply any duty in interval $i+1$. Instead of sending the surplus heat from interval i into cold utility, it can be send down into interval $i+1$. The result of cascade diagram is shown in Figure 7.3. Figure 7.3a is performed under the assumption that no heat from hot utility is supplied into interval 1. This result indicates that the heat flows between interval 1 and 2 has negative flow of 1945.51 W, which is thermodynamically infeasible. To solve this problem, the heat of 1945.51 W must be added from hot utility as shown in Figure 7.3b, and cascaded right through the system. By enthalpy balance, all energy flows are increased by 1945.51 W. The results of this cascade are shown that the minimum utilities require have been predicted. The minimum hot utility requirement is 1945.51 W and the minimum cold utility requirement is 5442.31 W. Moreover, the position of pinch has been located at the interval boundary with a shifted temperature of 578.52 K (i.e., hot streams at 588.52 K and cold streams at 568.52 K) where the heat flow is zero.

Shifted temperature

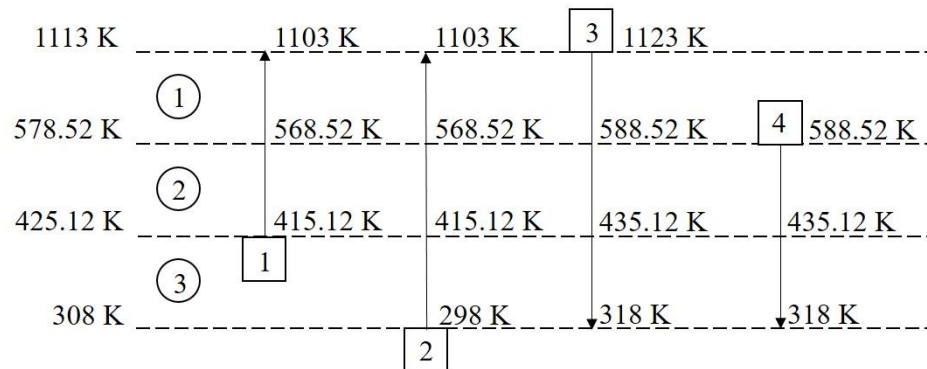


Figure 7.2 Streams and temperature intervals

Table 7.4 The temperature intervals and heat loads for process streams.

Shift temperature (K)	Interval number, i	$S_i - S_{i+1}$ (K)	$\sum CP_H - \sum CP_C$ (W K ⁻¹)	ΔH_i (W)	Surplus or deficit
$S_1 = 1113$	1	534.48	-3.64	-1945.51	Deficit
$S_2 = 578.52$	2	153.40	+14.52	+2227.37	Surplus
$S_3 = 425.12$	3	117.12	+27.45	+3214.94	Surplus
$S_4 = 308$					

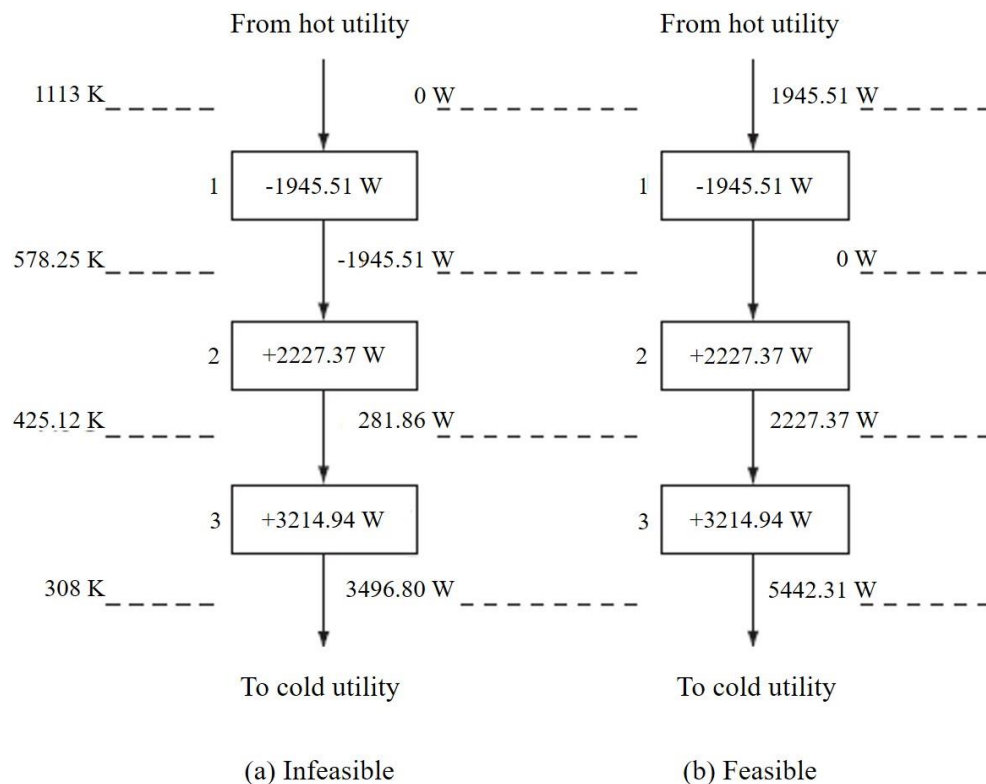


Figure 7.3 The cascade diagram of (a) infeasible heat flow and (b) feasible heat flow.

7.3 Heat exchanger network design

For designing a heat exchanger network, the most helpful tool that uses for this method is grid diagram. In this work, the grid diagram of the H-SOEC/DMR process is shown in Figure 7.4. In Figure 7.4, the streams are drawn as horizontal lines with hot streams at the top and high temperatures on the left. The grid represents the countercurrent nature of the heat exchange, making easier to check exchanger temperature feasible. The pinch temperature of 588.52 K for hot streams and 568.52 K for cold streams are presented in the grid diagram according to result from section 7.2. The pinch can be divided the grid diagram into 2 parts included above pinch and below pinch. Additionally, according to section 7.2, when ΔT_{\min} is specified and the minimum energy targets are calculated, then the minimum number of heat exchangers that will be used to perform heat exchanger network design should be calculated in order to reach the effective target of this process. The minimum number of heat exchangers can be

calculated according to Eq. 7.1. For this process, the minimum number of heat exchanger units is 7 units.

$$N_U = (N_{\text{above}} + U_{\text{above}} - 1) + (N_{\text{below}} + U_{\text{below}} - 1) \quad (7.1)$$

when N_U is the minimum number of heat exchanger units, N_{above} and N_{below} are the number of streams above and below the pinch temperature, respectively, and U_{above} and U_{below} are the number of utility above and below the pinch temperature, respectively.

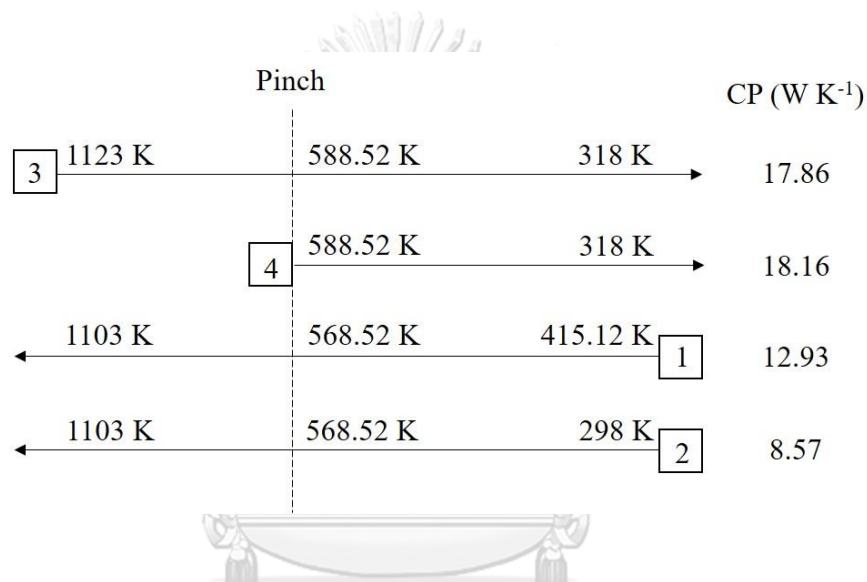
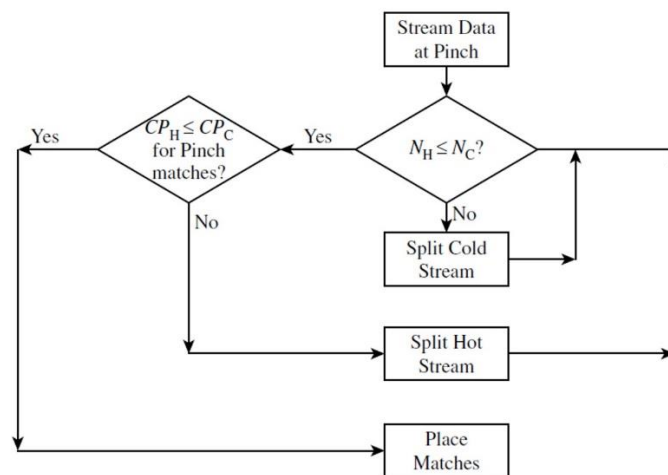


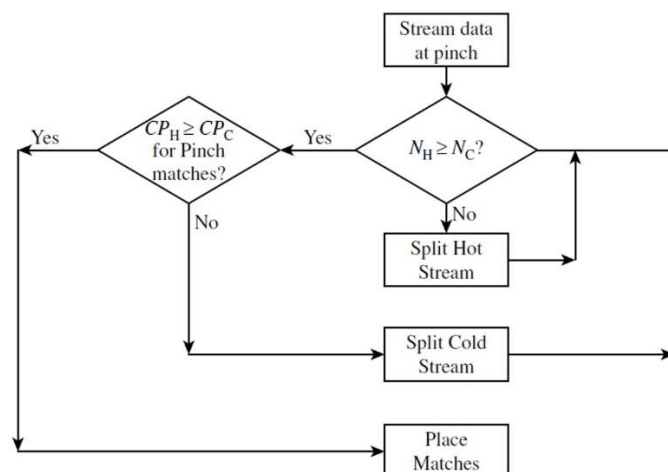
Figure 7.4 Grid diagram of the H-SOEC/DMR process.

In order to design heat exchanger network, the design is performed separately at above pinch and below pinch. The heat exchanger network design is carry out following 2 criteria included the stream number criteria and the CP inequality criteria. If streams of above pinch or below pinch are not satisfied, the streams splitting is required. The algorithms for the overall approach for stream splitting of both above pinch and below pinch are shown in Figure 7.5. For above pinch, in order to matching hot and cold streams, the stream number criteria and CP inequality criteria must be satisfied, which is the number and the heat capacity flow rate of the hot streams must be less than the cold streams. If the number the hot streams, or the capacity flow rate of the hot streams are more than the cold streams, the hot stream splitting is required. According to the pinch design rules, the cold utility cannot be used at the above pinch,

thus if the number or CP of the hot streams are more than the cold streams, result in some hot streams are remain from the match and need cold utility to eliminate that remain heat, which break the pinch design rules. For the below pinch, it is inversely with above pinch. In order to splitting stream, it is performed by splitting the streams flow rate, under assumption that C_p is constant, when the ratio of flow rate decreases, resulting in a decreased of CP.



(a) Above the pinch



(b) Below the pinch

Figure 7.5 Stream splitting algorithm for (a) above and (b) below the pinch (Smith, 2016).

The grid diagram of above pinch and below pinch are shown in Figures 7.6 and 7.7, respectively. For above pinch, the hot SYNGAS stream is split into two streams with the CP value of 9.29 and 8.57. The SYNGAS stream that has the CP value of 8.57 is exchanged with cold CARBON stream with 4850.49 W. The SYNGAS stream that has the CP value of 9.29 is exchanged with cold STEAMH stream with 4969.55 W, then the hot utility of 1945.51 W is used to heat the STEAMH stream in order to reach the target temperature. For below pinch, the hot SYNGAS stream is exchanged with cold STEAMH stream with 1982.25 W, then the cold utility of 2848.03 W is used to cool the SYNGAS stream to reach the temperature target. The hot SCOMP2 stream is exchanged with cold CARBON stream with 2317.13 W, then the cold utility of 2594.28 W is used to cool the SCOMP2 stream in order to reach the target temperature. The overall of grid diagram is shown in Figure 7.8. It is indicated that the hot utility of 1945.51 W and cold utility of 5442.31 W are used in this process, which it is agreed to the minimum energy target that calculated in section 7.2. Moreover, from the matching of hot and cold streams, the 7 heat exchanger units are used, which is agreed to the minimum number of heat exchanger units calculation. The process flowsheet of the H-SOEC/DMR process with heat exchanger network design is illustrated in Figure 7.9. In summary, a perform of heat exchanger network design for the H-SOEC/DMR process, resulting in an increases of the energy efficiency from 72.80 % to 81.46 %

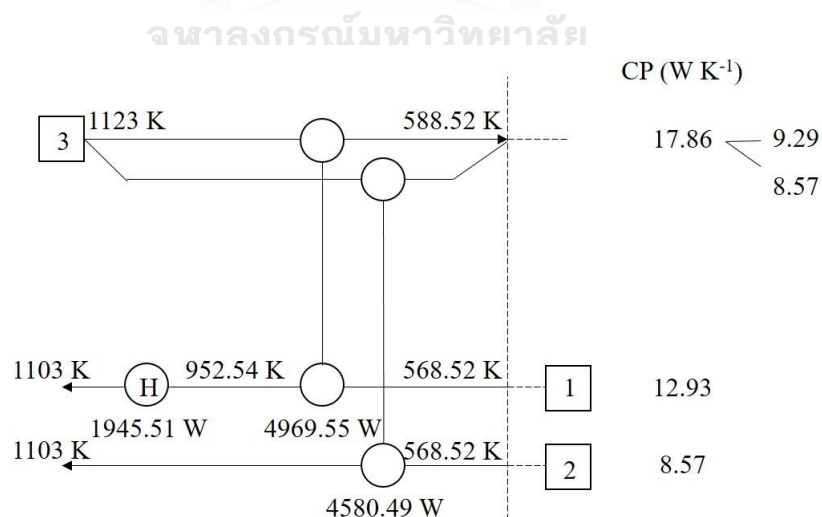


Figure 7.6 Above pinch network design.

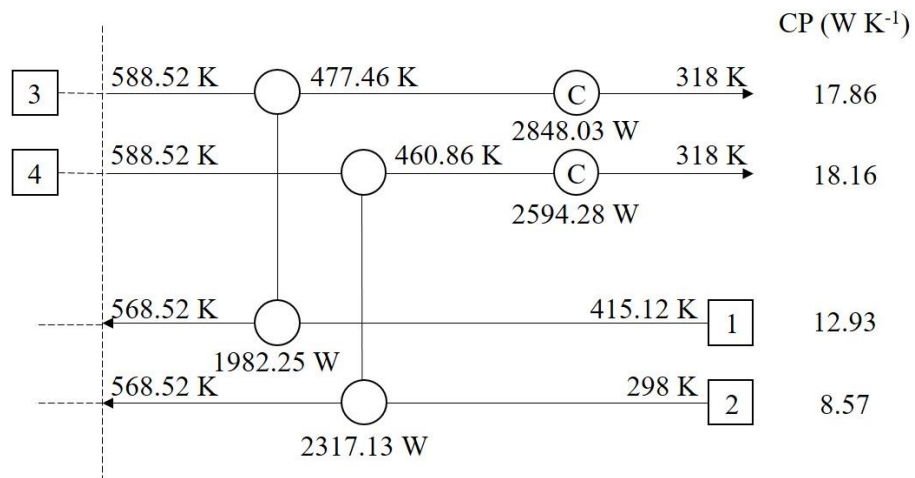


Figure 7.7 Below pinch network design.

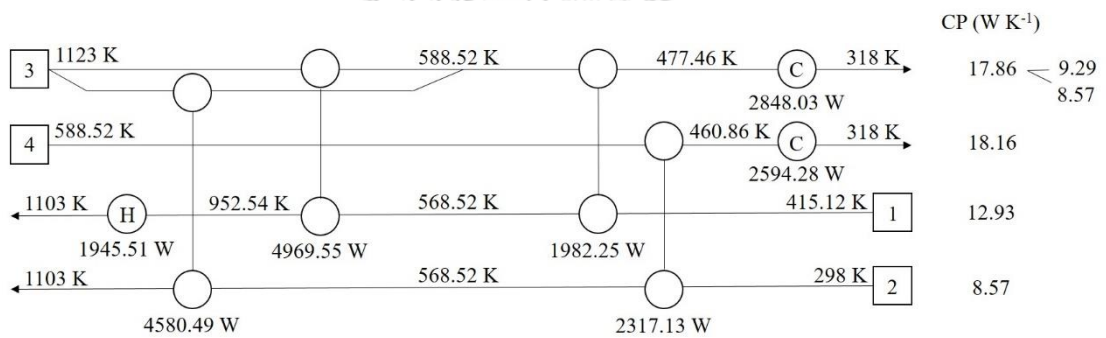


Figure 7.8 Overall network design achieving energy target.

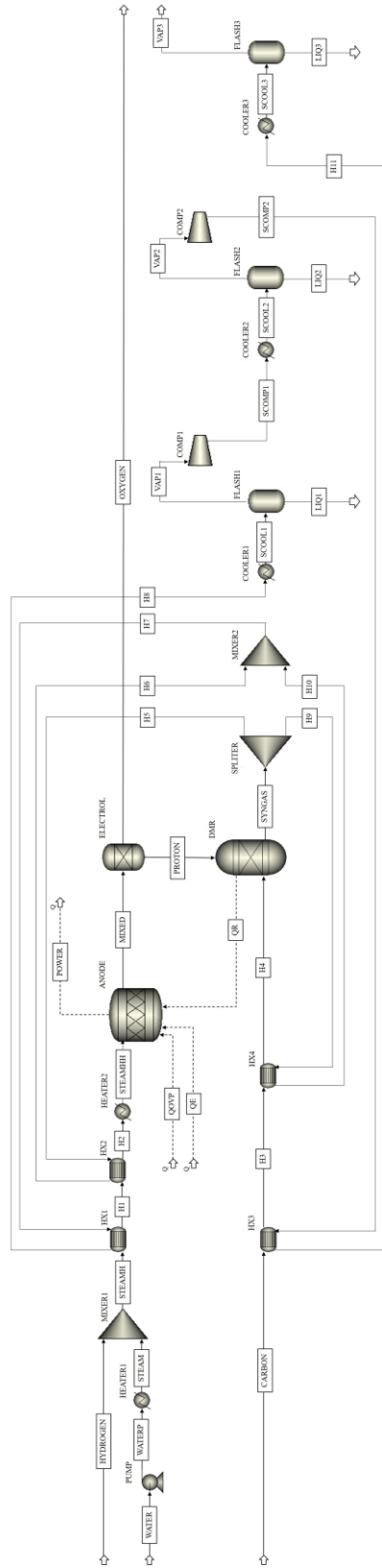


Figure 7.9 Simulation process flowsheet of the H-SOEC/DMR process with heat exchanger network design.

CHAPTER VIII

EXERGY ANALYSIS

According to the previous chapters, the energy analysis of the H-SOEC/DMR process is performed in order to evaluate the effect of the operating parameters on the energy efficiency, then the operating condition that gives the highest of the energy efficiency is selected as the optimum condition of the process. The energy efficiency is further improved by the heat exchanger network design through the pinch analysis method in order to achieve maximum heat recovery and minimum utilities requirement of the process. The energy analysis and heat exchanger network design are based on only the quantity of energy following the first law of thermodynamics. The exergy analysis is different from those, it is can be evaluated the quality of energy usage of the process. Exergy is the maximum theoretical useful work received from the system. Exergy can be lost (or exergy destruction), which account to the loss of the potential of work due to the irreversibility of the system. Thus, the exergy analysis is a useful tool that can be indicated that which part is inefficiency energy usage of the process. In this chapter, the exergy analysis of the H-SOEC/DMR at the optimum condition is performed in order to determine the exergy efficiency and exergy destruction, which can be indicated that which part of the process is inefficient, leading to decision for the plant modification of the process for improvement of efficiency of the process. Additionally, the effect of operating parameters on the exergy efficiency is also presented in this chapter.

8.1 Exergy analysis of the optimum condition

In this section, the exergy analysis of the process is performed under the optimum operating conditions, which are shown in Table 7.1. The process flowsheet simulation with heat exchanger network design for exergy analysis is shown in Figure 7.9. The exergy efficiency of the overall process (η_{ex}) and exergy efficiency of each unit ($\eta_{ex,k}$) can be calculated according to Eqs. 2.84 and 2.85, respectively. For the

exergy destruction, it can be calculated through the exergy balance according to Eq. 2.75. The considered units for exergy analysis of each unit, such as steam generator (SG), HX1, HX2, HX3, HX4, HEATER2, H-SOEC/DMR, COOLER1, syngas compressor (SC), and COOLER3 units, because the irreversibility (e.g., reaction, heat and work transfer) can be archived from these units and the changes of state (changes of composition or temperature of input and output streams), which can be generated the entropy and exergy destruction of the streams that flow through these units. In addition, the mixing, splitting, and flash units are not considered for the exergy analysis of each unit because these units do not generate the entropy, resulting in zero of exergy destruction of these units. Additionally, the exothermic heat that is achieved from the H-SOEC/DMR unit is considered as the waste heat released from the process, which does not provide to the exergy output of the process. Moreover, the heat of overpotential that is generated due to the entropy change is considered as the irreversibility of the process.

For the exergy analysis result of the process, the exergy destruction value of each unit is shown in Figure 8.1 and the exergy efficiency of each unit is shown in Figure 8.2. The result shows that H-SOEC/DMR unit is a unit that has the highest exergy destruction value of 73.50% of the total exergy destruction value because this unit is the unit that several reactions are taking place, resulting in a high irreversibility and destruction of exergy. The high in exergy destruction of this unit can be explained by following reasons. This unit uses both electrical and thermal energy for electrochemical and chemical reactions. The large electrical energy is used, resulting in a high exergy input of a unit. Although, this unit has a heat supply by the heat of overpotential, but this heat energy is generated via the entropy generation, which is considered as the irreversibility, resulting in exergy destruction of this unit. In addition, the one of the main reactant is used in this unit is CH_4 , which gives a high chemical exergy compared with CO and H_2 products, which give a lower chemical exergy than CH_4 . Moreover, this unit is operated as an exothermic process, which gives a heat as by-product. The heat released from this unit is considered as a waste heat that is useless and the exergy of this heat is zero, resulting in a high exergy destruction of this unit,

leading to the lowest of exergy efficiency of this unit when compared with another units. The exergy efficiency of 90.39% is achieved from the H-SOEC/DMR unit.

A steam generator (SG) unit is a second order of the lowest exergy efficiency, which given the exergy efficiency of 92.08%. This unit has a low exergy efficiency because the objective of this unit was a change of liquid into gas phases. A water feed through this process was changed into steam, which consume a large of heat. Although, this process was consume an exergy flow of water, exergy of heat, and exergy of work, but a product out of this process was an exergy flow of steam, which given a low chemical exergy, result in a low exergy efficiency and high exergy destruction. However, this process was given a low exergy destruction value of 1.79% of total exergy destruction value of process. A low exergy destruction value of this unit because a low of exergy value of both exergy of this unit, result in a low exergy destruction value compared with another units.

The second order of exergy destruction value is a syngas compressor (SC) unit, which gives an exergy destruction value of 12.24% of total exergy destruction value of process. The work that supplies to the compressors are lost because gas will always experience friction which result in some of work will be converted into heat, result in energy loss from compressors and exergy destruction of this unit. In addition, a high in the exergy value of this unit results in a high of exergy destruction value compared with another units. However, this unit is given a high exergy efficiency of 98.24% because it is given a high physical exergy of output stream and this unit is operated under the multi stages with perfect intercooling compressor, which minimum work demand, resulting in a high exergy efficiency of this unit.

For heater and cooler units, all of these units have a low exergy destruction due to low difference temperature exchange, resulting in a low heat transfer through these units. The exergy efficiencies of HEATER2, COOLER1, and COOLER3 units are 99.40%, 99.62%, and 99.67%, respectively, with exergy destruction value of 0.34%, 2.49%, and 2.21% of total exergy destruction value of process, respectively. For heat exchanger units, all of these units have a low exergy destruction because low difference temperature exchange between hot and cold streams and calculate through heat

exchanger network design. Moreover, when the chemical exergy of input and output streams are constant, the summation of physical exergies output is almost equal to input of these units, resulting in a high exergy efficiency. The exergy efficiency of HX1, HX2, HX3, and HX4 are 99.92%, 99.42%, 99.83%, and 99.54%, respectively, with exergy destruction value of 0.56%, 2.29%, 1.65%, and 2.93%, of total exergy destruction value of process, respectively.

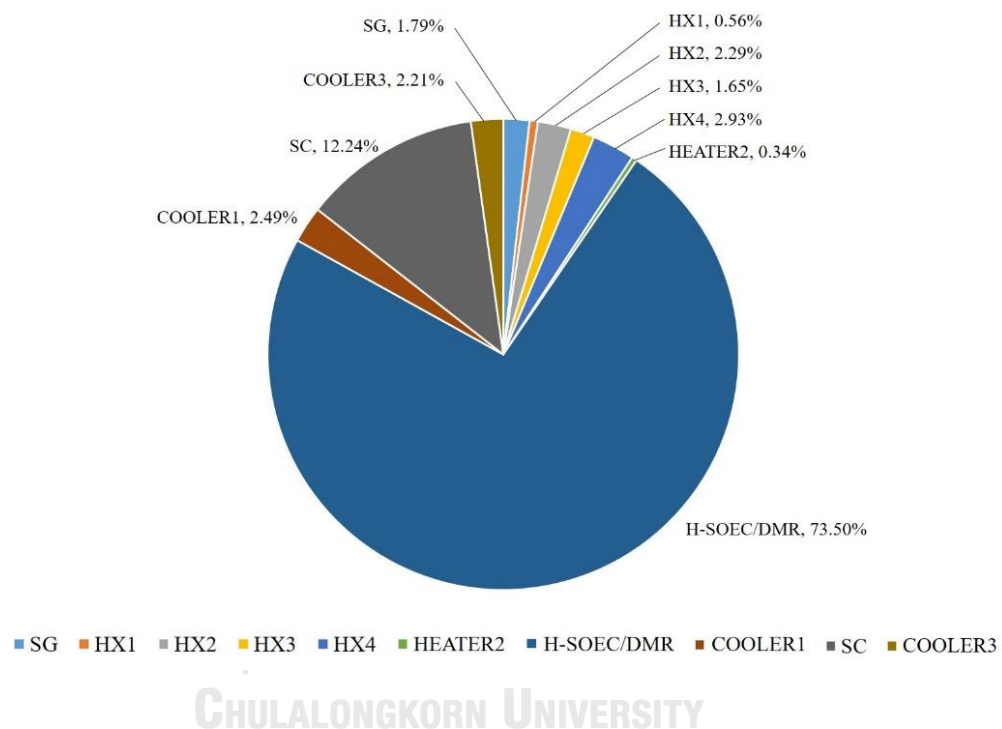


Figure 8.1 %Exergy destruction value of each unit in the H-SOEC/DMR process.

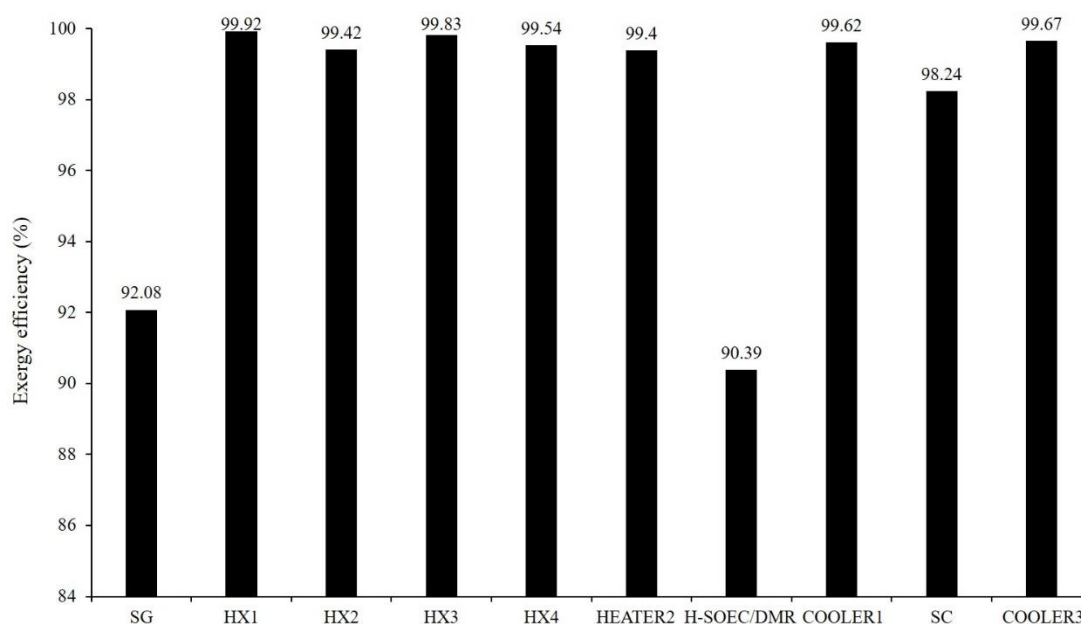


Figure 8.2 Exergy efficiency of each unit in the H-SOEC/DMR process.

For the overall exergy efficiency of the H-SOEC/DME process, the energy and exergy efficiencies and the exergy destruction of process are summarized in Table 8.1. The energy efficiency of 81.46% and the exergy efficiency of 82.64% with exergy destruction of 30031.77 W can be achieved, when the system is operated under optimum conditions (temperature of 1123 K, pressure of 1 atm, current density of 2500 A m⁻², and number of cell of 500 cells) with 0.3239 mol s⁻¹ of water, 0.0170 mol s⁻¹ of hydrogen, and 0.1619 mol s⁻¹ of carbon (CO₂ and CH₄ mixture) are used to produce 0.5773 mol s⁻¹ of syngas product. The energy and exergy efficiencies can be further improved by analyzing the exergy efficiency of each unit in process. According to Figure 8.2, the H-SOEC/DMR unit gives the lowest exergy efficiency. The one reason that this unit gives low exergy efficiency because of an exothermic heat released from this unit, which is used as waste heat, resulting in a high exergy destruction of this unit. In order to improvement, exothermic heat should be supplied to the steam generator (SG) unit, as shown in Figure 8.3, and can reduce the exergy destruction and increase the exergy efficiency (from 90.39% to 92.84%) of the H-SOEC/DMR unit and also

increase the energy and exergy efficiencies of the overall process. The efficiencies value after improvement are summarize in Table 8.1, energy efficiency of 84.18% and exergy efficiency of 83.47% with exergy destruction of 28315.58 W are achieved, when the system is operated under optimum conditions.

Table 8.1 Energy and exergy efficiencies of the optimal H-SOEC/DMR process.

Before improvement		After improvement	
Parameters	Value	Parameters	Value
η_{en} (%)	81.46	η_{en} (%)	84.18
η_{ex} (%)	82.64	η_{ex} (%)	83.47
EX _d (W)	30031.77	EX _d (W)	28315.58

8.2 Effect of operating parameters on exergy efficiency and destruction

In this section, effect of operating parameters on the exergy efficiency and destruction are analyzed in order to characterize that how operating parameters are effect on the exergy of the H-SOEC/DMR process. The operating parameters are considered in this section consist of temperature, pressure, current density, and number of cell. The simulation results and discussion are described as below.

The effect of operating temperature is investigated by varying the temperature in the range of 1123 to 1273 K, under operating conditions (pressure of 1 atm, current density of 2500 A m⁻², and number of cell of 500 cells). The exergy efficiency and destruction value result are shown in Figure 8.4. The exergy efficiency increases with an increasing of temperature because of the decreasing of exergy destruction from electrical energy used, which reduces when temperature increases. Although, an increase of temperature results in an increasing of reaction occur from process, which increases an irreversibility, but heat of overpotential, which relates to irreversibility, decreases, resulting in decreasing of exergy destruction and increasing of exergy efficiency. Moreover, syngas product increases with an increasing of temperature, resulting in high of chemical exergy output of process; therefore, exergy efficiency increases. For the effect of pressure, it is investigated in the range of 1 to 5 atm, under operating conditions (temperature of 1123 K, current density of 2500 A m⁻², and number of cell of 500 cells). The exergy efficiency and destruction results are shown in Figure 8.5. The exergy efficiency decreases, while exergy destruction increases with an increasing of pressure because of an increase of electrical usage and heat of overpotential. In addition, syngas product decreases with an increasing of pressure, resulting in low of chemical exergy output; thus, exergy efficiency decreases.

For the effect of current density, results are shown in Figure 8.6, which current density are varied from 500 to 2500 A m⁻², under operating condition (1123 K, 1 atm, and 500 cells). The exergy efficiency decreases with an increasing of current density because of an increase of exergy destruction from electrical energy demand and heat of overpotential, which increase with an increasing of current density. It is clearly that the exergy destruction value shows the same trend as electrical energy demand and heat of

overpotential (according to chapters V and VI). In addition, exergy destruction increases when current density increases due to an increase of substance input and output of process. In case of the effect of number, exergy efficiency is constant with an increasing of number of cell as shown in Figure 8.7, when number of cell is varied from 100 to 500 cells, under operating conditions (1123 K, 1 atm, and 2500 A m⁻²). According to chapters V and VI, number of cell has only effect on quantity term for both energy and syngas production. Thus, the increasing of number of cell, result in an overall input feed increases proportionally with an overall output product of process influent a constant exergy destruction and exergy efficiency. Moreover, exergy destruction steadily increases with an increasing of number of cell because of an increasing proportionally of overall input and output of process.

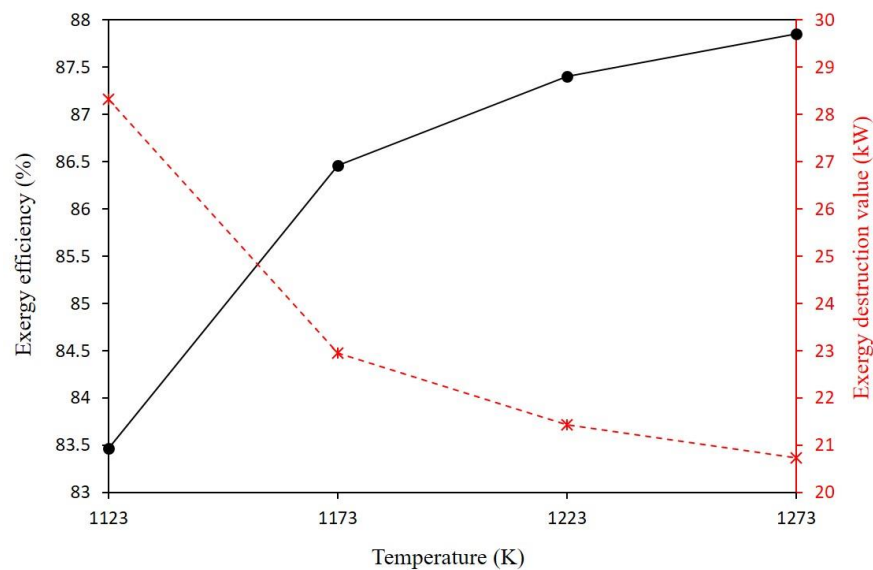


Figure 8.4 Effect of temperature on exergy efficiency and destruction value.

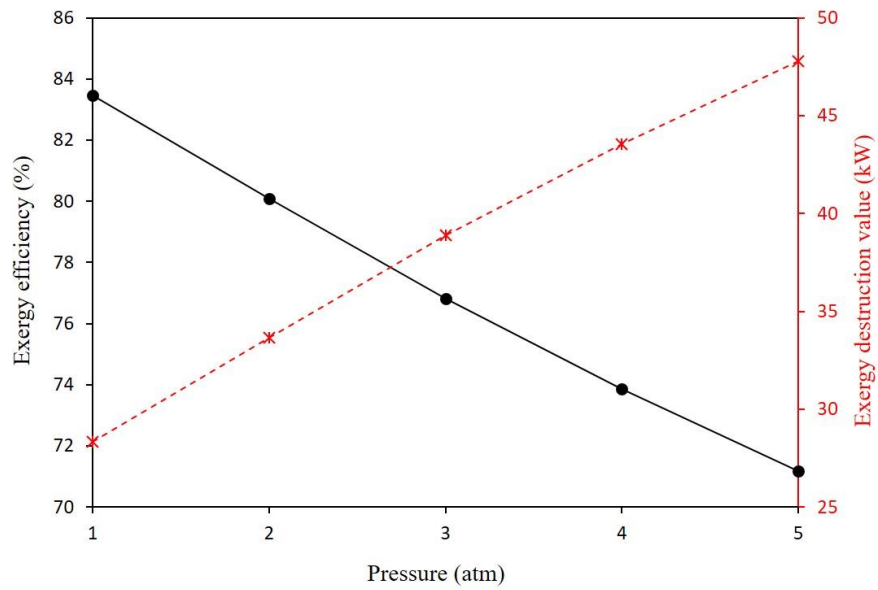


Figure 8.5 Effect of pressure on exergy efficiency and destruction value.

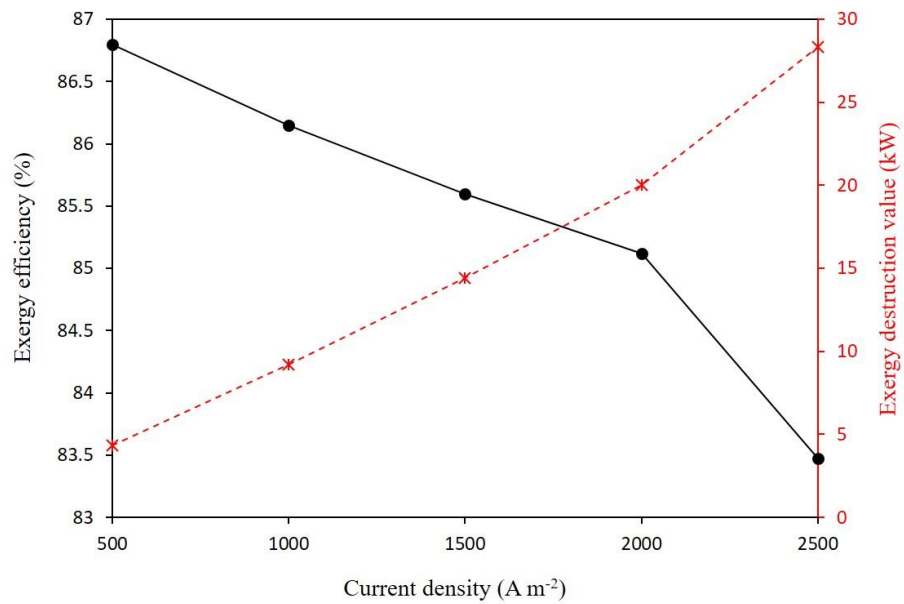


Figure 8.6 Effect of current density on exergy efficiency and destruction value.

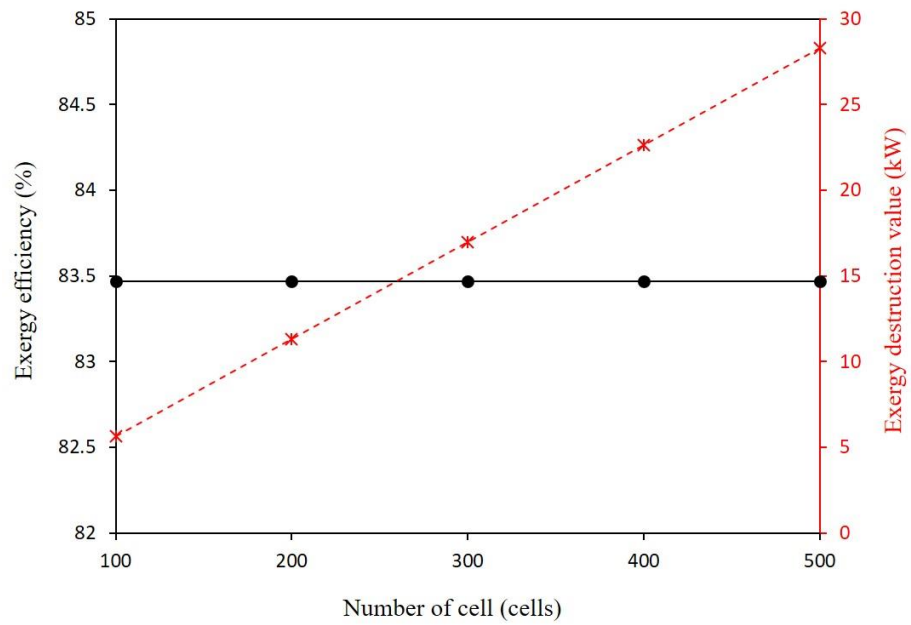
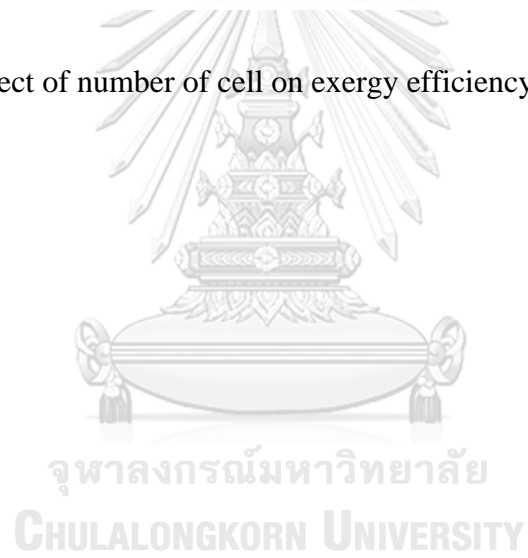


Figure 8.7 Effect of number of cell on exergy efficiency and destruction value.



CHAPTER IX

CONCLUSION AND RECOMMENDATIONS

This chapter, the summary results of this thesis and the recommendation of future works are presented. In this thesis, the proton-conducting solid oxide electrolysis cell coupling with a dry methane reforming (H-SOEC/DMR) process for syngas production was designed and studied. The effect of structural and operational parameters on the process performance in both electrochemical and syngas production terms were investigated using an electrochemical model and flowsheet simulation via Aspen Plus under steady-state condition. In order to obtain the process that given a high of both syngas production and efficiency terms, the energy analysis was performed. The effect of operating parameters on energy efficiency was investigated, then the condition that the highest energy efficiency achieved was selected to be the optimum condition of this process. Additionally, the energy efficiency was further improved through the heat exchanger network design of the H-SOEC/DMR process at optimum condition aim to achieve maximum heat recovery. Moreover, the exergy analysis was also performed at the optimum condition of the process to determine which part of the process was inefficient, leading to the decision for the plant modification of the process for improvement of efficiency of the process. Then, the effect of operational parameters on the exergy was performed in order to evaluate the effect of operating parameters on the exergy of the H-SOEC/DMR process.

9.1 Conclusion

The H-SOEC/DMR process was designed by adding the catalyst layer of DMR into a cathode side of H-SOEC in order to improve the problem in the syngas production term of the H-SOEC process. For the H-SOEC/DMR process, the water, CO₂, and CH₄ were used as main feedstock to produce syngas product. For the simulation term, the electrochemical model and flowsheet simulation model using Aspen Plus were used to investigate the performance of the H-SOEC/DMR process. The simulation results in

both cell voltage and syngas production terms were first validated with experimental data that result showed a good agreement. The effect of structural parameters (i.e., the thickness of cell and supported-structure, pore size, porosity, and tortuosity) on cell voltage was investigated. The results show that the thickness of cell effect on the cell voltage. The cell voltage increase with an increase of thickness of cell. In addition, the lowest cell voltage value was received when operated under the cathode-supported configuration. Moreover, the cell voltage decreases with an increase of pore size and porosity, while the tortuosity showed an opposite trend. According to the simulation result, the pore size of 0.5, porosity of 0.5, and cathode-supported configuration with anode, electrolyte, and cathode thickness of 50, 50, and 500 μm , respectively, were selected as constant structural parameters value in this thesis because the lowest cell voltage can be achieved, which can be minimize an electrical energy of this process.

The effect of operating parameters (i.e., S/C molar ratio, temperature, pressure, current density, and the number of cell) on both electrochemical and syngas production terms were investigated. For the S/C molar ratio, the value of 2 by adjusting a carbon stream was selected as a suitable ratio because this condition is given a low of cell voltage value and high of H/C molar ratio of syngas product, which higher than 2. In term of temperature effect, in the range of 1073 to 1273 K, the %CO₂ and %CH₄ conversions higher than of 90% and 80%, respectively, with a reduce of H₂O content in product stream were achieved from this process and those increased with temperature, while the pressure effect has given an opposite trend. In addition, the H/C molar ratio of syngas product higher than 2 was achieved from this process. Moreover, the amount of products increased with an increase in current density and number of cells. The result indicates that this process is given a high performance in term of syngas production. On the other hand, in term of energy demand, it needed high energy to sufficient both electrochemical and chemical reactions. The result shows that the total energy demand increase with an increase of syngas production to sufficient an energy demand of process. Therefore, the energy analysis of this process should be performed in order to evaluate the energy efficiency of this process. Moreover, the design of the process should be performed to improve the energy efficiency of the process, aim to

achieve the process that given a high in both syngas production and energy efficiency terms.

The energy analysis was performed by evaluating the effect of operating parameters on the energy efficiency of the process. The result shows that the operating parameters were the effect on energy efficiency. The temperature of 1123 K, pressure of 1 atm, current density of 2500 A m^{-2} , and number of cell of 500 cells was selected as optimum condition, which given the highest energy efficiency of 72.80% and amount of syngas production of $0.5773 \text{ mol s}^{-1}$ with %CO₂ and %CH₄ conversions of 97.18% and 88.77%, respectively. The energy efficiency can be further improved through heat exchanger network design by heat integration to achieve a maximum heat recovery of process. The pinch analysis of the H-SOEC/DMR process under the optimum condition with ΔT_{\min} of 20 K was performed. The result indicated that the pinch temperature was represented in the grid diagram, which 588.52 K for hot streams and 568.52 K for cold streams with minimum hot and cold utility requirements of 1945.51 W and 5442.31 W, respectively. The number of the heat exchanger of the optimal H-SOEC/DMR process consisted of 7 heat exchangers. In addition, after heat integration, the energy efficiency of the optimal H-SOEC/DMR process was improved from 72.80% to 81.46%.

Moreover, in order to realize which part of the process was inefficient and guideline to improvement, the exergy analysis was performed and the effect of operating parameters on exergy efficiency was investigated. The result shows that, at optimum condition, the lowest exergy efficiency of 90.39% and highest exergy destruction were achieved from the H-SOEC/DMR unit because of the high electrical energy usage and occurrence of several reactions taking place, which leads to the high irreversibility. Additionally, exothermic heat, which treated as waste heat released, resulting in the high of exergy destruction of this unit. In terms of overall exergy efficiency, at optimum condition, the exergy efficiency of 82.64% was achieved. The exergy efficiency of the process could be improved by utilizing waste heat released from the H-SOEC/DMR unit to the steam generator (SG) unit in order to reduce the exergy destruction of this unit. After an improvement, at optimum condition, the result shows that the exergy efficiency of the H-SOEC/DMR unit was increased from 90.39%

to 92.84% and the exergy of the overall process was increased from 82.64% to 83.47%. Moreover, after an improvement, the energy efficiency also increase from 81.46% to 84.18%, when $0.3239 \text{ mol s}^{-1}$ of water, $0.0170 \text{ mol s}^{-1}$ of hydrogen, and $0.1619 \text{ mol s}^{-1}$ of carbon (CO_2 and CH_4 mixture) were used to produce $0.5773 \text{ mol s}^{-1}$ of syngas product with % CO_2 and % CH_4 conversions of 97.18% and 88.77%, respectively, under the optimum condition with heat exchanger network design. Additionally, the result of the effect of the operational parameters on exergy efficiency indicated that the exergy efficiency increase with temperature, but decrease with pressure and current density, while constant with the number of cell.

9.2 Recommendations

9.2.1 The optimization of the H-SOEC/DMR process should be performed in order to find the operating condition that the highest energy efficiency and % CO_2 and % CH_4 conversions are achieved.

9.2.2 Currently, the experimental data of the H-SOEC/DMR process is limited, thus in the future, the aim to improve the reliability of the simulation, the experimental should be performed to obtain experimental data, which used as a simulation tool.

9.2.3 The economic analysis should be performed in order to determine the economically feasible and cost estimation of the H-SOEC/DMR process.

REFERENCES

- Abdullah, B., Abd Ghani, N., & Vo, D. (2017). Recent advances in dry reforming of methane over Ni-based catalysts. *Journal of Cleaner Production*, 162, 170-185.
- Aramouni, N., Touma, J., Tarboush, B., Zeaiter, J., & Ahmad, M. (2018). Catalyst design for dry reforming of methane: Analysis review. *Renewable and Sustainable Energy Reviews*, 82, 2570-2585.
- Arvidsson, M., Morandin, M., & Harvey, S. (2015). Biomass gasification-based syngas production for a conventional oxo synthesis plant-greenhouse gas emission balances and economic evaluation. *Journal of Cleaner Production*, 99, 192-205.
- Bonilla-Petriciolet, A., Rangaiah, G., & Segovia-Hernández, J. (2011). Constrained and unconstrained Gibbs free energy minimization in reactive systems using genetic algorithm and differential evolution with tabu list. *Fluid Phase Equilibria*, 300(1), 120-134.
- C. Reid, R., Sherwood, T., & Street, R. (1959). *The Properties of Gases and Liquids* (Vol. 12).
- Cao, P., Adegbite, S., & Wu, T. (2017). Thermodynamic Equilibrium Analysis of CO₂ Reforming of Methane: Elimination of Carbon Deposition and Adjustment of H₂/CO Ratio. *Energy Procedia*, 105, 1864-1869.
- Çengel, Y., Boles, M., & Kanoglu, M. (2019). *Thermodynamics : an engineering approach* (Ninth edition, International student edition. ed.). New York: McGraw-Hill Education.
- Challiwala, M., Ghouri, M., Linke, P., El-Halwagi, M., & Elbashir, N. (2017). A combined thermo-kinetic analysis of various methane reforming technologies: Comparison with dry reforming. *Journal of CO₂ Utilization*, 17, 99-111.
- Chan, S., Chen, X., & Khor, K. (2004). Cathode Micromodel of Solid Oxide Fuel Cell. *Journal of The Electrochemical Society - J ELECTROCHEM SOC*, 151.
- Chan, S., & Xia, Z. (2001). Anode Micro Model of Solid Oxide Fuel Cell. *Journal of The Electrochemical Society - J ELECTROCHEM SOC*, 148.
- Chein, R., Chen, Y., Yu, C., & Chung, J. (2015). Thermodynamic analysis of dry reforming of CH₄ with CO₂ at high pressures. *Journal of Natural Gas Science and Engineering*, 26, 617-629.

- Chen, B., Xu, H., Sun, Q., Zhang, H., Tan, P., Cai, W., Ni, M. (2018). Syngas/power cogeneration from proton conducting solid oxide fuel cells assisted by dry methane reforming: A thermal-electrochemical modelling study. *Energy Conversion and Management*, 167, 37-44.
- Dale, N., Mann, M., & Salehfar, H. (2008). Semiempirical model based on thermodynamic principles for determining 6kW proton exchange membrane electrolyzer stack characteristics. *Journal of Power Sources*, 185(2), 1348-1353.
- Delikonstantis, E., Scapinello, M., & Stefanidis, G. (2017). Investigating the Plasma-Assisted and Thermal Catalytic Dry Methane Reforming for Syngas Production: Process Design, Simulation and Evaluation (Vol. 10).
- Dimian, A., Bildea, C., & Kiss, A. (2014). Chapter 13 - Pinch Point Analysis. In A. Dimian, C. Bildea, & A. Kiss (Eds.), *Computer Aided Chemical Engineering* (Vol. 35, pp. 525-564): Elsevier.
- Dincer, I., & Rosen, M. (2013). Chapter 3 - Chemical Exergy. In I. Dincer & M. Rosen (Eds.), *Exergy (Second Edition)* (pp. 31-49): Elsevier.
- Dinh, D., Choi, S., Lee, D., Jo, S., Kim, K., & Song, Y. (2018). Energy efficient dry reforming process using low temperature arcs. *Plasma Processes and Polymers*, 15(5), 1700203.
- Dominguez-Ramos, A., Singh, B., Zhang, X., Hertwich, E., & Irabien, A. (2015). Global warming footprint of the electrochemical reduction of carbon dioxide to formate. *Journal of Cleaner Production*, 104, 148-155.
- Ebbesen, S., Høgh, J., Nielsen, K., Nielsen, J., & Mogensen, M. (2011). Durable SOC stacks for production of hydrogen and synthesis gas by high temperature electrolysis. *International Journal of Hydrogen Energy*, 36(13), 7363-7373.
- Er-rbib, H., Bouallou, C., & Werkoff, F. (2012). Production of Synthetic Gasoline and Diesel Fuel from Dry Reforming of Methane. *Energy Procedia*, 29, 156-165.
- Evgeny, Y. (2006). Book Review: *Exergy Method - Technical and Ecological Applications* by Szargut. *International Journal of Thermodynamics*, 9.
- Ghannadzadeh, A., They-Hetreux, R., Baudouin, O., Baudet, P., Floquet, P., & Joulia, X. (2012). General methodology for exergy balance in ProSimPlus® process simulator. *Energy*, 44(1), 38-59.

- Gopaul, S., & Dutta, A. (2015). Dry reforming of multiple biogas types for syngas production simulated using Aspen Plus: The use of partial oxidation and hydrogen combustion to achieve thermo-neutrality. *International Journal of Hydrogen Energy*, 40(19), 6307-6318.
- Guan, J., Ramamurthi, B., Ruud, J., Hong, J., Riley, P., & Minh, N. (2006). High performance flexible reversible solid oxide fuel cell.
- Hajjaji, N., Pons, M., Houas, A., & Renaudin, V. (2012). Exergy analysis: An efficient tool for understanding and improving hydrogen production via the steam methane reforming process. *Energy Policy*, 42, 392-399.
- Hamzehlouia, S., A. Jaffer, S., & Chaouki, J. (2018). *Microwave Heating-Assisted Catalytic Dry Reforming of Methane to Syngas (Vol. 8)*.
- Hawkes, G., O'Brien, J., M. Stoots, C., & Herring, J. (2007). *CFD MODEL OF A PLANAR SOLID OXIDE ELECTROLYSIS CELL FOR HYDROGEN PRODUCTION FROM NUCLEAR ENERGY (Vol. 158)*.
- Hernández-Pacheco, E., Singh, D., Hutton, P., Patel, N., & Mann, M. (2004). A macro-level model for determining the performance characteristics of solid oxide fuel cells. *Journal of Power Sources*, 138(1), 174-186.
- Herrera Delgado, K., Maier, L., Tischer, S., Zellner, A., Stotz, H., & Deutschmann, O. (2015). *Surface Reaction Kinetics of Steam- and CO₂-Reforming as Well as Oxidation of Methane over Nickel-Based Catalysts (Vol. 5)*.
- Im-orb, K., Visitdumrongkul, N., Saebea, D., Patcharavorachot, Y., & Arpornwichanop, A. (2018). Flowsheet-based model and exergy analysis of solid oxide electrolysis cells for clean hydrogen production. *Journal of Cleaner Production*, 170, 1-13.
- Kasemanand, S., Im-orb, K., Tippawan, P., Wiyaratn, W., & Arpornwichanop, A. (2017). Exergy analysis of the biogas sorption-enhanced chemical looping reforming process integrated with a high-temperature proton exchange membrane fuel cell. *Energy Conversion and Management*, 149, 485-494.
- Kemp, I. (2007). 2 - Key concepts of pinch analysis. In I. Kemp (Ed.), *Pinch Analysis and Process Integration (Second Edition)* (pp. 15-40). Oxford: Butterworth-Heinemann.

- Lavoie, J. (2014). Review on dry reforming of methane, a potentially more environmentally-friendly approach to the increasing natural gas exploitation (Vol. 2).
- Li, Q., Zheng, Y., Guan, W., Jin, L., Xu, C., & Wang, W. (2014). Achieving high-efficiency hydrogen production using planar solid-oxide electrolysis stacks. *International Journal of Hydrogen Energy*, 39(21), 10833-10842.
- Lu, J., Zhu, C., Pan, C., Lin, W., Lemmon, J., Chen, F., Xie, K. (2018). Highly efficient electrochemical reforming of CH₄/CO₂ in a solid oxide electrolyser (Vol. 4).
- Matyka, M., Khalili, A., & Koza, Z. (2008). Tortuosity-porosity relation in porous media flow. *Physical review. E, Statistical, nonlinear, and soft matter physics*, 78, 026306.
- Menon, V., Janardhanan, V., & Deutschmann, O. (2014). A mathematical model to analyze solid oxide electrolyzer cells (SOECs) for hydrogen production. 110, 83-93.
- Mingyi, L., Bo, Y., Jingming, X., & Jing, C. (2008). Thermodynamic analysis of the efficiency of high-temperature steam electrolysis system for hydrogen production. *Journal of Power Sources*, 177(2), 493-499.
- Muradov, N., & Smith, F. (2008). *Thermocatalytic Conversion of Landfill Gas and Biogas to Alternative Transportation Fuels* (Vol. 22).
- Namwong, L., Authayanun, S., Saebea, D., Patcharavorachot, Y., & Arpornwichanop, A. (2016). Modeling and optimization of proton-conducting solid oxide electrolysis cell: Conversion of CO₂ into value-added products. *Journal of Power Sources*, 331, 515-526.
- Ni, M. (2012). An electrochemical model for syngas production by co-electrolysis of H₂O and CO₂. *Journal of Power Sources*, 202, 209-216.
- Ni, M., Leung, M., & Leung, D. (2006). A modeling study on concentration overpotentials of a reversible solid oxide fuel cell. 163(1), 460-466.
- Ni, M., Leung, M., & Leung, D. (2007a). Energy and exergy analysis of hydrogen production by solid oxide steam electrolyzer plant. *International Journal of Hydrogen Energy*, 32(18), 4648-4660.

- Ni, M., Leung, M., & Leung, D. (2007b). Parametric study of solid oxide steam electrolyzer for hydrogen production. *International Journal of Hydrogen Energy*, 32(13), 2305-2313.
- Ni, M., Leung, M., & Leung, D. (2008a). Electrochemical modeling of hydrogen production by proton-conducting solid oxide steam electrolyzer. *International Journal of Hydrogen Energy*, 33(15), 4040-4047.
- Ni, M., Leung, M., & Leung, D. (2008b). Technological development of hydrogen production by solid oxide electrolyzer cell (SOEC). *International Journal of Hydrogen Energy*, 33(9), 2337-2354.
- Nikoo, M., & Amin, N. (2011). Thermodynamic analysis of carbon dioxide reforming of methane in view of solid carbon formation. *Fuel Processing Technology*, 92(3), 678-691.
- Perry, R., & Green, D. (2008). *Perry's chemical engineers' handbook* (8th ed. / ed.). New York: McGraw-Hill.
- Riazat, M., Baniassadi, M., Mazrouei, M., Tafazoli, M., & Moghimi Zand, M. (2015). The Effect of cathode Porosity on Solid Oxide Fuel Cell Performance (Vol. 3).
- Ruiz-Trejo, E., & Irvine, J. (2012). Ceramic proton conducting membranes for the electrochemical production of syngas. *Solid State Ionics*, 216, 36-40.
- S. Spacil, H., & S. Tedmon, C. (1969). *Electrochemical Dissociation of Water Vapor in Solid Oxide Electrolyte Cells* (Vol. 116).
- Shin, T., Myung, J., Naeem, K., Savaniu, C., & Irvine, J. (2015). Ce(Mn,Fe)O₂–(La,Sr)(Fe,Mn)O₃ composite as an active cathode for electrochemical reduction of CO₂ in proton conducting solid oxide cells. *Solid State Ionics*, 275, 106-109.
- Smith, R. (2016). *Chemical process design and integration* (Second edition ed.). Chichester, West Sussex, United Kingdom: John Wiley & Sons, Inc.
- Stempien, J., Sun, Q., & Chan, S. (2013a). Performance of power generation extension system based on solid-oxide electrolyzer cells under various design conditions. *Energy*, 55, 647-657.
- Stempien, J., Sun, Q., & Chan, S. (2013b). Solid oxide electrolyzer cell modeling: A review. 93(4), 216-246.

- Stroud, T., Smith, T., Le Saché, E., Santos, J., Centeno, M., Arellano-Garcia, H., Reina, T. (2018). Chemical CO₂ recycling via dry and bi reforming of methane using Ni-Sn/Al₂O₃ and Ni-Sn/CeO₂-Al₂O₃ catalysts. *Applied Catalysis B: Environmental*, 224, 125-135.
- T. Whipple, D., & Kenis, P. (2010). *Prospects of CO₂ Utilization via Direct Heterogeneous Electrochemical Reduction (Vol. 1)*.
- Tsai, C., & Schmidt, V. (2011). Tortuosity in anode-supported proton conductive solid oxide fuel cell found from current flow rates and dusty-gas model. *Journal of Power Sources*, 196(2), 692-699.
- Tungkamani, S., Phongaksorn, M., Narataruksa, P., Sornchamn, T., Kanjanabat, N., & Siri-Nguan, N. (2013). *Developing carbon tolerance catalyst for dry methane reforming (Vol. 2013)*.
- Udagawa, J., Aguiar, P., & Brandon, N. (2007). Hydrogen production through steam electrolysis: Model-based steady state performance of a cathode-supported intermediate temperature solid oxide electrolysis cell. *Journal of Power Sources*, 166(1), 127-136.
- Udagawa, J., Aguiar, P., & Brandon, N. (2008). Hydrogen production through steam electrolysis: Control strategies for a cathode-supported intermediate temperature solid oxide electrolysis cell. *Journal of Power Sources*, 180(1), 354-364.
- Veldsink, J., van Damme, R., Versteeg, G., & van Swaaij, W. (1995). The use of the dusty-gas model for the description of mass transport with chemical reaction in porous media. *The Chemical Engineering Journal and the Biochemical Engineering Journal*, 57(2), 115-125.
- Wang, S., & Lu, G. (1996). *Carbon Dioxide Reforming of Methane To Produce Synthesis Gas over Metal-Supported Catalysts: State of the Art (Vol. 10)*.
- Wang, Y., Liu, T., Fang, S., Xiao, G., Wang, H., & Chen, F. (2015). A novel clean and effective syngas production system based on partial oxidation of methane assisted solid oxide co-electrolysis process. *Journal of Power Sources*, 277, 261-267.
- Xiang, J., Cali, M., & Santarelli, M. (2004). Calculation for physical and chemical exergy of flows in systems elaborating mixed-phase flows and a case study in an IRSOFC plant. *International Journal of Energy Research*, 28, 101-115.

- Xie, K., Zhang, Y., Meng, G., & Irvine, J. (2010). Electrochemical reduction of CO₂ in a proton conducting solid oxide electrolyser (Vol. 21).
- Yan, C., Yang, A., Chien, I., Wei, S., Shen, W., & Ren, J. (2019). Advanced exergy analysis of organic Rankine Cycles for Fischer-Tropsch syngas production with parallel dry and steam methane reforming. *Energy Conversion and Management*, 199, 111963.
- Yang, P., Columbus, E., Wooten, J., Batchelor, W., Buchireddy, P., Ye, X., & Wei, L. (2009). Evaluation of Syngas Storage Under Different Pressures and Temperatures. *Applied Engineering in Agriculture*, 25, 121-128.
- Zhang, H., Lin, G., & Chen, J. (2010). Evaluation and calculation on the efficiency of a water electrolysis system for hydrogen production. *International Journal of Hydrogen Energy*, 35(20), 10851-10858.
- Zhang, M., Xiao, M., Wang, S., Han, D., Lu, Y., & Meng, Y. (2015). Cerium oxide-based catalysts made by template-precipitation for the dimethyl carbonate synthesis from Carbon dioxide and methanol. *Journal of Cleaner Production*, 103, 847-853.
- Zhang, W. (2004). Simulation of a tubular solid oxide fuel cell stack using AspenPlus™ unit operation models (Vol. 46).
- Zhang, X., O'Brien, J., O'Brien, R., & Housley, G. (2013). Durability evaluation of reversible solid oxide cells. *Journal of Power Sources*, 242, 566-574.
- Zhang, X., Song, Y., Wang, G., & Bao, X. (2017). Co-electrolysis of CO₂ and H₂O in high-temperature solid oxide electrolysis cells: Recent advance in cathodes. *Journal of Energy Chemistry*, 26(5), 839-853.
- Zhao, F., & Virkar, A. (2005). Dependence of polarization in anode-supported solid oxide fuel cells on various cell parameters. *Journal of Power Sources*, 141(1), 79-95.
- Zhu, H., Kee, R., Janardhanan, V., Deutschmann, O., & Goodwin, D. (2005). Modeling elementary heterogeneous chemistry and electrochemistry in solid-oxide fuel cells. 152(12), A2427-A2440.
- Zhu, L., Zhou, M., Shao, C., & He, J. (2018). Comparative exergy analysis between liquid fuels production through carbon dioxide reforming and conventional steam reforming. *Journal of Cleaner Production*, 192, 88-98.



จุฬาลงกรณ์มหาวิทยาลัย
CHULALONGKORN UNIVERSITY

VITA

NAME Wissawa Chalee

DATE OF BIRTH 06 August 1995

PLACE OF BIRTH Roi-et

INSTITUTIONS ATTENDED

- Bachelor's Degree in Industrial Chemistry from Department of Chemical Science, Faculty of Science, King Mongkut's Institute of Technology Ladkrabang in 2017
- Master Study in the major in Chemical Engineering at Chulalongkorn University, Thailand in August 2017

HOME ADDRESS 234/13 Dok-mai, Suvarnabhumi, Roi-et 45130

PUBLICATION Pure and Applied Chemistry International Conference 2019: Model development of proton-conducting solid oxide electrolysis cell for hydrogen production

